

UCSF

UC San Francisco Electronic Theses and Dissertations

Title

Investigating the Use of Protein and Liposomal Therapeutics for the Treatment of Glioblastoma

Permalink

<https://escholarship.org/uc/item/5dx4m2f9>

Author

Serwer, Laura

Publication Date

2011

Peer reviewed|Thesis/dissertation

Investigating the Use of Protein and Liposomal Therapeutics for the
Treatment of Glioblastoma

by

Laura Patterson Serwer

DISSERTATION

Submitted in partial satisfaction of the requirements for the degree of

DOCTOR OF PHILOSOPHY

in

Pharmaceutical Sciences and Pharmacogenomics

in the

GRADUATE DIVISION

of the

UNIVERSITY OF CALIFORNIA, SAN FRANCISCO

Copyright © 2011

by

Laura Patterson Serwer

ACKNOWLEDGEMENTS

This thesis is dedicated to my family, who are my inspiration in everything.

To my parents, Gerald and Sheryl Serwer for always encouraging my curiosities, enduring my endless stream of scientific "fun facts", and for providing unconditional love and support throughout all the stages of education that have led me to this point.

To my husband, Paul Karayan, whose love and support have given me strength, courage, and the faith to keep going.

To my siblings, Bradley Serwer, Valerie Serwer, Kathleen Corey, and James Corey who have taught me endless lessons in humility, humor, and happiness.

This thesis is also dedicated to all my teachers and mentors who have given their time and energy, even when I resisted their efforts.

To my PhD mentor, C. David James who has worked tirelessly to ensure that I have everything I need to be successful.

To my undergraduate mentor, Gerard C. Blobe, who first sparked my interest in cancer biology, and taught me the joys of independent discovery.

Finally, this thesis is dedicated to all my friends and classmates who have been a sounding board for my frustrations, and a happy break from the drudgery of writing.

Investigating the Use of Protein and Liposomal Therapeutics for the Treatment of Glioblastoma

by Laura Patterson Serwer

ABSTRACT

Glioblastoma, the most aggressive form of primary brain tumors, has disappointingly few treatment options, leading to a dismal prognosis for patients. While there are many traditional small molecule drugs that are effective against glioblastoma cell lines in vitro, the vast majority of these drugs are ineffective in vivo, owing to poor delivery of these drugs across the blood brain barrier into the brain tumor. This dissertation presents a series of studies into drug delivery to the brain, with a specific emphasis on delivery to brain tumors.

Chapter 3 of this thesis explores the use of yeast cytosine deaminase in an enzyme prodrug therapy paradigm. In this study, an active enzyme, yCD was delivered directly to the tumor by convection-enhanced delivery, and the prodrug, 5-fluorocytosine was delivered orally. While our efficacy studies did show that this treatment regimen was able to statistically enhance survival time, a rapid clearance of the yCD protein limits the utility of this approach.

Chapters 4 and 5 of this thesis explore the use of liposomally formulated drugs to treat GBM. Liposomes are small vesicles with phospholipid bilayers that can carry drugs either within the bilayer, or within the aqueous core of the liposomes. In this thesis, we explored the use of liposomes loaded with topotecan, a DNA topoisomerase I inhibitor. Chapter 3 addressed the systemic administration of liposomal topotecan, and found that this

route of delivery offered substantial efficacy in multiple models of GBM. Chapter 4 attempted to increase the specificity of liposomal topotecan by attaching an antibody against the epidermal growth factor receptor (EGFR) to the liposome surface. When we delivered these targeted liposomes by CED, we saw a significant increase in survival in two mouse models of GBM. While encouraging, the invasive nature of CED will likely limit the use of this therapeutic in the clinic.

In total, these studies highlight the potential utility of two popular themes in drug delivery: the use of protein-based therapeutics as well as nanoscale drug carriers, and offers insight into the future of GBM treatment.

Table of Contents

CHAPTER 1: INTRODUCTION	1
1.1 Challenges in drug delivery to tumors of the central nervous system (CNS)	1
1.1.1 The blood-brain barrier (BBB) in normal brain and in brain tumors	1
1.2 Approved treatments for glioma	2
1.2 Local Delivery Strategies	4
1.2.1 Convection-enhanced delivery (CED)	4
1.2.2 Intranasal delivery	10
1.2.3 Intrathecal delivery	11
1.3 Pharmacological Methods for Improving Drug Delivery to CNS Tumors	14
1.3.1 Chemical disruption of the BBB	15
1.4 Conclusions.....	16
CHAPTER 2: SYSTEMIC AND LOCAL DRUG DELIVERY METHODS FOR MOUSE MODELS OF BRAIN TUMORS	18
2.1 Abstract	18
2.2 Systemic Delivery Methods.....	19
2.2.1 Intravenous (tail vein) injection.....	20
2.2.2 Intraperitoneal injection.....	21
2.2.3 Oral gavage.....	22
2.3 Local Delivery (Acute Convection-Enhanced Delivery)	23
2.3.1 Probe construction	23
2.3.2 Infusion procedure.....	25
2.3.3 <i>In vivo</i> imaging	28
2.4 Representative Results	29
2.5 Discussion	29

CHAPTER 3: CED OF YEAST CYTOSINE DEAMINASE FOR TREATMENT OF AN ORTHOTOPIC MODEL OF GLIOBLASTOMA.....	32
3.1 Abstract	32
3.2 Introduction	33
3.3 Methods	34
3.3.1 Cell Culture.....	34
3.3.2 Tumor Implantation.....	35
3.3.3 Bioluminescent Tumor Imaging.....	35
3.3.4 Protein Expression and Purification	36
3.3.5 Protein Activity Assay.....	37
3.3.6 Convection-Enhanced Delivery of Proteins	38
3.3.7 Delivery of 5-fluorocytosine	39
3.3.8 Confocal Microscopy	39
3.3.9 Biodistribution of 3CD	40
3.4 Results.....	40
3.4.1 Verification of brain tumors by bioluminescence imaging	40
3.4.2 Survival advantage of 3CD/5-FC treatment in early and late stages of tumor growth	41
3.4.3 Effect of 3CD treatment on tumor volume.....	43
3.4.4 Localization of Katushka, a 26 kDa fluorescent protein	45
3.4.5 Elimination rate of radiolabeled 3CD from the brain.....	46
3.5 Discussion	47
3.6 Acknowledgements	50
CHAPTER 4: INTRAVENOUS DELIVERY OF TOPOTECAN LIPOSOMES.....	51
4.1 Abstract	51
4.2 Introduction	52

4.3 Methods	53
4.3.1 Cell cultures	53
4.3.2 Tumor implantation	54
4.3.3 Preparation of nanoliposomal topotecan	54
4.3.4 Biodistribution studies	55
4.3.5 Blood cell analysis	56
4.3.6 In vitro luciferase assay	56
4.3.7 Bioluminescence imaging	57
4.3.8 Topotecan treatment	57
4.3.9 Immunohistochemistry	58
4.3.10 Statistical analysis	58
4.4 Results	59
4.4.1 Biodistribution of nLS-TPT and free TPT	59
4.4.2 Effect of nLS-TPT on tumor growth	61
4.4.3 Effect of nLS-TPT on animal survival	64
4.4.4 Effect of liposomal packaging on drug efficacy <i>in vitro</i>	66
4.4.5 Analysis of biologic effect from TPT treatment <i>in vivo</i>	66
4.4.6 Toxicity	68
4.5 Discussion	74
4.6 Acknowledgements	77
CHAPTER 5: CONVECTION-ENHANCED DELIVERY OF EGFR-TARGETED TOPOTECAN LIPOSOMES	78
5.1 Abstract	78
5.2 Introduction	80
5.3 Methods	81
5.3.1 Materials	81
5.3.2 Cell culture	81

5.3.3 C225 Fab' and p2/4 preparation	82
5.3.4 <i>In vitro</i> binding/uptake of EGFR-LS	83
5.3.5 Tumor implantation	83
5.3.6 Convection-enhanced delivery	84
5.3.7 Effect of EGFR targeting on liposome distribution via CED.....	85
5.3.8 <i>In Vitro</i> luciferase assay	85
5.3.9 <i>In vivo</i> binding/uptake of EGFR (C225)-LS	85
5.3.10 Bioluminescence imaging (BLI)	86
5.3.11 Western blots	86
5.4 Results.....	87
5.4.1 <i>In vitro</i> binding/internalization of EGFR-TPT-LS	87
5.4.2 <i>In Vitro</i> drug uptake and cytotoxicity.....	88
5.4.3 Efficacy of systemic administration of EGFR-TPT-LS in EGFR-expressing xenografts	90
5.4.4 Efficacy of local administration of EGFR-TPT-LS in EGFR-expressing xenografts	91
5.4.5 Effect of EGFR targeting on tumor distribution of immunoliposomes infused via CED	97
5.5 Discussion	98
CHAPTER 6: CONCLUSION	100
6.1 Summary of findings	100
6.2 Future directions.....	102
6.2.1 Cytosine deaminase therapy	102
6.2.2 Ongoing clinical trials using liposomal drugs to treat GBM.....	102
6.2.3 Potential combination therapies with liposomal topotecan	103
REFERENCES	105

List of Figures

Figure 1-1 Protein therapeutics in clinical development for glioma treatment by CED.	6
Figure 1-2 Liposomal distribution after CED into a mouse bearing an intracranial tumor.....	8
Figure 1-3 Small molecule therapeutics investigated for ITD.	12
Figure 2-1 Procedure filming in the HDFCCC Vivarium	19
Figure 2-2 CED cannula and surgical set-up.....	24
Figure 2-3 Mouse skull suture lines.	27
Figure 2-4 Representative results from successful CED.	28
Figure 2-5 Representative image of successful CED into the rat brainstem.....	30
Figure 3-1 Thermostable CD (3CD) has an extended half-life at 37°C.	38
Figure 3-2 Verification of brain tumors by bioluminescent imaging.	41
Figure 3-3 Survival advantage for rats treated with 3CD at an early or late stage of tumor growth.....	43
Figure 3-4 Treatment with 3CD reduces tumor volume when administered early in tumor growth.....	44
Figure 3-5 Localization of a fluorescent surrogate protein.	46
Figure 3-6 Clearance of radiolabeled 3CD.....	47
Figure 4-1 Pharmacokinetic analysis of nLS-TPT retention in tumor-bearing brain and plasma.....	60
Figure 4-2 AUC_{∞} of topotecan in tumor-bearing mice	61
Figure 4-3 Effects of nLS-TPT treatment on tumor growth in vivo	63
Figure 4-4 Effect of nLS-TPT treatment on survival in mice bearing intracranial tumors.	65
Figure 4-5 <i>In vitro</i> analysis of nLS-TPT effect on cell luminescence.....	66
Figure 4-6 Comparison of free TPT versus nLS-TPT pro-apoptotic activity as indicated by DNA fragmentation analysis.	67
Figure 4-7 Caspase-3 activation in cells treated with nLS-TPT.....	68
Figure 4-8 Effect of nLS-TPT and free TPT on body weight.	69
Figure 4-9 Effect of nLS-TPT treatment on hemoglobin and hemaocrit levels.....	71
Figure 4-10 Effect of nLS-TPT treatment on platelet levels.....	72
Figure 4-11 Neutrophil levels in mice treated with nLS-TPT.....	73

Figure 4-12 Neutrophil levels in mice treated nLS-TPT, with or without prior temozolomide treatment.	73
Figure 4-13 Distribution of topoisomerase I expression among GBM subtypes	76
Figure 5-1 Binding/internalization studies of fluorescently labeled NT-TPT-LS and EGFR-TPT-LS.	87
Figure 5-2 Binding/internalization studies of fluorescently labeled NT-TPT-LS and EGFR (C224)-TPT-LS	88
Figure 5-3 TPT uptake in cells that overexpress EGFR.....	89
Figure 5-4 Luciferase assay of TPT-LS treated cells.	90
Figure 5-5 Systemic administration of EGFR-TPT-LS in mice bearing intracranial tumors that overexpress EGFRvIII.....	91
Figure 5-6 Effect of a single administration (0.26 mg/kg) of either EGFR-TPT-LS or NT-TPT-LS in mice bearing U87-EGFRvIII tumors.....	92
Figure 5-7 Effect of two administrations of EGFR-TPT-LS treatment on U87-EGFRvIII tumor growth and survival.....	93
Figure 5-8 Effect of EGFR-TPT-LS treatment on i	95
Figure 5-9 Effect of EGFR-TPT-LS on cell sources that lack EGFR.	96
Figure 5-10 Distribution of NT-LS or EGFR (C225)-LS in U87-EGFRvIII tumors.....	97
Figure 6-1 Combination of liposomal topotecan with whole brain radiotherapy in mice bearing SF767 intracranial tumors.	104

Chapter 1: Introduction

This chapter contains reprinted material from the review article “Challenges in drug delivery to tumors of the central nervous system: an overview of pharmacological and surgical considerations” by Laura P. Serwer and C. David James submitted to Advanced Delivery Drug Delivery Reviews on July 15, 2011.

1.1 CHALLENGES IN DRUG DELIVERY TO TUMORS OF THE CENTRAL NERVOUS SYSTEM (CNS)

1.1.1 The blood-brain barrier (BBB) in normal brain and in brain tumors

The central nervous system is uniquely protected by the Blood-Brain Barrier (BBB), which separates circulating blood and from the CNS. Composed of endothelial cells lacking intracellular fenestrations and linked by tight junctions, the BBB serves to dramatically restrict the types of compounds that can freely diffuse from the blood stream into the brain [1-3]. While there is evidence of transcytosis of positively charged serum proteins, such as albumin, the movement of simple molecules, such as glucose, as well as some larger molecules, including hormones and growth factors, is regulated by specific carrier proteins[3, 4]. In addition to the well-characterized network of influx transporters in the BBB, there also exists a BBB network of efflux transporters, such as p-glycoprotein and members of the multidrug resistance-associated protein family, that actively pump substrates from the brain into the blood stream[5, 6]. In combination, the efflux pumps, the highly specific influx transporters, and the relatively impermeable physical structure of the BBB, result in a substantial challenge in the treatment of CNS cancer due to the difficulty in achieving efficacious drug levels in the CNS from systemic administration of therapy.

While the composition and function of the BBB has been extensively described for normal brain, changes that occur to the BBB in association with CNS tumor development are less well understood. CNS tumor magnetic resonance (MR) imaging, based on gadolinium enhancement of tumor, is generally accepted as indicating BBB compromise or breakdown. However, extent of compromise may be quite variable between individual tumors, as well as within a single heterogeneous tumor, creating significant variation in therapeutic access and distribution within tumor. In support of this consideration, Schlageter *et al.* studied a small panel of preclinical models of CNS cancer and found considerable variation in the structure of the BBB within their model cohort[7]. Specifically they found that some models maintained nearly intact barriers lacking detectable pores or intracellular fenestrations, whereas others contained large pores, up to 3 millimeters in diameter[7]. In all cases they found that the vascularity of the tumor was highly irregular, and with greater intervessel distance than observed in normal brain[7]. Furthermore, clinical studies of anti-angiogenic agents have shown CNS tumor BBB to be highly dynamic, with changes in contrast-enhancement detectable as early as 24 hours after the onset of therapy[8]. These studies suggest that the state of the tumor BBB is not only variable, but highly changeable as well.

1.2 Approved treatments for glioma

There remain few approved chemotherapeutics for malignant glioma, the most common type of CNS tumor in adults. In fact, prior to incorporating the DNA alkylating agent temozolomide (TMZ) into standard treatment during the past decade, surgery and radiation therapy were the only routinely used treatments [9]. While TMZ confers survival benefit to the glioma patient population as a whole, extent of efficacy is largely influenced by the methylation status of the *MGMT* gene promoter, with promoter methylation occurring in

35-45% of these tumors[10, 11]. In patients whose tumors have un-methylated MGMT promoter regions, *MGMT* protein (O-6-methylguanine-DNA methyltransferase) is expressed and repairs DNA damage caused by TMZ, negating its tumoricidal effects[12]. However, even in the best case scenario of complete MGMT silencing due to promoter methylation, malignant glioma patient mean survival is extended approximately 6 months, relative to patients with unmethylated MGMT, with average survival for all malignant glioma patients now between 15 and 22 months[11]. This clinical reality makes it patently clear that there is a dire need for improved therapeutic approaches.

As malignant glioma is essentially incurable, newly diagnosed patients receiving standard of care therapy will invariably have recurrent disease, at which time patients are routinely treated with bevacizumab[13]. Bevacizumab, a monoclonal antibody that targets vascular endothelial growth factor - A (VEGFA), has been shown to extend malignant glioma patient progression-free survival in Phase II studies compared to historical controls[14-16]. In light of the paucity of options for recurrent malignant glioma, the FDA granted, in 2009, approval for bevacizumab in treating patients with recurrent disease, while necessary Phase III studies are being completed.

Lastly, there is one additional FDA approved option for local therapy of glioma, Gliadel (proliferon 20 with carmustineinplant)[17]. Gliadel is a biodegradable polymer that is impregnated with carmustine (BCNU), a DNA alkylating agent. After resection of the tumor bulk, Gliadel wafers are placed in the resection cavity, enabling steady local, carmustine release, contributing to the reduction of residual tumor cells at the resection margin. Gliadel treatment increases patient survival by two months on average, which is considered significant survival benefit for recurrent disease[18].

Conventional thinking and predominant effort, as concerns achieving improved treatment outcomes for brain tumor patients, has been focused on the development of therapeutics that target and inhibit activated signaling mediators in malignant glioma. In fact, an impressive armamentarium of these inhibitors already exist, though their use in clinical trials have yielded unimpressive results, due in part, if not entirely to biodistribution and pharmacokinetic limitations. In the remainder of this review, we will focus on several strategies for improving drug delivery to glioma that encompass novel physical routes of administration as well as innovative pharmacological strategies to increase drug efficacy.

1.2 LOCAL DELIVERY STRATEGIES



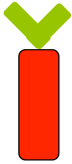


1.2.1 Convection-enhanced delivery (CED)

Intraoperative injection of anti-cancer agents into brain tumors has experienced minor success as a result of diffusion-limited drug distribution as well as infusate leakage away from the target site. Convection-enhanced delivery (CED) is a type of direct administration that uses positive pressure to increase circulation of drug throughout the tumor, and to reduce the influence of therapeutic molecular weight on distribution. While successful in this regard, CED remains technically challenging and a subject of ongoing preclinical and clinical research.

Cannula trajectories, as well as the number of cannulas used, have a substantial impact on the success of CED infusion. Poor cannula placement can result in leakage of drug away from the target site, potentially leading to adverse effects, such as chemical meningitis[19]. The highly variable intracranial distribution of glioma tumors adds to the challenge for the use of CED by requiring an individualized cannula placement plan for each patient. Optimal cannula placement can be aided by the FDA-approved software iPlan by BrainLAB, which models fluid flow in the brain and provides feedback regarding cannula

location. By comparing actual infusion distributions of radiolabeled albumin to drug distributions predicted by iPlan, Sampson *et al.* found the software to be accurate in 5 of the 7 instances[20]. iPlan algorithms are rapidly evolving to assist in more accurate cannula placements and more thorough drug distribution, although, even in its current state, use of the software is proving clinically beneficial.

Due to high molecular weight, therapeutic proteins have been common candidates for delivery by CED. Most therapeutic proteins investigated for the treatment of malignant glioma consist of a cytotoxic moiety, often a bacterial toxin, combined with a targeting moiety for selective therapeutic effect on glioma cells (**Figure 1-1**). In Chapter 3 of this thesis, we explored the use of CED to deliver yeast cytosine deaminase (yCD), a nontargeted therapeutic protein to orthotopic xenograft models of glioblastoma.

	IL4-PE (PRX321)	IL13- PE38QQR (cintredekin besudotox)	Anti-EGFRvIII scFv-PE (MR1-1)	Tf-CRM107 (TransMID)	chTNT-1/B mAb -I ¹³¹ (Cotara)
					
Cytotoxic Agent	Pseudomonas exotoxin	Pseudomonas exotoxin	Pseudomonas exotoxin	Diphtheria exotoxin	I ¹³¹
Target	Interleukin-4 receptor	Interleukin-13 receptor	Epidermal growth factor receptor, variant III	Transferrin receptor	DNA - histone complex
Clinical Status	Phase IIb	Phase III	Phase I	Withdrawn*	Phase II









	Pseudomonas exotoxin
	Diphtheria exotoxin
	I ¹³¹
	Interleukin-4
	Interleukin-13
	scFv against EGFRvIII
	mAb against DNA-histone complex
	Transferrin protein

Figure 1-1 Protein therapeutics in clinical development for glioma treatment by CED.

*TransMD was withdrawn from Phase III trials in the US, but has been included in order to illustrate that other bacterial toxins, in addition to the pseudomonas exotoxin, have been investigated.

An extensively investigated cytotoxic moiety is derived from *Pseudomonas aeruginosa* exotoxin (PE). PE inhibits elongation factor 2 (EF-2), an essential component of protein synthesis machinery. Several PE fusion proteins have made it through multiple rounds of clinical testing, notably IL4-PE (PRX321) and IL13-PE38QQR (cintredekin besudotox). Both target interleukin receptors that are over-expressed in malignant glioma, and promote tumor cell death via EF-2 inhibition. Phase I and II trials have shown acceptable safety profiles of both drugs, but neither has reached acceptable efficacy standards for obtaining FDA approval. Cintredekin besudotox has been tested in the Phase III PRECISE trial, with results indicating no significant survival advantage from this treatment, in relation to treatment with Gliadel wafers. MR1-1, a novel PE fusion protein that combines PE with a monoclonal antibody fragment against a mutant form of EGFR commonly overexpressed in malignant glioma tumors[21], has been investigated in preclinical studies, with associated results showing that the drug is well-tolerated, thereby clearing the way for future studies in patients[21].

Other notable fusion proteins being investigated for efficacy by CED include TransMD-107 (tf-CRM107) as well as Cotara. TransMD-107 is a diphtheria exotoxin fused to transferrin, and binds to transferrin receptor that is commonly overexpressed in malignant glioma. The safety of TransMD-107 has been demonstrated in Phase I and Phase II studies, with partial responses noted in the Phase II trial[22]. Cotara consists of a radioactive isotope (I^{131}) labeled antibody that is targeted against DNA histone complexes in dying tumor cells. By localizing to dying cells, Cotara delivers radiation to surrounding viable tumor cells. Preliminary Phase II results with Cotara show improved patient survival relative to historical controls, with full Phase II study analysis to be completed later this year.

In addition to its use in administering protein-based drugs, CED is also the delivery method of choice for large molecules, nanoparticles, and biologics, such as oligonucleotides, drug bearing liposomes, and viral-mediated therapies, respectively. Trabedersen (AP-12009) is an antisense oligonucleotide that targets the transcript for transforming growth factor-beta 2 (TGF- β 2), a protein involved in various aspects of tumor growth and survival. Phase II results show significant survival benefit for patients treated with Trabedersen, relative to historical controls, with Phase III analysis of this therapeutic currently underway.

Liposomal drug carriers encapsulate small molecule chemotherapeutics and can improve the pharmacokinetic profile of these agents by reducing drug clearance time. When delivered by CED, liposomal agents achieve acceptable tumor coverage, as indicated by magnetic resonance imaging, using gadolinium-loaded liposomes, or by fluorescent microscopy (Figure 1-2).

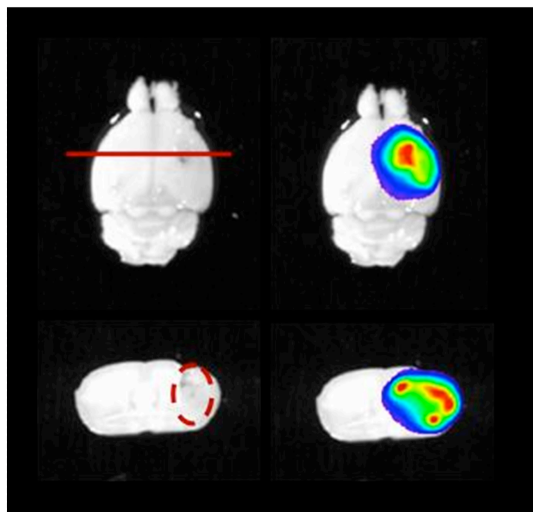


Figure 1-2 Liposomal distribution after CED into a mouse bearing an intracranial tumor.

Fluorescently-labeled liposomes were infused by CED into a nude mouse bearing a human intracranial xenograft. After the infusion, the brain was resected and imaged. Upper left photograph shows the location of the coronal section shown in the lower left and right images, with outline of the tumor indicated by the dashed line in the lower left image. Right panels show fluorescent liposome coverage of the tumor.

Among the chemotherapeutics being investigated in association with liposomal formulation is irinotecan, which has shown impressive efficacy in preclinical studies when delivered by CED in rodent and canine models[23, 24]. The canine studies, in fact, involve the treatment of pets with glioma, which closely resembles human disease. Substantial variation in liposomal irinotecan tumor coverage has been demonstrated in studies conducted thus far (0.02-90%), due in part to the variable locations of the canine tumors. In areas where tumor coverage was determined to be reasonably thorough, tumor cells responded with a 15-fold reduction in proliferation, as measured by Ki-67 immunohistochemistry[25]. In rodent models of glioma, CED administration of liposomal irinotecan decreased tumor laminin and vascular density, suggesting the therapeutic may have an anti-angiogenic effect, in addition to its known pro-apoptotic and anti-proliferative effects [26]. These preclinical studies were of fundamental importance in providing motivation for my studies of liposomal topotecan, which are described in Chapter 5 of this thesis.

Liposomes can also serve as vectors for gene transfer to glioma cells. For instance, Gupta *et al.* used liposomes modified with the HIV tat peptide to transfect green fluorescent protein (GFP) expression constructs into rodents bearing orthotopic gliomas[27]. As concerns clinical studies, Voges *et al.* have used liposomes to deliver the herpes simplex virus-1 thymidine kinase gene to human glioma patients in a Phase I/II clinical study. After CED treatment with liposomes, patients were given systemic ganciclovir, and in 6 of 8 instances a change in tumor cell metabolism was noted by positron emission tomography (PET), with two of the tumors showing >50% reduction in volume, as indicated by MRI.

Though it has tremendous potential to improve clinical outcomes for malignant glioma patients, CED faces several challenges for achieving more widespread use. In addition to the highly variable nature of CED-associated therapeutic distribution in tumors, the procedure is highly invasive, which limits the number of patients that can be treated by CED, and further limits the number of dosing cycles that can be applied to CED eligible patients.

1.2.2 Intranasal delivery

The trigeminal and olfactory nerves that innervate the nasal epithelium represent the only direct connection between the external environment and the brain[28]. Given the ease of administering drugs by nasal inhalation, this route of delivery has received considerable interest for its potential in treating cognitive and neurodegenerative disorders[29-31]. In regard to brain tumor therapy, intranasal delivery (IND) has seen only minor investigation thus far, though published results indicate intriguing potential for this approach in treating CNS cancer. Methotrexate, raltitrexed, and 5-fluorouracil (5-FU) have all been shown to accumulate in the brain after intranasal delivery (IND)[32-34], and in the case of 5-FU, IND results in significantly greater 5-FU brain exposure than IV dosing, with further 5-FU exposure achieved by co-treating animal subjects with inhibitors of cerebrospinal fluid secretion[34]. In spite of the promising pharmacokinetic indications for administering 5-FU by IND, this therapeutic approach has yet to be evaluated in preclinical brain tumor models, and as such there are no results with which to assess efficacy.

To date, the only controlled efficacy study of IND in a brain tumor model was conducted by Hashizume *et al.*, using an oligonucleotide telomerase inhibitor (GRN163)[35]. When administered by IND to rats with intracranial glioblastoma, detectable accumulation of

GRN163 was evident, which resulted in a highly significant extension of animal survival. In addition to this preclinical study, there has been a single human subject study in which an oligodendroglioma patient was administered perillyl alcohol by IND[36-38], which resulted in partial tumor regression following treatment[37]. While encouraging, there has yet to be a follow-up study from the use of this treatment approach in a clinical trial.

In total, as concerns the treatment of brain tumors, IND administration has received minor attention, with most investigations and applications of this treatment approach being directed to neurodegenerative disease[39].

1.2.3 Intrathecal delivery

In some glioma patients tumor cells disseminate along the leptomeninges (meningeal gliomatosis, neoplastic meningitis), resulting in tumor spread along the neuraxis[40, 41]. Since neuraxis disseminated tumors remain protected by the blood-brain barrier, intrathecal delivery (ITD) is a reasonable treatment approach for achieving improved outcomes for this patient population. By bypassing the blood-brain barrier, ITD allows for the use of many agents that do not have favorable CNS distribution when administered systemically. Drug circulation in the intrathecal space is largely determined by the bulk flow rate of cerebrospinal fluid, with drug exposure subject to the same pharmacokinetic factors as apply to other routes of administration[42, 43]. Unfortunately, not all drugs are acceptable ITD candidates, as irritants can cause dose-limiting chemical arachnoiditis, as was seen in a single patient trial of ITD topotecan[44]. Below, studies are discussed for ITD of small molecule and macromolecular drugs.

ITD administration of many small molecules has been investigated (**Figure 1-3**), including methotrexate[45], cytosine arabinoside[46], neocarzinostatin[47], ACNU[48],

mafosfamide[49], and thiotriethylenephosphoramidate (thio-TEPA)[50]. The results for thio-TEPA were particularly encouraging in showing radiologic response in 5 of 14 patients, with a corresponding 5.5 month gain in survival time for responders in comparison to non-responders[50].

Drug	Mechanism of Action	Reference	Comments
Topotecan	DNA topoisomerase I inhibitor	Clayton 2008[44], Groves 2008[51]	Chemical arachoniditis observed
Methotrexate	Antimetabolite	Edwards 1981[45], Yoshimura J 2008[52]	
Cytosine Arabinoside	Antimetabolite	Fulton 1982[46]	Currently used in liposomal formulation
Neocarzinostatin	Induces DNA breaks	Uemura 1985[47]	Caused a decreased number of malignant cells in CSF
ACNU	Alkylating agent	Levin 1989[48]	8 of 21 patients showed a decrease in CSF cytology
Mafosfamide	Alkylating agent	Blaney 2005[53], Slavic 2003[54]	Phase I trial, with headaches as dose-limiting toxicity
Thiotriethylenephosphoramidate (thio-TEPA)	Alkylating agent	Witham 1999[50]	Radiologic response in 5 of 14 patients
Etoposide	DNA topoisomerase II inhibitor	Slavic 2003[54]	No toxicity observed

Figure 1-3 Small molecule therapeutics investigated for ITD.

While there are many investigational agents being administered intrathecally, only one, liposomal cytarabine, has been approved for clinical use. As is the case for all liposomal drugs, the liposomal formulation of cytarabine, a potent antimetabolite, promotes controlled drug release and extended drug exposure after administration. While the approved indication is for lymphomatous meningitis, the nonspecific cytotoxicity of cytarabine makes

it a good candidate drug for treating other forms of cancer. Indeed, in a single patient with a low grade oligodengrogloma displaying leptomenigeal dissemination, treatment with ITD liposomal cytarabine combined with oral temozolomide resulted in complete tumor regression, with no signs of recurrence at 24-month follow-up[55]. In a recent randomized clinical trial for patients with neoplastic meningitis, intrathecal liposomal cytarabine treatment demonstrated anti-tumor effect in 13 of 18 patients, compared to only 3 of 17 responders who received unencapsulated cytarabine[49], supporting the importance of the liposomal formulation for increasing therapeutic efficacy.

Currently there is a diverse portfolio of experimental agents being tested in preclinical models of neoplastic meningitis. For instance, 81C6, an anti-tenascin antibody, is being used as a delivery vector for ¹³¹I intrathecal brachytherapy. Tenascin is an extracellular matrix protein that is ubiquitously expressed in gliomas, particularly in glioblastomas[56]. In a Phase I trial, ITD of ¹³¹I-81C6 was able to stabilize disease in 42% of patients[57].

Oncolytic viruses have also been explored for efficacy by ITD. For example, glioblastomas are known to express CD155, the poliovirus receptor, which provides a point of tumor cell access for a tumoricidal recombinant poliovirus[58]. Indeed, in a preclinical rodent model of neoplastic meningitis, ITD of recombinant poliovirus resulted in significant animal survival extension[59]. While encouraging, concerns about safety, as well as pre-existing immunity in vaccinated adults, have limited enthusiasm for the clinical development of this therapy.

Finally, recent work has revealed that stem cells can be used as vehicles for delivering anti-cancer agents. Seminal work by Aboody *et al.*, has shown that both neural stem cells (NSC) and mesenchymal stem cells (MSC) display tropism for glioma cells,

thereby suggesting the use of stem cells for delivering therapy in treating residual disease[60]. Further support for this treatment approach has been presented by Shimato *et al.* who used NSCs, transduced to express cytosine deaminase, in treating a rodent model of leptomeningeal medulloblastoma[61]. When the prodrug 5-fluorocytosine was administered, transduced NSCs were able to produce sufficient amounts of cytotoxic 5-fluorouracil to demonstrate anti-tumor effect and prolong animal survival[61].

With respect to the use of mesenchymal stem cells, thymidine kinase transduced MSCs have been used to treat neoplastic meningitis in a rat model[62]. When combined with ganciclovir administration, this therapy demonstrated substantial anti-tumor effect, although treatment was initiated at a time when animal subjects had minor tumor burden, and therefore the experiment was not necessarily representative of the context in which glioma patients would be treated[62].

1.3 PHARMACOLOGICAL METHODS FOR IMPROVING DRUG DELIVERY TO CNS TUMORS

While bypassing the BBB through physical methods has achieved a degree of preclinical and clinical success, CED and ITD remain invasive approaches that carry significant risks for patients. The development of pharmacological strategies to reduce BBB effects have been sought not only for their potential in decreasing patient risk, but also for the potential of these approaches in achieving greater therapeutic distribution in tumors, and for compatibility with repeated drug administration. Here, we review various strategies for increasing the transport of drugs across the BBB, focusing on strategies that have shown preclinical efficacy in the treatment of malignant glioma.

1.3.1 Chemical disruption of the BBB

It has long been known that the BBB can be disrupted via infusion of either a hyperosmotic fluid, such as mannitol[63], or through the administration of a vasoactive compound, such as bradykinin[64]. Hyperosmotic mannitol infusions cause a transient shrinkage of cerebrovascular endothelial cells, resulting in an enlargement of the tight junctions and BBB leakiness[63]. The use of mannitol has been shown to promote CNS access for a wide range of compounds, including small molecules such as methotrexate[65], and larger biologics such as monoclonal antibodies and viruses[66-68]. While increases in the CNS concentration of therapeutics after mannitol infusion has indicated significant potential for this approach[65], preclinical efficacy results have been highly variable[69]. Furthermore, clinical studies have shown that although mannitol infusions increase BBB permeability at the tumor site, the permeability of normal brain is also increased, thereby increasing the risk of enhanced neurotoxicity from therapy[70].

Infusions with vasoactive agents have also yielded promising results in preclinical studies, and suggest that tumor vasculature may be more sensitive to vasoactive agent than normal brain vasculature[71]. Vasoactive peptides that have been used to increase drug transport to brain tumors include leukotrienes[64], bradykinin[64], and RMP-7[72]. Use of the latter, RMP-7, an analogue of bradykinin, has been shown to increase animal survival in a rodent model of glioma, when combined with systemic administration of carboplatin[72]. Though promising, delivery of vasoactive agents requires intra-arterial infusion, and as such creates a barrier for clinical translation of this treatment approach.

Other strategies for addressing BBB effects include exploiting the function of specific BBB proteins. In this regard the transferrin receptor has long been an attractive target, due to its ability to bind ligand and transcytose ligand conjugates from the blood stream into the

brain. In addition to transferrin ligand, intravenously administered antibodies targeting the transferrin receptor can be detected in the brain parenchyma at rates significantly higher than labeled control antibodies, indicating their transport across the BBB[73]. Transferrin antibodies can be conjugated to drug carriers, such as liposomes, which, in turn, can serve as vehicles for numerous therapeutics. Investigators have used this approach to transport detectable quantities of both small molecule inhibitors, as well as RNAi constructs into the brain[74, 75]. Though preclinical results give reason for optimism regarding the use of BBB transport proteins for improving therapeutic access to tumor, there has yet to be a clinical demonstration of targeted drug carriers crossing the BBB in sufficient concentration for demonstrating anti-tumor effect in patients.

The modulation of BBB efflux pump function, such as p-glycoprotein (Pgp) and the breast cancer resistance protein (BCRP), provide an alternative approach for increasing therapeutic concentrations in brain tumors. For example, Carcaboso *et al.* found that systemic treatment with gefitinib, an inhibitor of Pgp and BCRP, resulted in increased intratumoral concentration of intravenously administered topotecan [76].

1.4 CONCLUSIONS

Delivering drugs for effective treatment of CNS cancer has long been hampered by a lack of effective approaches that either modulate or circumvent the BBB. Despite these obstacles, significant progress has been made in utilizing less conventional routes of administration, especially CED and ITD, as well as with regard to novel drug formulations, and this progress is being actively investigated in numerous clinical trials. In this thesis, we explored both local delivery by CED of a protein therapeutic (Chapter 3), as well as a targeted liposomal therapeutic (Chapter 5), and additionally investigated the systemic

delivery of a nontargeted liposomal therapeutic (Chapter 4). Collectively, the related research that has been conducted in recent years provides promise of a future in which CNS tumor patients will have multiple, efficacious treatment options for improved clinical management of their disease.

CHAPTER 2: Systemic and Local Drug Delivery Methods for Mouse Models of Brain Tumors

This chapter contains material from the article “Systemic and Local Drug Delivery for Treating Diseases of the Central Nervous System in Rodent Models” by Laura P. Serwer, Rintaro Hashizume, Tomoko Ozawa, and C. David James, published in the Journal of Visualized Experiments, 2010. The accompanying video, demonstrating the procedures described in this chapter can be viewed at: <http://www.jove.com/details.php?id=1992>

2.1 ABSTRACT

Thorough preclinical testing of central nervous system (CNS) therapeutics includes a consideration of routes of administration and agent biodistribution in assessing therapeutic efficacy. Between the two major classifications of administration, local vs. systemic, systemic delivery approaches are often preferred due to ease of administration. However, systemic delivery may result in suboptimal drug concentration being achieved in the CNS, and lead to erroneous conclusions regarding agent efficacy. Local drug delivery methods are more invasive, but may be necessary to achieve therapeutic CNS drug levels. Here, we demonstrate proper technique for three routes of systemic drug delivery: intravenous injection, intraperitoneal injection, and oral gavage. In addition, we show a method for local delivery to the brain: convection-enhanced delivery (CED). The use of fluorescently-labeled compounds is included for *in vivo* imaging and verification of proper drug administration. The methods are presented using murine models, but can easily be adapted for use in rats.

2.2 SYSTEMIC DELIVERY METHODS

Although systemic delivery of drugs is not the most efficient approach for achieving high drug concentrations in the CNS, systemic deliveries are convenient and well accepted by patients. Here, we will demonstrate proper procedures for three routinely used systemic administration approaches: intravenous injection, intraperitoneal injection, and oral gavage. All procedures were filmed in the Helen Diller Family Comprehensive Cancer Center (HDFCCC), behind a sterile barrier, following UCSF IACUC and LARC protocols. All methods are described in a list-like manner, intended to facilitate application in the laboratory.



Figure 2-1 Procedure filming in the HDFCCC Vivarium

2.2.1 Intravenous (tail vein) injection

Before beginning the procedure, the body weight of each mouse should be recorded. No more than 1% of the mouse's body weight in volume should be injected at a single time. For example, no more than 0.2mL of fluid should be injected in a 20g mouse. All fluids injected intravenously should be sterilized by an appropriate method.

The mouse should be warmed for 5-10 minutes using either a heating pad or a heat lamp to dilate the tail vein. If using a heat lamp, monitor the mouse at all times to avoid hyperthermia. The mouse is then transferred to a holding device, which restrains the mouse while allowing access to the tail vein (see video). In the mouse tail there are four visible vessels: the vessels on the dorsal and lateral sides are veins, and the vessel on the ventral side is an artery. To access the tail vein, the tail of the mouse is held at the most distal point, and rotated 90 degrees so that the vein is facing upwards. The injection site is cleaned with an alcohol swab and a 28g insulin syringe is inserted, beveled side up, into the vein (see video). If the needle is properly placed in the vein, it should move freely and without pressure. Slowly inject the drug with even pressure over 5-10 seconds. If a blister appears on the tail, stop injecting, as this indicates that the needle is no longer in the vein.

After injection, apply gentle pressure to the injection site until the bleeding stops. This normally takes 30-60 seconds. Monitor the mouse for 5-10 minutes after the injection to insure that there is no further bleeding.

2.2.2 Intraperitoneal injection

Before beginning the injection, the drug should be loaded into a syringe attached to a 28g needle. Make sure that there is space in the syringe for drawing back the plunger before the injection (e.g., if injecting 200 μ L, make sure that the syringe capacity is 300 μ L or greater). Remove the mouse from the cage by its tail and place it onto a textured surface, so that the mouse has something to grip. A cage lid is usually sufficient. Allow the mouse to stretch its body and then using your non-dominant hand, grasp the skin on the back of the mouse, taking care to lightly pinch as much skin as possible between your thumb and index and middle fingers (see video). Turn the mouse over so that the abdomen of the mouse is facing upwards. If the mouse can freely move its head, release the grip and try again, so as to avoid being bitten during the injection.

With your dominant hand, pick up the syringe and insert the needle at a 30 degree angle into the lower left quadrant of the mouse (see video). Holding the mouse slightly inverted will help move the organs away from the injection site. To ensure that the needle is in the intraperitoneal space, pull back on the syringe plunger. If any fluid or blood appears in the syringe, then the needle is not in the intraperitoneal space and should be removed. If no fluid is aspirated into the syringe, then inject the syringe contents with an even pressure over 1-5 seconds and release the mouse.

Monitor the mouse for 5-10 minutes after the injection to ensure that the mouse returns to normal activity levels.

2.2.3 Oral gavage

Before beginning the injection, record the weight of the mouse. The maximum volume that can be delivered by oral gavage is 10mL per kilogram of body weight. For example, the maximum volume for a 20g mouse would be 200 μ L. Attempting to inject larger volumes may result in reflux, which will cause incomplete drug delivery. If it is necessary to administer volumes greater than indicated above, as many as three doses may be administered over 24 hours.

To avoid puncturing the esophagus, it is important to measure the length of the gavage needle for each mouse. Hold an 18g ball tip curved gavage needle at the last rib of the mouse, and then mark the length at the tip of the mouse's head using a permanent marker (see video). During the gavage, this mark will be a stopping point as you insert the needle into the mouth of the mouse.

Restrain the mouse using the same hand grip as for an intraperitoneal injection. Insert the gavage needle in the mouth, over the tongue, and advance the needle through the pharynx. Do not insert the needle past the stopping mark. The needle should proceed smoothly without any pressure (see video). If you encounter pressure, stop and withdraw the needle to avoid injecting fluid into the lungs.

With the needle in place, depress the plunger over 1-5 seconds and then remove the needle at the same angle that it was inserted. Monitor the mouse for 5-10 minutes, paying close attention to any signs of labored breathing which may indicate that fluid has entered the lungs.

2.3 LOCAL DELIVERY (ACUTE CONVECTION-ENHANCED DELIVERY)

2.3.1 Probe construction

A reflux-resistant CED cannula for rodents is not yet commercially available. Here we will demonstrate a method for cannula construction that was adapted from a method first described by Krauze *et al* [77]. The cannula has three parts (**Figure 2-2**): 100 μ M diameter silica tubing through which the infusate flows, a rigid metal needle for structural support, and flexible Teflon tubing for loading the infusate. To obtain the rigid metal needle, use an open flame to melt the plastic on a Surflo IV Catheter (24g stylet) and using tweezers remove the metal needle. The rest of the catheter can be discarded. Cut a length of silica tubing (OD 0.163mm), slightly longer than the metal needle, using a single-edge razor blade. Role the silica tubing in a small drop of cyanoacrylate based fast-acting adhesive (e.g. Krazy Glue), taking care not to get any glue on the ends of the tubing. Insert the silica tubing in the metal needle and let dry for 5 minutes.

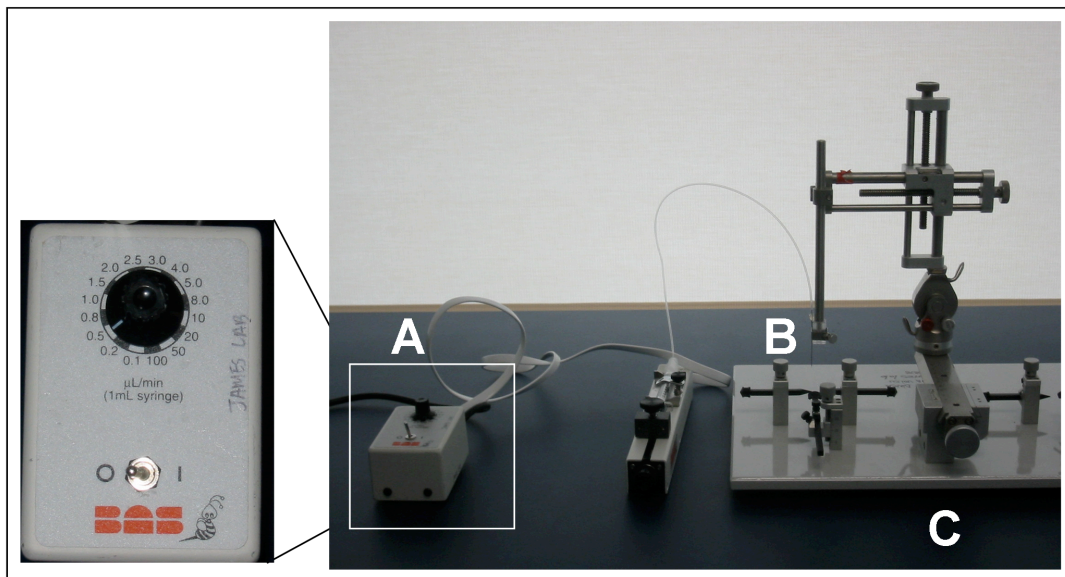
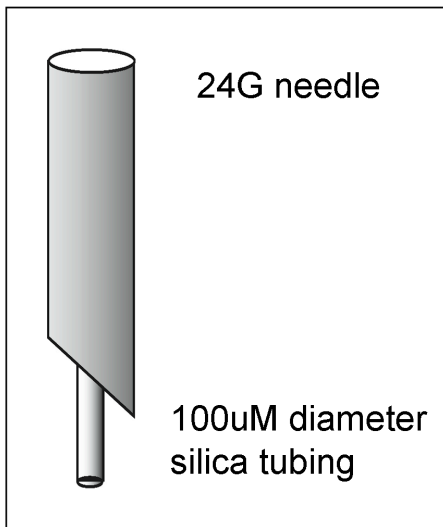


Figure 2-2 CED cannula and surgical set-up. The basic elements of the convection-enhanced delivery surgical set-up are shown. A microinfusion pump (A) is attached to the infusion cannula (B, shown enlarged at top). A stereotaxic frame (C) is used to position the probe. This image does not include heating and anesthetic equipment also used during the procedure.

Once dry, the silica tubing should be firmly affixed to the needle. The ends of the silica should be trimmed so that 2mm of silica tubing protrudes from the pointed end of the needle and 3mm of silica tubing protrudes from the flat end (see video). Cut a section of Teflon tubing 20 cm in length. Roll the metal needle in a small drop of adhesive, again taking care not to get glue on the ends of the silica tubing as this will clog the cannula. Insert the

needle into the Teflon tubing to a depth of 1 cm. Let dry for 1 minute. Using a glue gun, apply a drop of hot glue to the joint between the metal needle and the Teflon tubing (see video). Ensure that the entire joint is covered on all sides and let dry for at least 1 hour. Cannulas can be made up to a week in advance and stored at room temperature.

2.3.2 Infusion procedure

To prepare the surgical area, all surfaces should be sprayed with a disinfectant, such as a 2% chlorhexidine solution. The surfaces are then covered with absorbent drapes. The following supplies should be placed in the surgical area:

- Heating pad to maintain mouse body temperature
- Two small Petri dishes; one containing 3% hydrogen peroxide, and one containing 2% chlorhexidine
- Sterile gauze and cotton swabs
- Sterile disposable scalpels (Number 21)
- Sterile 22g needles
- Mouse stereotaxic frame
- Controlled rate syringe pump
- Autoclaved mouse skin stapler, staples, and staple remover

To set-up the CED cannula, attach a 1 mL syringe to the Teflon tubing using a set of plastic syringe adapters. The cannula should be affixed to the stereotaxic frame so that it is perpendicular to the surgical surface (see video). To disinfect the cannula, fill the 1 mL syringe with 70% ethanol and depress the plunger to run the ethanol through the cannula. Repeat this process using sterile saline, and check for any leaks around the cannula joints. To disinfect the outside of the cannula, gently wipe with a 70% ethanol wipe.

Fill the cannula with sterile saline and then pull back on syringe so that a small air bubble is drawn into the cannula. This air bubble will separate the infusate from the saline in

the cannula. Then, backload your infusate (see video). Connect the syringe to the syringe pump and prime the pump by briefly running the cannula. Sedate the mouse using an injected anesthetic and prepare the skin by swabbing several times (for 5-10 seconds) with a piece of sterile gauze dipped in the 2% chlorhexidine solution. Ophthalmic ointment should be applied to the mouse to maintain adequate eye moisture during the procedure. Using a sterile scalpel, create a sagittal incision along the center of the skull, approximately 1.5cm long (see video). The skull surface is then cleaned using a cotton swab soaked in a 3% hydrogen peroxide solution. Take care to avoid getting hydrogen peroxide in the eyes of the mouse. The suture lines of the skull should be apparent at this point: if they are not visible, gently swab the skull with a fresh cotton swab soaked in 3% hydrogen peroxide solution.

Identify the bregma (**Figure 2-3**) and then measure 2mm to the right and 1mm posterior of this structure to locate the infusion site. Using the sterile 22g needle, gently create a hole in the skull at this point by twisting the needle against the skull (see video). Avoid forcing the needle downward against the skull. At this point, the mouse should be placed in the stereotaxic frame and begin receiving inhaled anesthetic (see video). Administer the anesthetic at a low level (1%), and carefully monitor the mouse for changes in respiration rate, adjusting the anesthetic accordingly.

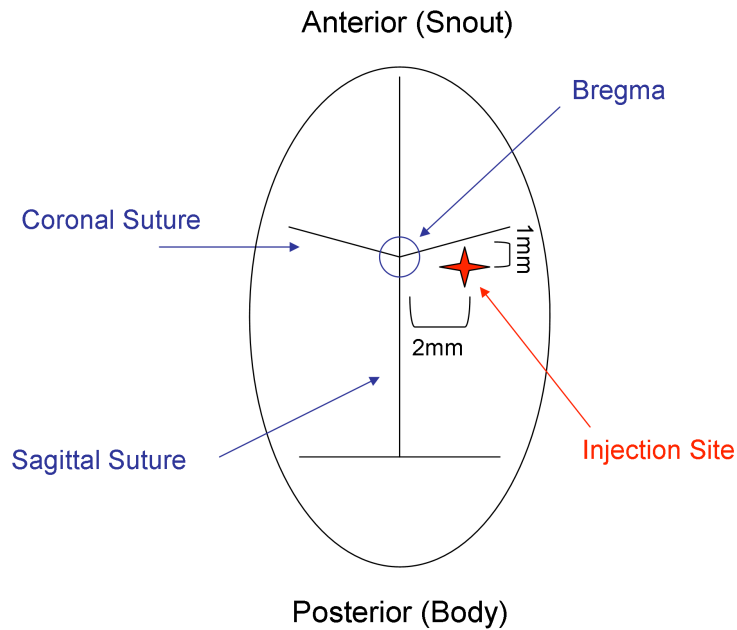


Figure 2-3 Mouse skull suture lines. The CED infusion site (red star) can be located by identifying the intersection of the sagittal and coronal sutures (the bregma) and then measuring 2mm lateral and 1mm posterior of the bregma.

Position the cannula over the skull hole and then lower 3mm below the skull surface.

Begin the infusion, using the following rates and durations:

0.1 $\mu\text{L}/\text{min}$ for 5 minutes

0.2 $\mu\text{L}/\text{min}$ for 5 minutes

0.5 $\mu\text{L}/\text{min}$ for 5 minutes

0.8 $\mu\text{L}/\text{min}$ for 7.5 minutes

OFF for 1 minute

Total Infused Volume: 10 μL

At the end of the infusion, slowly remove the cannula and swab the skull with 3% hydrogen peroxide. Apply sterile bone wax to the hole (see video). Using forceps, draw the skin together over the skull and staple to close. Buprenorphine should be administered for post-operative pain relief. Monitor the mouse post-operatively until it regains consciousness and mobility. Due to the length of the procedure, it may take up to an hour for the mouse to

regain full activity. During this time place the mouse cage on a heating pad to avoid hypothermia, and do not house the recovering mouse with other active mice. Skin staples should be removed one week after surgery.

2.3.3 *In vivo* imaging

Fluorescently-labeled infusate can be imaged following CED administration, and can be monitored for changes in signal intensity as well as signal location. Typically, it is best to wait 2-3 hours after the infusion to image, so as to allow the mouse to recover from the infusion. For anesthesia during imaging, use a low level of an inhaled anesthetic. Position the mouse, dorsal side up, in an imaging station (e.g., IVIS Lumina, Caliper Life Sciences, Alameda, CA). Using an appropriate filter setting for the fluor that is being imaged, acquire an image. For CED, a successful infusion should show most of the material in the brain near the infusion site (**Figure 2-4**).

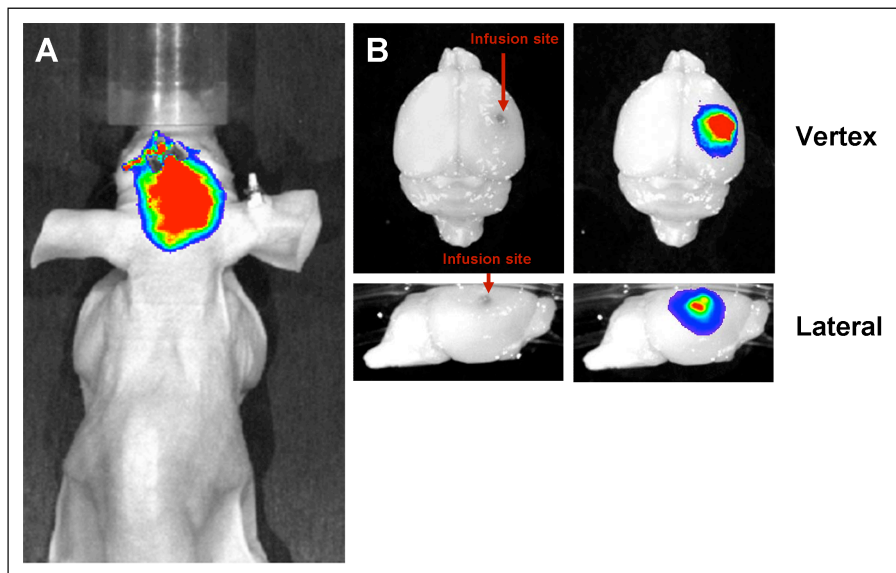


Figure 2-4 Representative results from successful CED. Liposomes labeled with a far-red fluorescent dye were infused into the mouse brain by CED and imaged both *in vivo* and *ex vivo*. A successful infusion shows a fluorescent signal localized to the site of infusion both *in vivo* (A) and *ex vivo* (B). The signal should be localized to the infused hemisphere without leakage into the contralateral hemisphere.

2.4 REPRESENTATIVE RESULTS

A lack of adverse reaction to administration of therapy is an important indicator of successful injection. For example, following tail vein injection there should be no change in appearance (e.g., size, color) of the tail. A bubble or blister following tail vein injection would indicate subcutaneous, rather than intravenous, delivery of therapy. For intraperitoneal injections, a bump on the skin or discoloration of the abdomen may indicate subcutaneous injection or damage to internal structures. In oral gavage, a mouse with labored breathing or coughing may indicate that fluid was injected into the lungs, rather than into the stomach. For CED, neurologic function is important for assessing successful administration of therapy. A mouse that is exhibiting seizures or hemiparesis may have received an improper infusion. If a fluorescent infusate is used, *in vivo* imaging can be applied for assessing successful distribution of infusate (**Figure 2-4**). If the infusate is not localized to the site of injection, the infusion was not successful.

2.5 DISCUSSION

Preclinical evaluation of the efficacy of any therapeutic agent must take into account pharmacological properties of the agent and the target tissue of interest. While systemic methods of administration are in general more facile and better tolerated by patients, the selectivity of the blood-brain barrier often necessitates local delivery of therapy for treating CNS disease. Here, we have demonstrated one method of direct delivery to the brain: CED. Other forms of local delivery to the brain include direct administration to the cerebrospinal fluid, intratumoral bolus injection, and ventricular injection. For these methods, diffusibility of therapeutic is critically important, with poor diffusion limiting the region of coverage to a

few millimeters from the injection site[78, 79]. In contrast, CED uses positive pressure to increase the area of drug distribution[79] while still enabling therapeutic targeting to specific neuroanatomical structures. In our laboratory, we have successfully performed CED into the brainstem as well as into the caudate putamen in rodents (**Figure 2-5**).

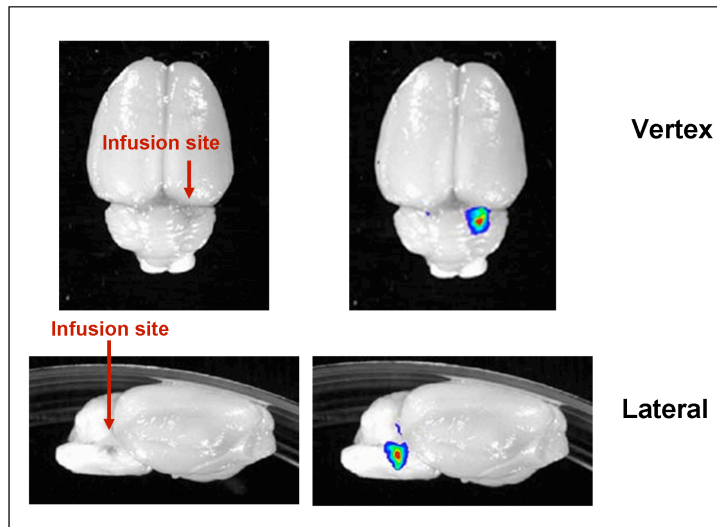


Figure 2-5 Representative image of successful CED into the rat brainstem. Fluorescently-labeled liposomes were infused into the rat brainstem. In rats, as much as 20 μ L can be infused. The increased thickness of the rat skull and depth of injection precluded *in vivo* imaging, but correct infusion location could be verified by *ex vivo* imaging of the dissected brain.

The ability to conduct CED in rodent models has become increasingly important in association with increasing interest in maximizing therapeutic efficacy when treating various types of CNS disease. CED can be used to deliver a variety of agents, including purified proteins, small molecule drugs, and viruses[80, 81]. The range of diseases that can be treated with CED includes cancers of the CNS[82] as well as neurodegenerative diseases such as Parkinson's disease[80]. As CED research continues to expand, the need for *in vivo* imaging of CED administered therapy is similarly increasing. While the fluorescent imaging

demonstrated here would likely not be visible through the human skull, other methods employing co-infusion of MRI contrast agents[24] are attracting interest for monitoring infusates in patients with CNS disease.

CHAPTER 3: CED of Yeast Cytosine Deaminase for Treatment of an Orthotopic Model of Glioblastoma

3.1 ABSTRACT

The use of 5-fluorouracil has been limited in the treatment of brain tumors due to its high systemic toxicity. In the study described below we utilized yeast cytosine deaminase (yCD) for converting nontoxic 5-fluorocytosine (5-FC) to 5-fluorouracil (5-FU) to treat an intracranial model of glioblastoma multiforme, a highly aggressive form of glioma. Luciferase-modified U87MG cells were intracranially implanted in athymic rats, allowing us to ensure successful tumor implantation by bioluminescence imaging. Tumors were infused by convection-enhanced delivery (CED) with a thermostable version of yCD (3CD). We chose a conservative dose of 4.2U, where 1U is defined as the ability to convert 1 μ mol of 5-FC to 5-FU in one minute, for subsequent preclinical testing, after determining that doses as high as 33U could be tolerated without neurological impairment. 5-FC was delivered orally at a dose of 50mg twice a day for 5 days, for a total dose of 500 mg per rat. Treating at both early and late time points in tumor progression yielded statistically significant results between control and treatment groups ($p=0.0057$, 0.05 , respectively). However, survival benefit was relatively modest. We also examined the localization and clearance of the 3CD protein from the brain using both fluorescent and radioactive tracers and from this analysis we concluded that the protein is cleared from the brain within 48 hours. This work suggests that the 3CD/5-FC prodrug enzyme system is efficacious in an aggressive model of glioma, whose efficacy may be a short clearance time from the tissue.

3.2 INTRODUCTION

CED, first described in 1994, was developed as a method to bypass the blood-brain barrier and increase drug distribution in the brain parenchyma[79]. The ability of CED to safely deliver agents to the brain has been well-documented in rodents, canines, and primates[83-85]. Anti-tumor compounds that are ineffective for glioma treatment when delivered intravenously are able to extend survival time in rodents when delivered by CED, validated examples of which include carboplatin and gemcitabine[86]. CED has also been used to deliver larger molecules to the brain including viral particles, liposomes, and purified proteins[26, 87, 88]. Yamashita and colleagues have shown that delivering a combination of liposomal topotecan and liposomal doxorubicin by CED can extend rodent survival time nearly three-fold relative to animal subjects receiving no treatment [89]. Notable protein therapeutics delivered by CED include the tumor necrosis factor-related apoptosis-inducing ligand (TRAIL) peptide and the chimeric IL13-PE protein[90, 91]. Here, we demonstrate the use of CED as an effective delivery system for yeast cytosine deaminase (yCD) for use in enzyme prodrug therapy with 5-fluorocytosine (5-FC).

The enzymatic ability of CD to convert the nontoxic 5-fluorocytosine to highly cytotoxic 5-fluorouracil (5-FU) has been well-documented[92, 93]. Several groups have attempted to deliver CD to the tumor site through transfection of tumor cells with the CD; this strategy is also known as Gene Directed Enzyme Prodrug Therapy (GDEPT)[92]. While GDEPT has shown efficacy in preclinical models, viral mediated CD expression was required to achieve sufficient protein production[92]. The safety issues associated with viral use prompted the development of an alternative CD delivery strategy[94]; Antibody Directed Enzyme Prodrug Therapy (ADEPT) which conjugates enzyme to an antibody targeted to the site of delivery. However, for CD, ADEPT results in a long circulation time of the antibody-

enzyme conjugate, resulting in production of active drug in the circulation and subsequent systemic toxicity. To overcome the obstacles encountered in GDEPT and ADEPT, we have delivered purified CD protein directly to the tumor using CED. This approach allows greater control over the timing and location of yCD treatment as well as the amount of active yCD protein administered. In association with local administration of yCD protein, the prodrug, 5-FC can be delivered orally for conversion to 5-FU at the tumor site. Alternatively, 5-FC can be administered before CED delivery of CD for immediate production of 5-FU at the tumor site.

The efficacy of this approach was assessed in an orthotopic xenograft model of human glioblastoma, in which the implanted GBM cell line, U87MG, has been modified with firefly luciferase for tumor bioluminescence imaging. We compared two different treatment dates to establish efficacy in models of both minor and substantial tumor burden. Finally, we explored the localization and clearance of the yCD protein from the brain.

3.3 METHODS

3.3.1 Cell Culture

The U-87MG human glioblastoma cell line was modified to stably express firefly luciferase and was a generous gift from Dr. Graeme Hodgson in the Department of Neurological Surgery at the University of California, San Francisco. Cells were maintained as monolayers in Eagle's minimal essential medium supplemented with 10% fetal calf serum. Cells were cultured at 37°C with 5% CO₂. For implantation, cells were harvested by trypsinization, washed with Hanks' Balanced Salt Solution and resuspended in Hanks' Balanced Salt Solution.

3.3.2 Tumor Implantation

All animal experiments were conducted using protocols approved by the University of California, San Francisco, Institutional Animal Care and Use Committee (UCSF IACUC). Six to eight-week old male congenitally athymic rats (rnu/rnu) purchased from the National Cancer Institute were anesthetized with ketamine (60 mg/kg) and xylazine (7.5 mg/kg) and placed in a stereotactic frame (Stoelting, Wood Dale, IL, USA). A 1.5cm saggital incision was made into the scalp and the skull suture lines were exposed. A small burr hole was drilled 3mm to the right of the bregma using a dental drill, and a guide screw was implanted in the burr hole. Using a sterile needle, the dura was punctured and 1.5×10^6 cells in a 10 μ l volume were injected at a depth of 4mm over 60 seconds using a 10 μ l Hamilton syringe (Stoelting). After injection, the syringe was held in place for 30 seconds and then slowly removed. The guide screw was cleaned with hydrogen peroxide and then sealed with bone wax. The scalp was closed using 9mm surgical staples (Stoelting). Rats were housed in aseptic conditions that included filtered air and sterilized water, bedding, food, and cages. Rats were monitored daily and were euthanized if they exhibited any neurological symptoms or a greater than 15% reduction in body weight.

3.3.3 Bioluminescent Tumor Imaging

Either 7 or 10 days after tumor implantation, rats were anesthetized by an intraperitoneal injection of ketamine (60 mg/kg) and xylazine (7.5 mg/kg) and then injected intraperitoneally with 33.3 mg of D-luciferin (potassium salt, Gold Biotechnology, St. Louis, MO, USA) dissolved in sterile saline. Tumor luminescence was determined 7-12 minutes

after luciferin injection. Data was gathered using the IVIS Lumina System (Caliper Life Sciences., Alameda, CA, USA) and analyzed using the LivingImage software (Caliper Life Sciences.). Images were quantified as the sum of photon counts/sec in regions of interest defined by a lower threshold value of 25% of peak pixel intensity. Rats with detectable photon counts above background were considered to have been successfully engrafted with tumor. Rats showing background level luminescence were removed from the study.

3.3.4 Protein Expression and Purification

For CD and Katushka protein expression, plasmids expressing the protein of interest along with antibiotic resistance markers were transformed into BL21-Codon Plus (DE3)-RIPL *E.coli* cells (Stratagene, La Jolla, CA), which contain tRNAs to express mammalian proteins. The *E.coli* cells containing the plasmid were grown in 1 L of luria broth containing antibiotic at 37°C until OD_{600nm} reached 0.6. Protein expression was induced by adding isopropyl β -D-1-thiogalactopyranoside (IPTG, 0.5 mM final concentration; Invitrogen). For 3CD expression, zinc acetate (0.5mM final concentration) was also added. Bacteria were then incubated at 23°C overnight with constant shaking at 200 rpm. Bacteria containing expressed protein were collected by centrifugation at 6,000 x g for 30 minutes at 4°C, and resuspended in 20-25 ml of lysis buffer containing 300 mM NaCl, 20 mM Tris-Cl, 40 mM imidazole, 0.2% Triton X-100, and 0.5 mM PMSF. After three freeze-thaw cycles, the cells were lysed by lysozyme and sonication treatments and centrifuged at 12,000g for 30 minutes at 4 °C. The supernatant containing soluble proteins was collected and filtered through a 0.45 μ m membrane (Whatman, USA). The filtered supernatant was applied to a HisTrap FF affinity column (Amersham Biosciences, Piscataway, NJ) that was pre-equilibrated with

binding buffer containing 300 mM NaCl, 20 mM Tris-Cl, and 40 mM imidazole, pH 8. After the entire soluble fraction was passed through the column, the column was washed with 20 column volumes of the binding buffer. The bound protein was eluted using a buffer containing 300 mM NaCl, 20 mM Tris-Cl, and 300 mM imidazole, pH 8. The eluates were pooled and applied to a PD-10 desalting column (Biorad) to remove imidazole and change the buffer to 1x PBS. All proteins used in animal studies were run on a DetoxiGel polymixin B column (Pierce, Rockford, IL) to remove endotoxin.

3.3.5 Protein Activity Assay

Enzymatic conversion of 5-FC to 5-FU per μg of 3CD was measured using previously described methods[95]. Briefly, 1 μg 3CD was incubated in 1 mL PBS containing 5 mM 5-FC at 37 °C. Aliquots of the reaction mixture (20 μL) were removed at 10, 20 and 30 minutes, and enzymatic conversion quenched by dilution to 1 mL in 0.1 N HCl in PBS. The amount of 5-FU formed in the reaction was determined by measuring the UV absorbance at 255 and 290 nm. Concentration (mM) of 5-FU is calculated as $0.185*(\text{Abs } 255) - 0.049*(\text{Abs } 290)$ to adjust for presence of unconverted 5-FC. Assays were performed in triplicate.

3CD (**Figure 3-1**) has three point mutations that extend the thermostability of the protein. In our hands, 3CD had a >10-fold increase in enzymatic half-life at 37°C.

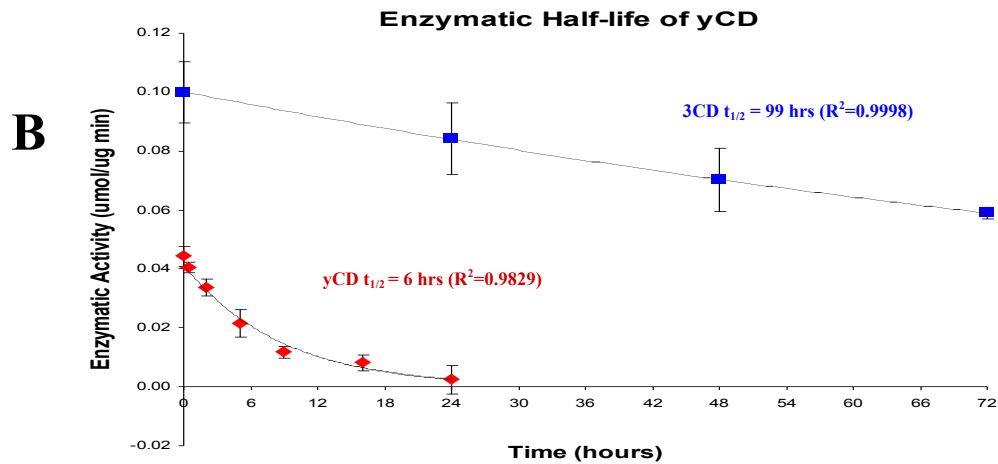
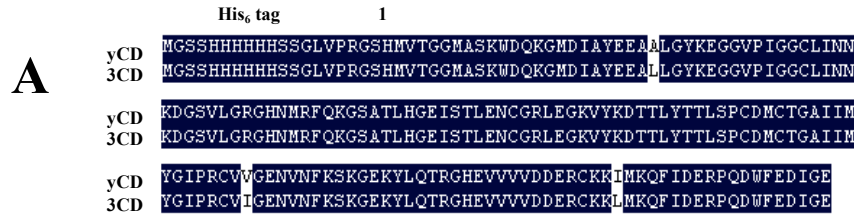


Figure 3-1 Thermostable CD (3CD) has an extended half-life at 37°C. The amino acid sequence alignment between wild-type yCD (yCD) and thermostable yCD (3CD) is shown in (A). A His₆ tag was added for facile purification. Three point mutations (shown in white) were created at the following sites, A23L, V108I and I140L, as described by Korkegian *et al*[96]. When compared to wild-type yCD, 3CD is more enzymatically active for an extended period of time (C).

3.3.6 Convection-Enhanced Delivery of Proteins

All proteins were administered intracranially by convection-enhanced delivery (CED). A step-design cannula was used to reduce reflux during the infusion and was assembled as previously described[77]. For the infusion, rats were anesthetized with ketamine (60 mg/kg) and xylazine (7.5 mg/kg) and then placed in a stereotactic frame (Stoelting, Wood Dale, IL, USA). Isoflurane was administered to the rats as needed to maintain a surgical plane of anesthesia. For animals with and without intracranial tumor, a 1.5cm saggital incision was made in the scalp and the skull suture lines were exposed. For rats with intracranial tumor, the guide screw was removed and the burr hole was used as the entry site for the cannula. For rats lacking intracranial tumor, a small burr hole was created as was done for tumor

implantation, but a guide screw was not implanted. The cannula was then positioned 5mm below the surface of the skull and a syringe pump was attached to the cannula. The infusion ran at the following speeds: 0.1µl/min for 5 minutes, 0.2µl/min for 5 minutes, 0.5µl/min for 5 minutes, and 0.8µl/min for 30 minutes. Infusion time was 45 minutes and the total volume infused was 28 µl. The infusion cannula remained in place for 1 minute after the infusion ended. After the cannula was removed, the burr hole was sealed with bone wax and the scalp was closed with 9mm surgical staples (Stoelting).

3.3.7 Delivery of 5-fluorocytosine

200 mg/kg 5-fluorocytosine was orally administered to rats twice a day beginning on the day of 3CD administration and continued for 4 consecutive days. 5-fluorocytosine (Sigma) was dissolved in sterile H₂O.

3.3.8 Confocal Microscopy

After the Katushka protein was infused by CED, rats were euthanized by trans-cardiac perfusion of 200 mL ice-cold phosphate-buffered saline followed by 200 mL of 4% paraformaldehyde. The brain was then dissected from the skull and soaked in 4% paraformaldehyde overnight at room temperature. Using a Vibratome 3000, the brain was cut as 200 µm coronal sections. Sections were stored in phosphate-buffered saline at 4°C until imaging, which was within a week of sectioning.

All confocal images were taken using LaserSharp Software on a Biorad 1024 Confocal Scanning Laser Microscope (Biorad, Hercules, CA) mounted on a Nikon Diaphot 200 microscope. The Katushka signals were acquired on photomultiplier 1 with excitation

from the 568-nm line of a krypton-argon laser. The FITC signals were acquired on photomultiplier 2 with excitation from the 488-nm line of a krypton-argon laser. The gain was set to avoid pixel overexposure in the images. Multiple regions of interest were imaged using a 4X or a 10X objective lens (Nikon) and saved as 8-bit PIC files. Images were analyzed by Image J version 10.2 (<http://rsb.info.nih.gov/ij/>).

3.3.9 Biodistribution of 3CD

Purified 3CD protein was labeled with ^{125}I and infused into the healthy brains of six to eight week-old Fisher 344 rats by CED. Rats were sacrificed at time points ranging from 0 to 48 hours post-infusion, $n \geq 3$ for each time point. After sacrifice, organs were removed and gamma radiation was determined using a Perkin Elmer Wizard Gamma Counter (Boston, MA).

3.4 RESULTS

3.4.1 Verification of brain tumors by bioluminescence imaging

In order to confirm the presence of intracranial tumor, we implanted each rat with U-87MG cells that were modified to stably express firefly luciferase. When luciferin was injected intraperitoneally, we were able to detect intracranial luminescent signal in the majority of animal subjects. **Figure 3-2** shows the same rat at 11 and 24 days post-tumor implantation. As tumor growth progresses, luminescent signal increases from 1.48×10^8 photons to 3.78×10^9 photons. Signal was always seen on the right side of the skull suggesting that the tumor cells remained at the site of injection and did not migrate to other areas of the brain. Previous work using luciferase-modified glioma cells in mice has shown that the

photon count increases proportionally with tumor volume[97]. Luminescent signal was most often assayed 11 days post-implantation, but positive signal could be observed as early as 7 days post-implantation. Only rats with a luminescent signal above background were used in treatment experiments. The luminescent signal was also used for distributing rats into treatment groups to ensure that each group had the same average tumor size at the start of treatment.

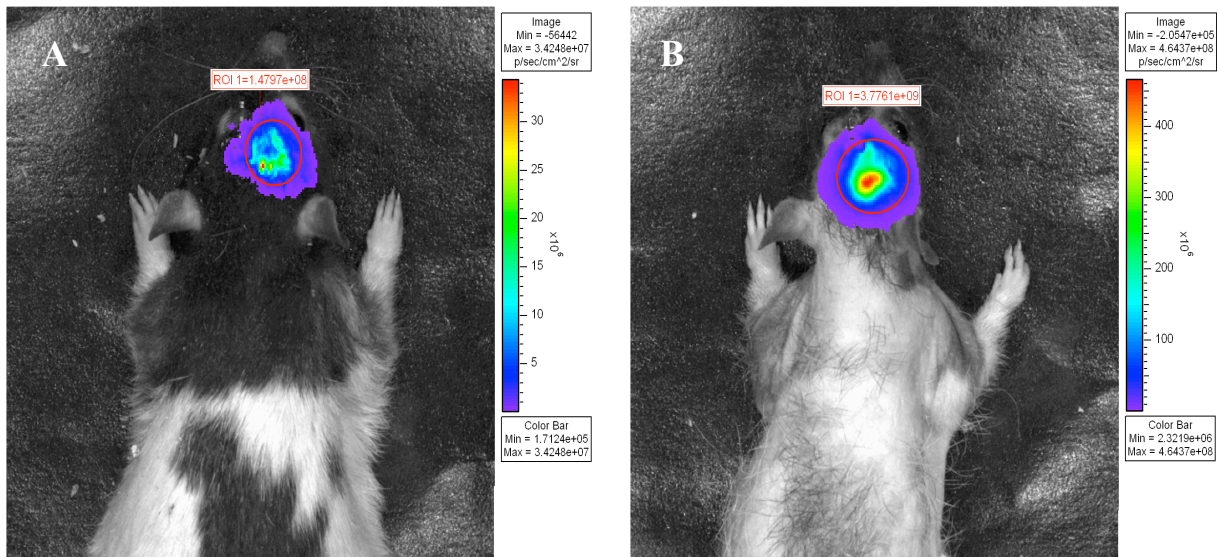


Figure 3-2 Verification of brain tumors by bioluminescent imaging.

Tumor implantation was evaluated by injecting animals with 33.3mg of luciferin and monitoring luminescence emitted from the luciferase-expressing tumor cells. Representative images taken from an animal subject at 11 days post-implantation (A) and 24 days post-implantation (B). The image was quantified by counting the total number of photons emitted in an automatically defined region of interest (ROI), shown by the red circles. The ROI at day 11 is 1.48×10^8 photons and by day 24 has increased to 3.78×10^9 photons.

3.4.2 Survival advantage of 3CD/5-FC treatment in early and late stages of tumor growth

Previous reports have shown efficacy using a virally delivered construct expressing yCD along with co-administration of 5-FC in the U-87MG xenograft model[92]. We hypothesized that delivering purified 3CD protein directly into the tumor would result in

greater protein concentration in the tumor, along with enhanced protein activity, due to the increased stability of 3CD compared to wild-type γ CD, and thus provide enhanced therapeutic effect. We infused either active 3CD protein or phosphate-buffer saline (PBS) intratumorally using convection-enhanced delivery (CED). The amount of 3CD infused was based on enzyme activity, rather than the protein mass since enzyme activity varied, according to the protein preparation and storage time before infusion. Starting the day of protein injection, 50 mg of 5-FC was delivered twice a day by oral gavage. The first dose of 5-FC was given before CED allowing for 5-FC to be present in the brain at the time of protein infusion. 5-FC administration continued twice a day for 4 days after protein administration. Only a single infusion of 3CD was studied.

As shown in **Figure 3-3**, treatment with 3CD and 5-FC provided a significant survival advantage compared to 5-FC alone, in both early and late stage tumor models. We found that the timing of treatment initiation impacted the extent of therapeutic benefit. When we delivered the protein 7 days after tumor cell implantation, we saw a larger statistical difference ($p = 0.0057$) between rats receiving 3CD/5-FC and those receiving 5-FC alone. While all the control rats had died by day 29, one long term survivor (60 days) resulted from early treatment. Upon dissection of the brain from the long-term survivor, no tumor could be found. When the protein was delivered 12 days after tumor implantation, the effect was more modest and no long-term survivors were observed so the more substantial tumor burden at day 12 reduced the efficacy of treatment. Efficacy at a later stage in glioma progression, when there is more substantial tumor burden, is critical, as many human gliomas are diagnosed only in an advanced state.

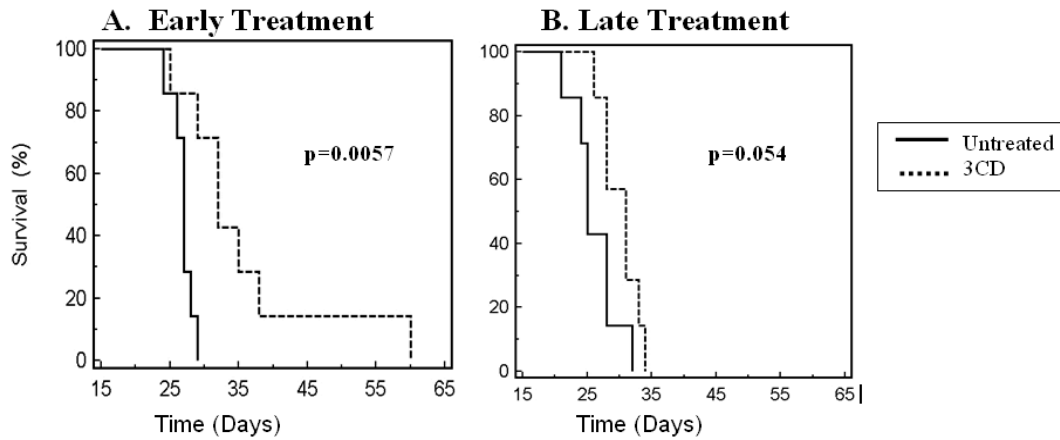


Figure 3-3 Survival advantage for rats treated with 3CD at an early or late stage of tumor growth. All rats were implanted with U87MG and were treated with either 3CD protein or PBS (untreated) by convection-enhanced delivery. 5-FC was administered to all rats starting on the day of CED and continued for 4 consecutive days. In figure **A**, protein delivery occurred 7 days after tumor implantation and resulted in a highly significant survival advantage, $p = 0.0057$. In figure **B**, protein delivery occurred 12 days after tumor implantation resulting in a smaller, but still significant benefit, $p = 0.054$. $N=7$, all groups.

3.4.3 Effect of 3CD treatment on tumor volume

When rats in all tumor studies reached a moribund condition, the tumors were resected from the brain and the mass of the tumor was determined. We hypothesized that animal death would occur when the tumor reached a certain size threshold, therefore, if tumor mass is recorded at the time of death of all animals, there should not be a difference in the average tumor mass between treated and control animals. Indeed, when treatment is delivered 12 days post-tumor implantation (late treatment), this is the case. As shown in **Figure 3-4**, the average tumor mass in the untreated (PBS) group (166.3 mg) is not statistically different from the average tumor mass in the 3CD group (199.1 mg).

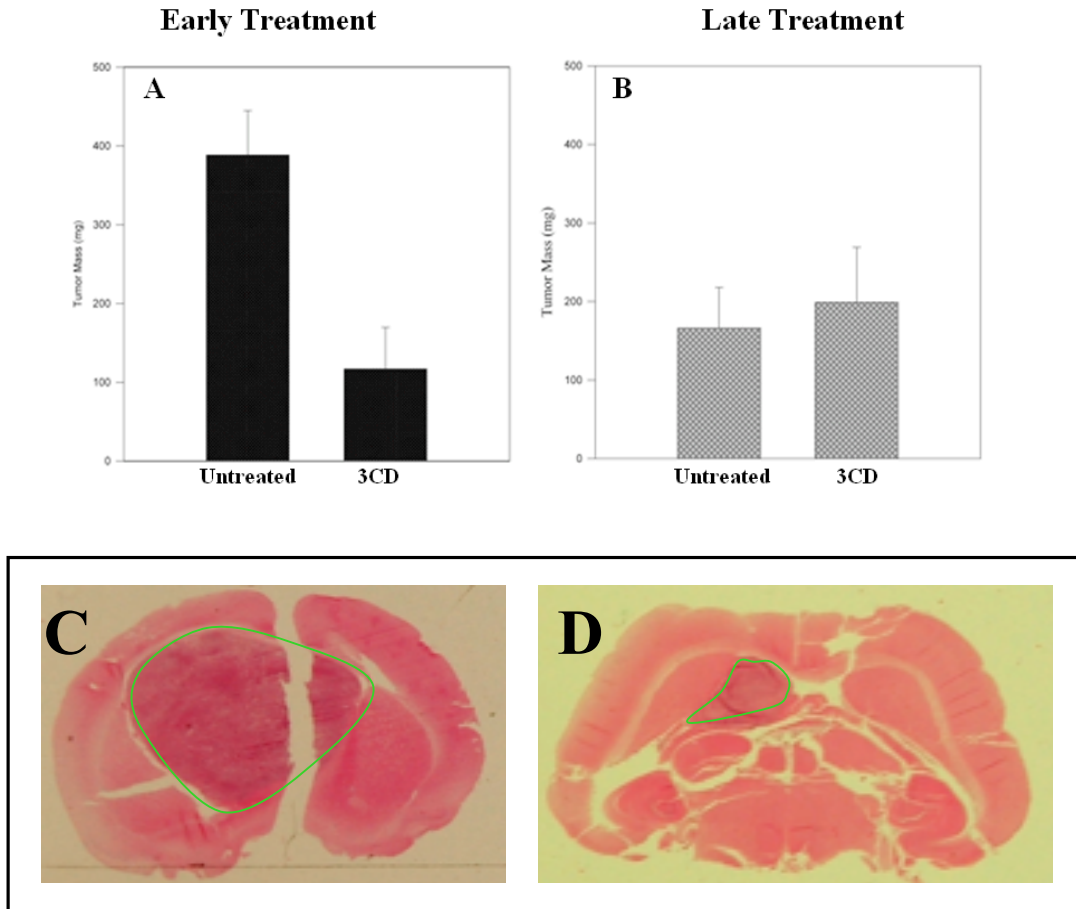


Figure 3-4 Treatment with 3CD reduces tumor volume when administered early in tumor growth. Tumors were removed from rats during autopsy and massed. When 3CD/5-FC treatment is begun 7 days after tumor implantation (**A**), a significant reduction in tumor mass is seen, $p = 0.006$. However, when the beginning of treatment is delayed until 12 days post-implantation (**B**), no difference in tumor mass is seen, $p = 0.713$. Bars represent group means; standard error of the mean is indicated, $n \geq 6$. Representative H&E sections were taken from untreated rats (**C**) or 3CD treated rats (**D**) at time of reaching a moribund condition, for the day 7 treatment experiment. The section with the largest tumor diameter is shown for each rat. Tumor mass is outlined in green.

However, this was not the case when treatment began 7 days post-tumor implantation. In these rats, there was a significant difference in tumor mass at the time of death between the treated and control animals ($p = 0.006$). As shown in **Figure 3-4**, the average tumor mass in the untreated (PBS) group (395.17 mg) was much larger than the average tumor mass in the 3CD group (116.83 mg). This difference suggests that rats in the treatment group were dying from causes in addition to tumor burden. We noted that three of the rats receiving

3CD treatment at day 7 were euthanized due to the development of torticollis. As torticollis can be indicative of a tumor in the pituitary fossa, we performed hematoxylin and eosin (H&E) staining on the brains to identify tumors outside the implantation site but did not find any infratentorial tumor masses. A potential explanation for this involves leakage of 3CD protein from the tumor into healthy brain, resulting in 5-FU neurotoxicity.

3.4.4 Localization of Katushka, a 26 kDa fluorescent protein

To determine how long 3CD remains at the site of infusion, we performed a series of imaging studies using the far-red fluorescent protein Katushka. We chose Katushka as a surrogate for 3CD distribution based on their shared dimeric structures and similar molecular weights (26.3 kDa for Katushka and 36 kDa for 3CD). As an internal control, we co-infused FITC labeled dextran that has a molecular weight of 10kDa. The infusions were performed by CED into the brains of healthy rats. As shown by confocal microscopy in **Figure 3-5**, 24 hours after administration detectable levels of both Katushka and FITC-dextran remained at the site of infusion. The compounds both localize in perivascular areas in the brain. Perivascular localization of FITC-dextran as well as liposomes has been previously reported following CED infusion[83, 98]. By 48 hours post-infusion, as shown in **Figure 3-5**, both FITC-dextran and Katushka are detectable. Both fluorophores display a weak punctate signal, suggesting that the remaining FITC-dextran and Katushka is localized to a subpopulation of perivascular cells. By 7 days after infusion both Katushka and FITC-dextran are almost entirely absent from the infusion site. A few areas of signal could be detected at day 7 and are shown in **Figure 3-5**. At day 7, FITC-dextran and Katushka are still colocalized to areas surrounding intracranial vasculature.

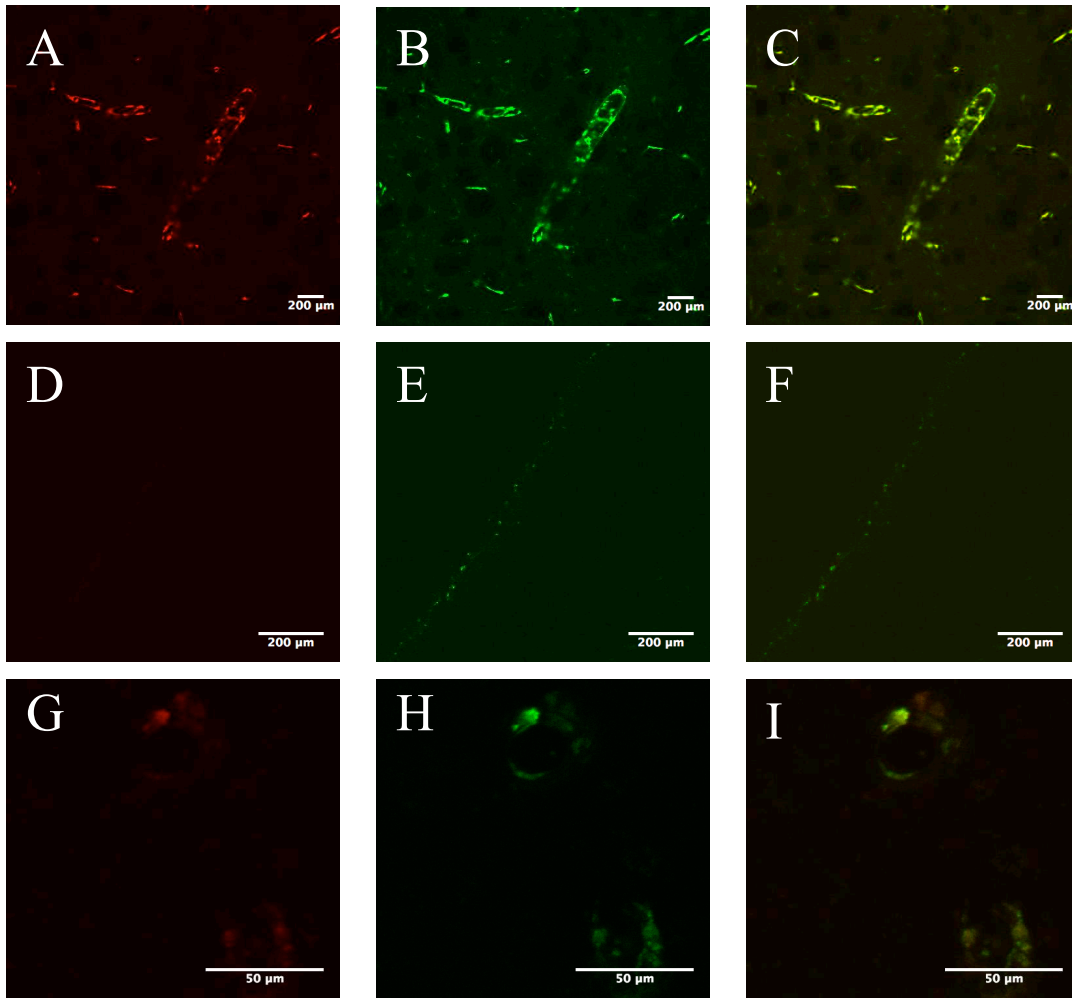


Figure 3-5 Localization of a fluorescent surrogate protein. Katushka, a far-red fluorescent protein of comparable size to 3CD was infused into a rat brain by CED along with FITC-dextran (10 kDa). Images were taken 24 hours (A-C), 48 hours (D-F) and 7 days post-infusion (G-I). At 24 hours post-infusion, detectable signals of both Katushka and FITC-dextran are seen colocalizing to the perivascular cells. By 48 hours the signal is dramatically reduced, but colocalization of Katushka and FITC-dextran is still seen near the vasculature. By 7 days, the signal is almost entirely absent, but a few areas of perivascular colocalization can still be seen at higher magnification.

3.4.5 Elimination rate of radiolabeled 3CD from the brain

We next looked directly at the clearance of the 3CD protein by infusing purified 3CD labeled with radioactive iodine (^{125}I). Rats were sacrificed ($n \geq 3$) at time points ranging from immediately after infusion to 48 hours post-infusion. The fraction of the initial dose per gram of tissue was determined and is shown in **Figure 3-6**. Radiolabeled 3CD appears to be

cleared faster than Katushka, with near complete clearance seen by 24 hours post-infusion. This observation reinforces our hypothesis that treatment efficacy of 3CD is limited by its clearance time from the site of action.

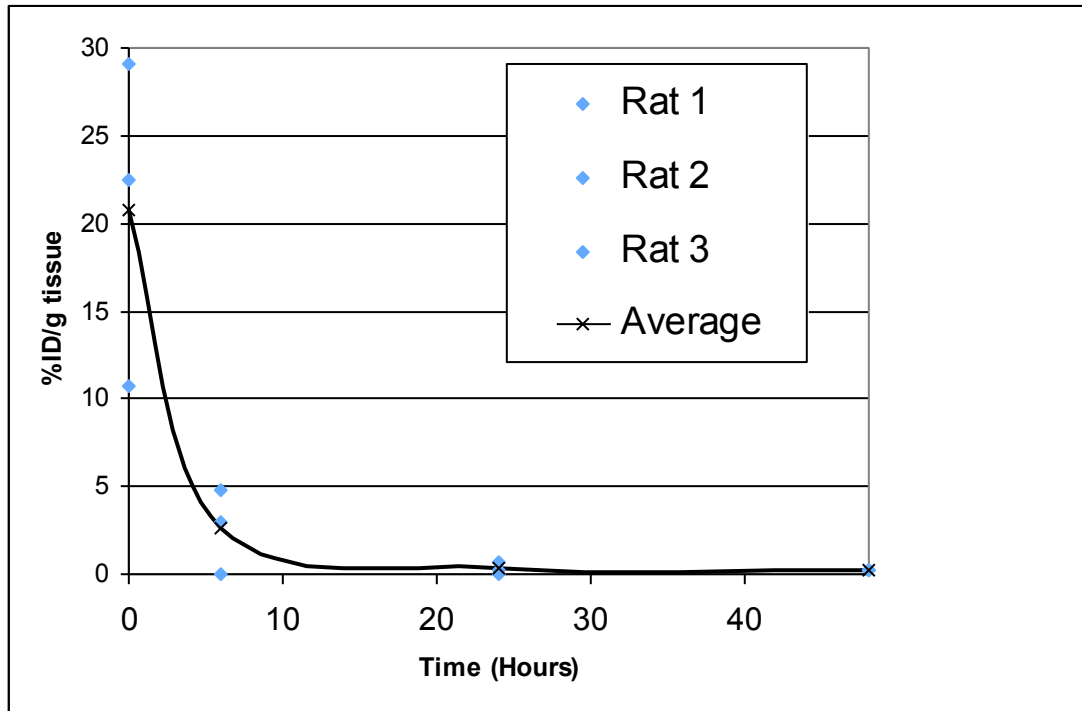


Figure 3-6 Clearance of radiolabeled 3CD. Purified 3CD protein was labeled with ^{125}I and delivered to the rat brain by CED. Blue diamonds indicate the individual rats with the black line representing the group average.

3.5 DISCUSSION

CED is a safe and effective method to deliver 3CD to intracranial tumor for enzyme prodrug therapy. While viral delivery systems have shown varying degrees of efficacy, the safety issues involved with viral delivery systems have not been adequately addressed. Direct administration of therapeutic proteins is an increasingly feasible option for the treatment of glioma, due to the advancement of both biologic drugs and CED technology. Our data show a statistically significant effect on overall rodent survival. Survival benefit is most likely limited by the short clearance time of 3CD from the brain, as shown in Figures 5 and 6.

Additionally, the U87MG cell line used is relatively resistant to 5-FU. Miller and colleagues determined the IC₅₀ of 5-FU in cultures of four glioma cell lines and found a wide range of sensitivity, with U87MG representing the least sensitive cell line with a 3-4 times greater IC₅₀ than the most sensitive glioma line[92]. Future efforts to increase efficacy should address 3CD residence time and potential biomarkers that would indicate individual tumor 5-FU resistance or sensitivity.

One of the advantages in delivering CD protein directly by CED, rather than through gene therapy, is the ability to accurately titrate the amount of protein delivered to the tumor site. The dose administered here represented a conservative dosing schedule and total amount 3CD per animal. Results of a maximum tolerated dose study showed that athymic rats are able to tolerate intracranial doses of up to 33U of 3CD, which is nearly 8 times higher than the therapeutic dose administered here. Rats receiving 33U of protein showed a slight weight loss which was resolved within a week of ending treatment and did not show any neurological symptoms (data not shown). These results suggest that a more aggressive 3CD regimen could be tolerated, particularly in larger tumors, and may increase the therapeutic benefit. Future studies should also explore any mutations to the CD protein that would increase its rate of 5-FC to 5-FU conversion, as well as address the immunogenicity of this yeast-derived protein in mammals[99].

Here, we have shown that delivery of a therapeutic protein by CED is a feasible and effective strategy for the treatment of a preclinical model of glioma. We have also shown that the treatment is effective in both early and more advanced stage of tumor burden. Distribution studies showed a perivascular localization of infused proteins and a rapid clearance from the infusion site. Future improvements to this treatment may include

increasing the dose of 3CD and using 3CD formulations that increase its residence time at the tumor site.

3.6 ACKNOWLEDGEMENTS

Dr. Marieke van der Aa provided invaluable assistance with both tumor implantation as well as with CED. Dr. Richard Cohen provided expert instruction on the confocal microscope.

CHAPTER 4: Intravenous Delivery of Topotecan

Liposomes

This chapter contains material from the article “Investigation of Intravenous Delivery of Nanoliposomal Topotecan for Activity Against Orthotopic Glioblastoma Xenografts” by Laura P. Serwer, Charles O. Noble, and Karine Michaud, et al. in press, Neuro-Oncology.

4.1 ABSTRACT

Achieving effective treatment outcomes for glioblastoma (GBM) patients has been impeded by many obstacles, including the pharmacokinetic limitations of anti-tumor agents, such as topotecan (TPT). Here, we demonstrate that intravenous administration of a novel nanoliposomal formulation of TPT (nLS-TPT) extends the survival of mice with intracranial GBM xenografts, relative to administration of free TPT, due to improved biodistribution and pharmacokinetics of the liposome formulated drug. In three distinct orthotopic GBM models, three weeks of biweekly intravenous dosing with nLS-TPT was sufficient to delay tumor growth and significantly extend animal survival compared to treatment with free TPT ($p \leq 0.03$ for each tumor tested). Analysis of intracranial tumors showed increased activation of cleaved caspase-3, as well as increased DNA fragmentation, both indicators of apoptotic response to treatment with nLS-TPT. These results demonstrate that intravenous delivery of nLS-TPT is a promising strategy in the treatment of GBM, and support clinical investigation of this therapeutic approach.

4.2 INTRODUCTION

Topotecan (TPT), an analogue of the chemotherapeutic camptothecin, is an approved treatment for many types of cancer, including recurrent small cell lung and ovarian tumors[100-103]. With respect to brain tumors, TPT has shown significant activity against the most common and malignant type of primary brain tumor, glioblastoma (GBM), both *in vitro* as well as in subcutaneous xenograft models of GBM[104, 105]. Results from preclinical studies, in combination with encouraging results regarding the distribution of TPT into cerebrospinal fluid (CSF) following systemic TPT administration, prompted clinical investigations of TPT monotherapy efficacy in treating GBM patients[104-106]. Unfortunately, results from phase II clinical trials involving TPT treatment of both newly diagnosed and recurrent GBM revealed only modest patient responses[107-109]. Though no longer being investigated as a monotherapy for treating GBM, TPT continues to see use in GBM clinical trials as a part of combination therapy approaches.

The minor efficacy of TPT as a monotherapy for GBM has been attributed to a rapid rate of TPT clearance from the CSF ($t_{1/2\text{CSF}} = 4.8$ hours), as well as to rapid TPT inactivation in plasma (active form $t_{1/2} = 23$ minutes)[110]. Liposomal encapsulation is a strategy being explored for improving the anti-tumor efficacy of camptothecin derivatives[111, 112], including TPT[26], and has been shown to increase drug circulatory half-life while helping maintain drug activity by providing an appropriate pH[111, 113].

In fact, systemic injection of nanoliposomal TPT has shown enhanced activity, relative to free TPT, against subcutaneous xenografts for several types of human cancer[112, 114]. Moreover, nanoliposomal TPT has demonstrated superior efficacy in treating orthotopic (intracranial) xenograft models of GBM when administered directly into the tumor by convection-enhanced delivery (CED)[26, 111]. Specifically, in a rat orthotopic GBM

xenograft model, CED administration of nanoliposomal TPT increased TPT half-life in the brain, relative to free TPT, and conferred a highly significant survival advantage to rodent subjects. In spite of such demonstrations, the invasive nature of CED, combined with the limited success of CED-associated clinical trials to date, has restrained enthusiasm for more widespread use of this route of therapeutic administration in treating brain tumor patients.

Here, we show for the first time the enhanced efficacy of systemically administered nanoliposomal TPT using three orthotopic xenograft models of GBM. The interpretation of enhanced efficacy is based on bioluminescence monitoring of tumor growth and therapeutic response, survival benefit to animal subjects, and immunohistochemical analysis of tumor apoptotic response to therapy, with the results from each consistent in their support for clinical investigation of this approach for treating glioblastoma.

4.3 METHODS

4.3.1 Cell cultures

U-87MG cells were maintained as monolayers in high glucose Dulbecco's minimal essential medium (DMEM) supplemented with 10% fetal calf serum, 1% non-essential amino acids, penicillin, and streptomycin. Cells were cultured at 37°C with 5% CO₂. GBM43 and GBM6 cells were maintained as serially-passaged subcutaneous xenografts in athymic mice. U-87MG, GBM43, and GBM6 were each modified by lentiviral infection for stable expression of firefly luciferase[97]. For intracranial injection of GBM43 and GBM6, subcutaneous tumor was removed, minced with a scalpel, and subjected to three rounds of passage through a 40µm pore filter, with centrifugation after each round of filtering (increasing speed: 158g, 355g, 631g, 10 minutes each). After the final round of

centrifugation, the cells were resuspended in 1mL of sterile DMEM media (without antibiotics), counted and diluted to 1×10^8 cells/mL for intracranial injection. U-87MG cells were harvested for intracranial injection by monolayer trypsinization and resuspended in DMEM at 1×10^8 cells/mL.

4.3.2 Tumor implantation

All animal experiments were conducted using protocols approved by the University of California, San Francisco, Institutional Animal Care and Use Committee. Four to six-week old female athymic nu/nu mice (Simonsen Labs: Gilroy, CA) were anesthetized by intraperitoneal injection of ketamine (100 mg/kg) and xylazine (10 mg/kg). A 1 cm sagittal incision was made along the scalp, and the skull suture lines exposed. A small hole was created by puncture with a 25g needle, at 2 mm to the right of the bregma and 0.5 mm anterior of the coronal suture. Using a sterile Hamilton syringe (Stoelting), 3×10^5 cells in 3 μ l were injected at a depth of 3 mm over a 60 second period. After injection, the syringe was held in place for 1 minute and then slowly removed. The skull was cleaned with 3% hydrogen peroxide and then sealed with bone wax. The scalp was closed using 7 mm surgical staples (Stoelting). Mice were monitored daily and euthanized when exhibiting significant neurological deficit or greater than 15% reduction from their initial body weight.

4.3.3 Preparation of nanoliposomal topotecan

A detailed description of nanoliposomal TPT preparation is given in previous work[112]. Briefly, liposomes for packaging topotecan consisted of hydrogenated soy phosphocholine and 1,2-distearoyl-*sn*-glycero-3-phosphoethanolamine-N-

[methoxy(polyethylene glycol)-2000] at a molar ratio of 3:2:0.015. A sucrose octasulfate gradient was used for loading TPT into the liposomes. Unencapsulated TPT was removed by Sephadex G-25 gel filtration chromatography, eluting with pH 6.5 HEPES buffered saline. The phospholipid concentration of the purified solution was measured spectrophotometrically using a standard phosphate assay[115]. Prior to HPLC column injection for TPT quantitation, liposome samples were solubilized in a solution containing 1% trifluoroacetic acid in methanol. TPT was detected by fluorescence (excitation 370 nm, emission 535 nm) with a retention time of 11.5 min. The nanoliposomal TPT (nLS-TPT) had a final drug to phospholipid ratio of 327.7 ± 5.31 g TPT·HCl/mol phospholipid. Liposome size was determined by photon correlation spectroscopy using a Coulter N4 Plus particle size analyzer (Beckman Coulter: Fullerton, CA), and reported as the volume-weighted average diameter \pm standard deviation of the liposome size distribution (100.1 ± 8.4 nm).

4.3.4 Biodistribution studies

Mice with intracranial U-87MG tumors were injected with 5 mg/kg of either free TPT or nLS-TPT via tail vein, then sacrificed at 1, 8, 24, or 48 hours post-injection by trans-cardiac perfusion with phosphate-buffered saline (PBS). Blood samples were obtained immediately before perfusion via cardiac puncture and centrifuged for 10 min at 8,154g. The plasma was then removed and frozen at -80°C. After perfusion with PBS, the tumor-bearing brain hemispheres were resected and frozen at -80°C. TPT was extracted from 10-20 μ l of plasma with 980-990 μ l of 1% trifluoroacetic acid in methanol. The mixture was vortexed for 5 seconds and stored at -80°C for 2 h followed by centrifugation at 13,400g for 10 min. The supernatant was transferred to an HPLC autosampler vial and stored at 4°C until analyzed for

TPT content. HPLC analysis was performed as described in *Preparation of Nanoliposomal Topotecan*. Brain tissues were processed with a mechanical homogenizer in water at 20% wt/wt ratio. 100 µl of the tissue homogenate was added to 400 µl of 1% trifluoroacetic acid in methanol and subjected to the same extraction and analysis procedure that was used for plasma. The spiked extraction recovery from tumor-containing brain tissue was 97.8%. The standard curve linearity averaged >0.998 with a detection limit of 0.1 ng/ml. Topotecan concentrations shown include both free, as well as encapsulated, topotecan. Area under curve (AUC) calculations used the trapezoidal rule[116].

4.3.5 Blood cell analysis

Athymic mice were treated with 1 mg/kg doses of either free TPT or nLS-TPT as described in *Topotecan Treatment*. Blood was collected weekly from the submandibular vein, into EDTA-coated tubes, according to the UCSF IACUC/LARC standard procedure[117], and analyzed using a Hemavet 850 (Drew Scientific: Oxford, CT) within two hours of collection.

4.3.6 In vitro luciferase assay

Luciferase-modified U-87MG cells were plated in a 96-well plate at a concentration of 5,000 cells per well. 24 hours later cells were treated for either 24 or 48 hours with 2.67×10^{-3} mg/mL free TPT or nLS-TPT. After incubation, the cells were washed in pre-warmed PBS, and fresh media, without phenol red, was added to the cells. D-luciferin was added to each well at a final concentration of 0.6 mg/mL. After a 10 minute incubation cells were

examined for luminescence using the IVIS Lumina System (Caliper Life Sciences, Alameda, CA, USA), as described below in *Bioluminescence Imaging*.

4.3.7 Bioluminescence imaging

Mice were anesthetized by intraperitoneal injection of ketamine (100 mg/kg) and xylazine (10 mg/kg), and then injected intraperitoneally with 33.3 mg of D-luciferin (potassium salt, Gold Biotechnology, St. Louis, MO, USA) dissolved in sterile saline. Tumor bioluminescence was determined 10 minutes after luciferin injection, using the IVIS Lumina System (Caliper Life Sciences, Alameda, CA, USA) and LivingImage software, as the sum of photon counts/sec in regions of interest defined by a lower threshold value of 25% of peak pixel intensity. Imaging was performed biweekly beginning three days after tumor implantation until completion of study.

4.3.8 Topotecan treatment

TPT (Fisher) was dissolved in pyrogen-free sterile water and stored at -20°C. Prior to treatment mice were randomized according to BLI score at most recent imaging. Both nLS-TPT and free TPT were administered to mice via tail vein injection[118]. Immediately prior to injection, nLS-TPT and free TPT were diluted to a concentration of 0.2 mg/mL in either 5mM HEPES (nLS-TPT) or sterile water (free TPT). Mice received TPT administrations twice weekly (T, F), for a maximum of 6 administrations.

4.3.9 Immunohistochemistry

After resection, mouse brains were fixed for 48 hours in 10% buffered formalin. Brains were then paraffin-embedded and sectioned (10 μ m) for hematoxylin and eosin (H&E) staining and immunohistochemical analysis. To assay DNA fragmentation, TUNEL staining was performed using the DeadEnd Colorimetric TUNEL system (Promega), according to the manufacturer's protocol for paraffin-embedded tissues. For the determination of cleaved caspase-3 reactivity, unstained sections were processed using a Ventana BenchMark XT automated system and a protocol consisting of pre-treatment with 3% ethanolic hydrogen peroxide for 16 min at room temperature, epitope retrieval in Tris buffer, pH 8, for 8 min at 90°C, and incubation with primary antibody to cleaved caspase-3 (Cell Signaling Tech) at 0.2 μ g/ml for 32 min at 37°C.

4.3.10 Statistical analysis

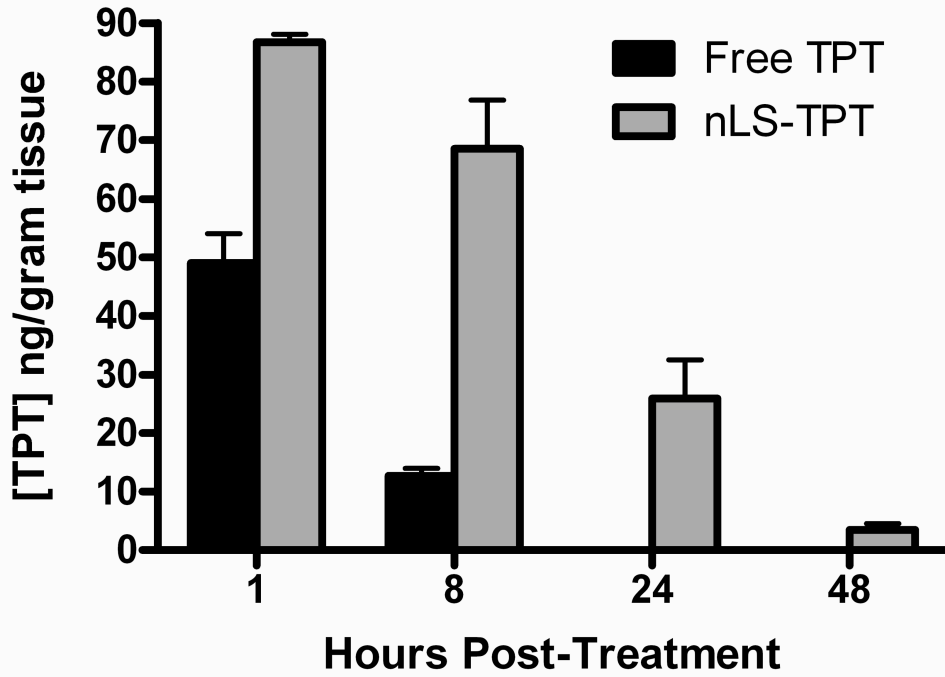
PRISM 5, Version 5.03 (GraphPad Software, Inc: La Jolla, CA) was used to conduct all statistical analysis. For survival analysis, significance was determined by the Log-rank (Mantel-Cox) test. For all other analyses, a two-tailed unpaired t-test was applied.

4.4 RESULTS

4.4.1 Biodistribution of nLS-TPT and free TPT

Athymic mice with intracranial U-87MG tumors were injected with a single dose of nLS-TPT or free TPT, and sacrificed at 1, 8, 24, and 48 hours post-injection with tissues removed for HPLC analysis of TPT content. At all time points following injection, there was significantly more TPT in tumor-bearing brain in mice treated with nLS-TPT than in mice treated with free TPT ($p < 0.005$, all time points: **Figure 4-1**). In fact, after 24 hours, mice treated with free TPT had no detectable TPT in tumor-bearing brain (limit of detection = 1.67 ng TPT/g tissue), whereas mice treated with nLS-TPT continued to show detectable TPT in brain at 48 hours post-administration of nLS-TPT, the last time point assayed. Furthermore, area under curve (AUC) calculations, indicating total drug exposure, revealed that brain tissue from mice receiving nLS-TPT was 5-fold greater than for mice receiving free TPT (**Figure 4-2**).

A



B

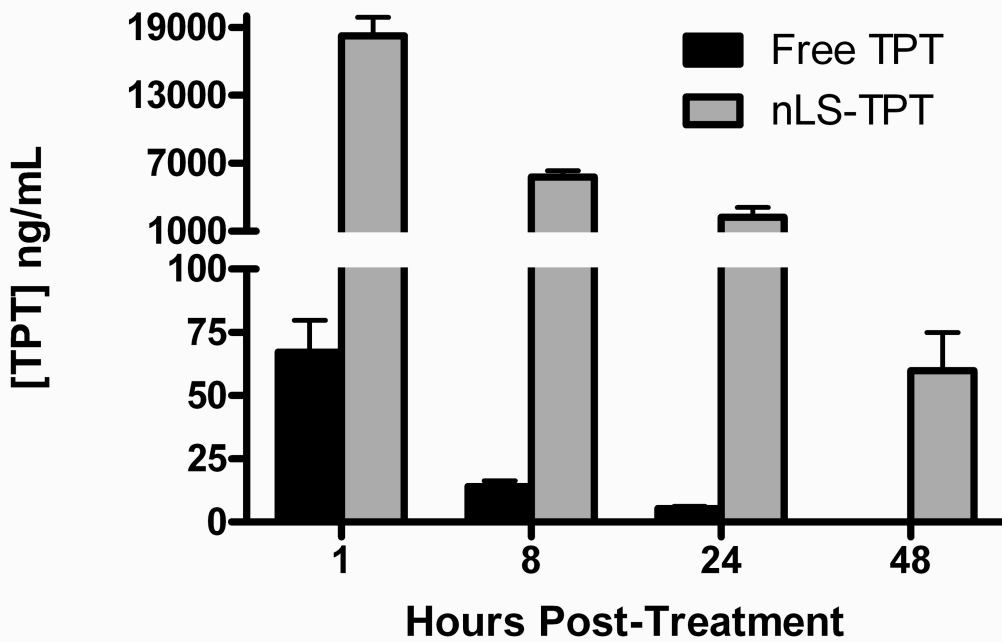


Figure 4-1 Pharmacokinetic analysis of nLS-TPT retention in tumor-bearing brain and plasma. A single dose of 5 mg/kg of free TPT or nLS-TPT was administered intravenously, with mice

sacrificed at the indicated time points subsequent to TPT administration. **A.** Brains were resected, and hemisphere containing tumor was dissected for isolation of TPT. **B.** Blood was drawn from mice immediately before sacrifice, with plasma separated and analyzed for TPT content as described in section 3.3.4. Group means with standard error of the mean (SEM) are indicated. Free TPT versus nanoliposomal TPT concentration comparisons are significantly different for each timepoint and for each type of tissue ($p < 0.05$ for all comparisons).

Figure 4-2 AUC_∞ of topotecan in tumor-bearing mice		
	Brain w/ Tumor (ng*hr/g)	Plasma (ug*hr/mL)
Free TPT	342	0.655
nLS-TPT	1745.7	197

Corresponding results for the analysis of plasma TPT showed that nLS-TPT treatment significantly increases the duration of and total exposure to TPT in circulation (**Figures 4-1, 4-2**). The plasma AUC_∞ for mice treated with nLS-TPT was 197 ug*hr/mL, over 200-fold higher than the AUC_∞ in mice treated with free TPT (0.655 ug*hr/mL). With respect to duration, TPT was not detectable in the plasma of mice 48 hours after administration of free TPT, whereas the 48 hour concentration of TPT in mice receiving nLS-TPT was readily detectable, and significantly greater than the 8 and 24 hour plasma concentrations for mice receiving free TPT.

4.4.2 Effect of nLS-TPT on tumor growth

Mice receiving treatment with free TPT or nLS-TPT, and bearing intracranial U87-MG xenografts, experienced a reduced tumor growth rate relative to untreated controls (**Figure 4-3**), with nLS-TPT significantly outperforming free TPT. To address the consistency of nLS-TPT efficacy *in vivo*, we applied the same experimental design, as used with the U-87MG experiment, to orthotopic GBM models in which the tumor cell sources were obtained from serially-propagated subcutaneous xenografts (**Figures 4-3b and 4-3c**). This approach for tumor maintenance has been previously shown to promote retention of

patient GBM molecular and biologic characteristics[119, 120]. Bioluminescence monitoring of response to treatment for xenografts GBM43 (proneural subtype) and GBM6 (classical subtype)[121] (**Figure 4-3**), revealed anti-tumor activity of nLS-TPT consistent with those indicated for the U-87MG model, supporting the finding that nLS-TPT is more effective in suppressing tumor growth.

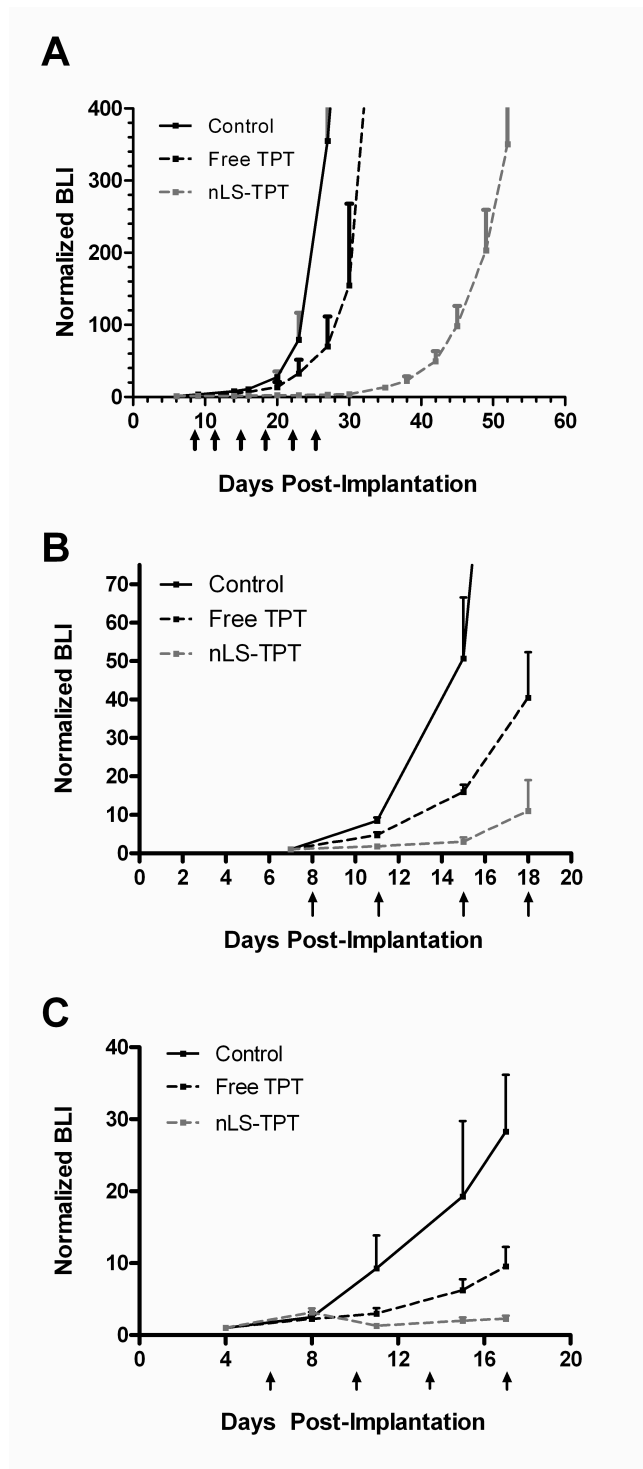


Figure 4-3 Effects of nLS-TPT treatment on tumor growth in vivo. Results from bioluminescence monitoring of intracranial tumor growth and response to intravenous TPT, either free or nanoliposomal. 1 mg/kg administrations are indicated by arrows (maximum of 6 administrations). Group means are plotted, with SEM indicated for each. **A.** U-87MG xenograft model of GBM. **B and C.** Subcutaneously-propagated GBM43 and GBM6, classified as proneural and classical subtypes of GBM, respectively[121].

4.4.3 Effect of nLS-TPT on animal survival

Consistent with our prior experience in using bioluminescence imaging for monitoring intracranial tumor response to therapy[97, 122], corresponding survival analysis for all three GBM models tested (U-87MG, GBM43, GBM6) showed that suppression of tumor growth is predictive of survival benefit. Mice treated with free TPT experienced increased median and mean survival relative to control group mice, but of lesser extent than mice treated with nLS-TPT (**Figure 4-4**). Importantly, in all three xenograft models, there was a statistically significant survival benefit from nLS-TPT treatment compared to free TPT treatment ($p \leq 0.03$ for all models).

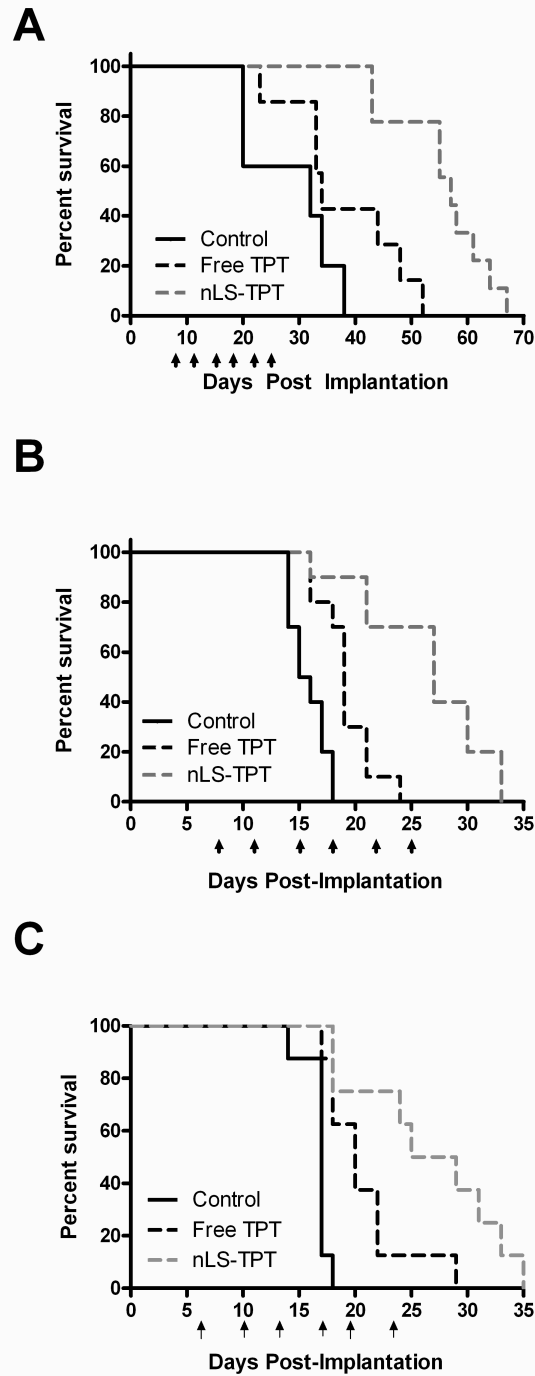


Figure 4-4 Effect of nLS-TPT treatment on survival in mice bearing intracranial tumors. Kaplan-Meier survival curves for mice bearing tumors described in **Figure 4-3**. 1 mg/kg doses are indicated by arrows (maximum of 6 administrations). **A.** U-87MG model. $N_{\text{control}} = 5$, $N_{\text{freeTPT}} = 7$, $N_{\text{nLS-TPT}} = 9$. **B.** GBM43 model. $N = 10$, all groups. **C.** GBM6 model. $N = 8$, all groups. In each experiment, survival comparisons for free TPT versus nLS-TPT treated mice indicated a statistically significant difference: $p = 0.001$ for **A** (U-87MG) and **B** (GBM43), $p = 0.03$ for **C** (GBM6).

4.4.4 Effect of liposomal packaging on drug efficacy *in vitro*

To rule out any intrinsic differences in TPT efficacy related to liposomal packaging, we compared free TPT and nLS-TPT anti-tumor effects *in vitro*, using the same luciferase-modified U-87MG cells as used *in vivo* (Figures 4-3, 4-4). Results for 24 and 48 hour incubations indicated similar activities for free TPT and nLS-TPT (Figure 4-5), supporting the differential efficacy observed *in vivo* as being attributable to improved drug distribution and stability from nanoliposomal formulation.

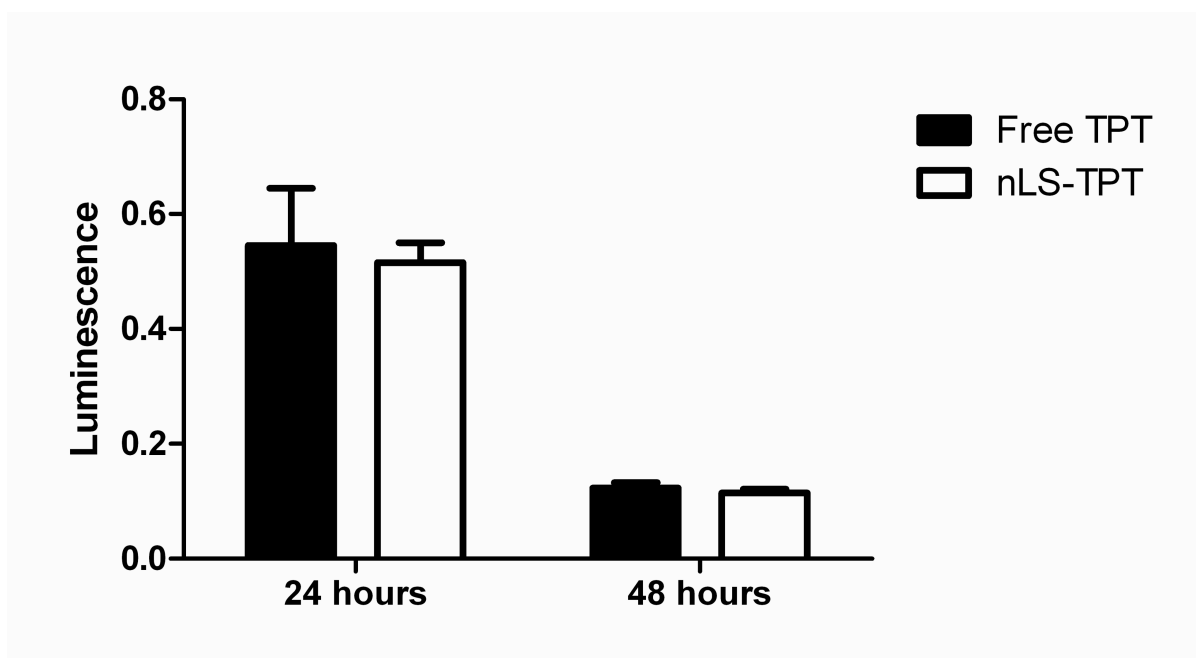


Figure 4-5 *In vitro* analysis of nLS-TPT effect on cell luminescence. U-87MG cells were incubated with either free TPT or nLS-TPT (2.67×10^{-3} mg/mL, final concentration) for the indicated times. Effect of TPT treatment on luminescence, relative to untreated control specimens, is indicated. N = 3 for all groups. Data are representative of and consistent with results from replicate experiments.

4.4.5 Analysis of biologic effect from TPT treatment *in vivo*

To assess mode of action and biologic consequences of nLS-TPT treatment *in vivo*, athymic mice bearing GBM43 tumors were injected with a single dose of either free TPT or nLS-TPT and sacrificed 24 hours after treatment. Brains were removed, fixed, embedded, then sectioned for molecular analysis of intracranial xenograft response to therapy. In

contrast to tumors from untreated mice, tumors from mice treated with free TPT or nLS-TPT showed significantly higher levels of TUNEL staining (**Figure 4-6**), indicative of more extensive DNA fragmentation, with cellular positivity in tumors exposed to nLS-TPT significantly higher than in tumors exposed to free TPT ($p < 0.01$ for all two-way comparisons). Cleaved caspase-3 staining showed a similar pattern of results, confirming that the highest tumor apoptotic response results from nLS-TPT treatment (**Figure 4-7**). Staining for Ki67, to address effects of therapy on tumor cell proliferation, showed no significant difference in cellular positivity between treatment groups.

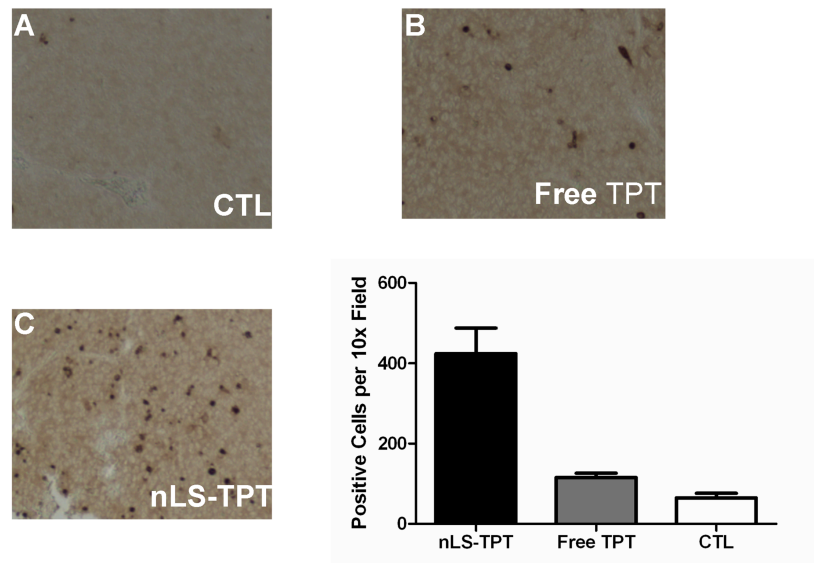


Figure 4-6 Comparison of free TPT versus nLS-TPT pro-apoptotic activity as indicated by DNA fragmentation analysis. Mice bearing GBM43 tumors were treated with a single dose of free TPT or nLS-TPT and euthanized 24 hours following treatment. Brains were immediately resected following euthanasia, fixed in formalin, then embedded in paraffin, and sectioned for immunohistochemical analysis of TUNEL positivity. Counting of positive cells in four 10x fields per tumor indicated a significant difference of effect of treatment on tumor apoptosis for all two-way comparisons ($p < 0.01$).

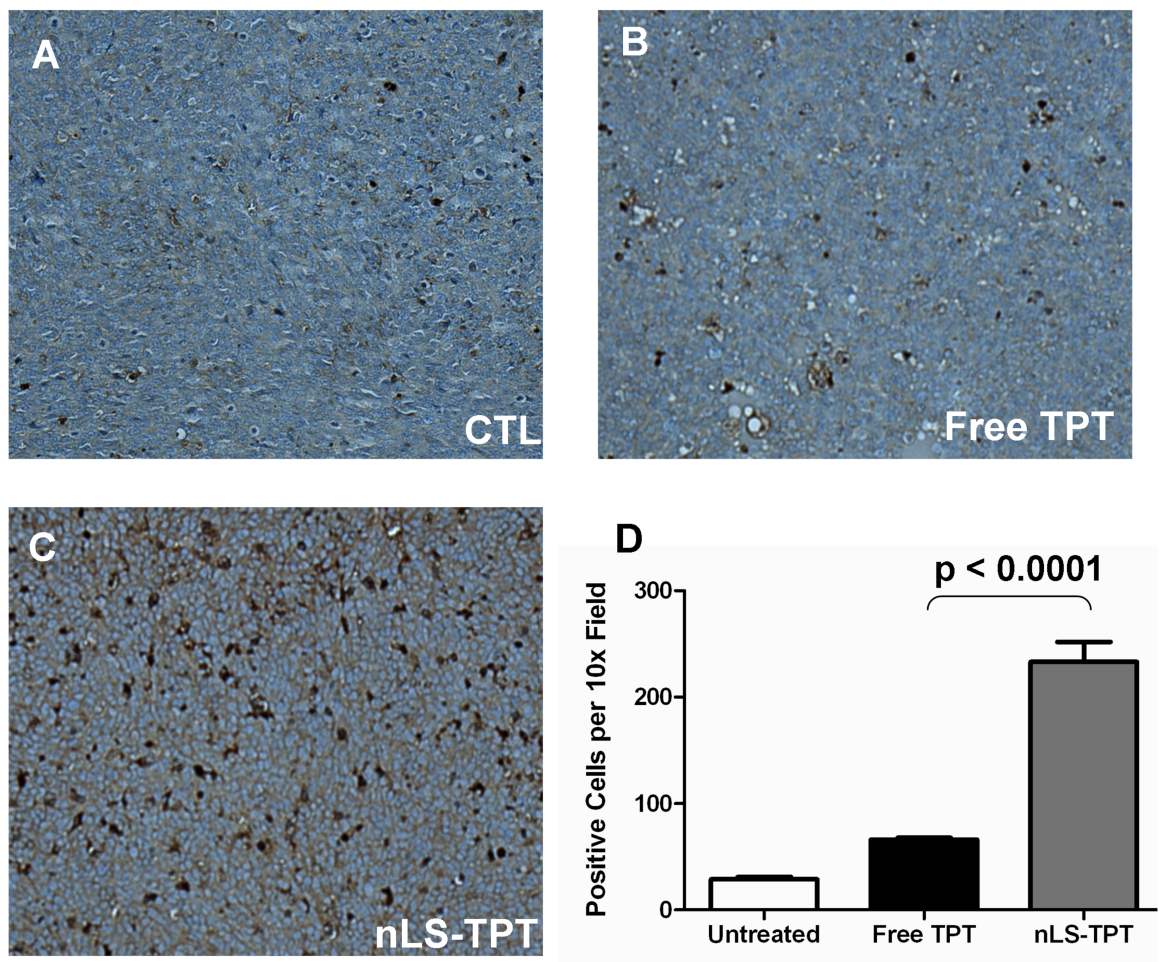


Figure 4-7 Caspase-3 activation in cells treated with nLS-TPT. Mice bearing GBM43 tumors were treated with a single dose of either free TPT or nLS-TPT and euthanized 24 hours following treatment. Brains were resected immediately following euthanasia, then fixed in 10% formalin and embedded in paraffin, then sectioned for immunohistochemical analysis of tumor cleaved caspase-3 positivity. Counting of positive cells in four 10x fields per tumor indicated a significant difference of effect of treatment on caspase 3 activation for all two-way comparisons ($p < 0.001$).

4.4.6 Toxicity

For each *in vivo* experiment the body weight of all animal subjects was monitored. There was no significant difference in average body weights between free TPT and nLS-TPT treated mice during the period in which mice remained asymptomatic of tumor burden, irrespective of tumor model being tested (Figure 4-8).

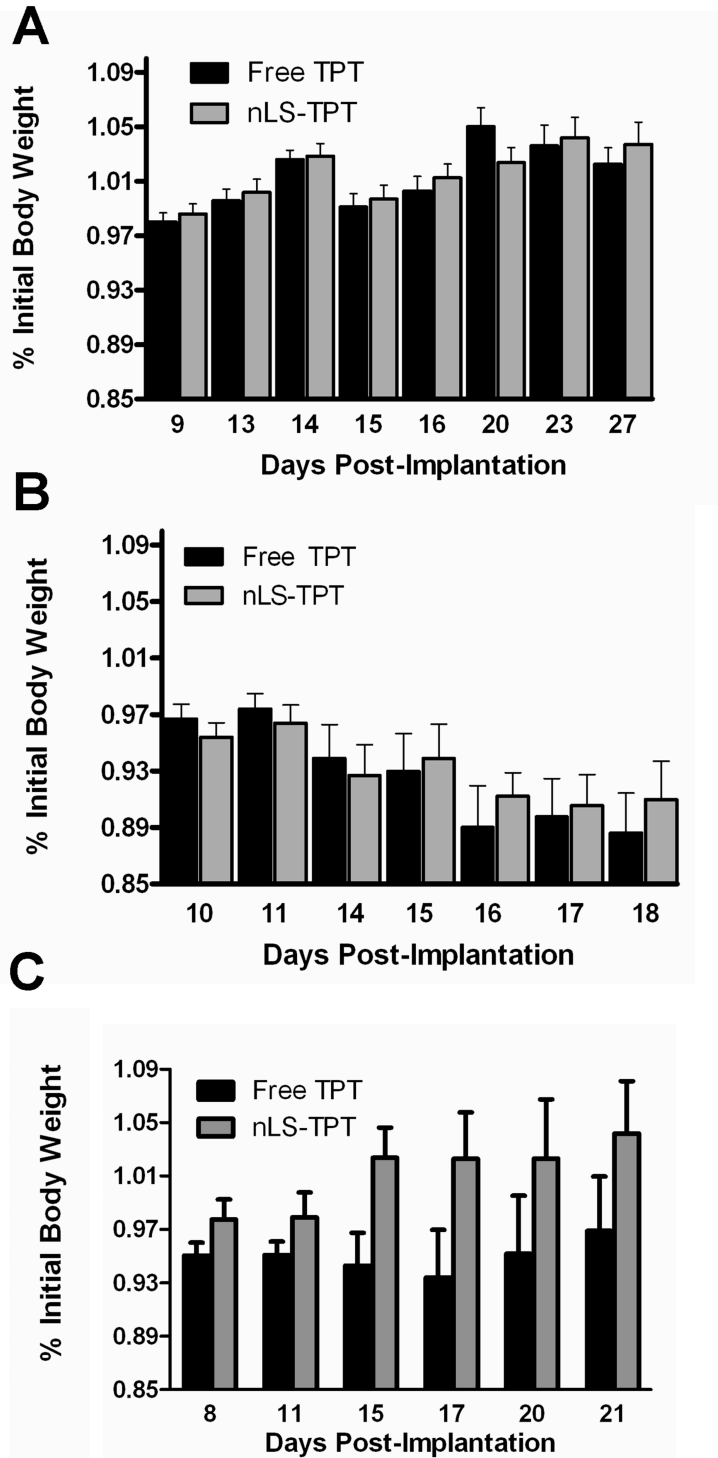


Figure 4-8 Effect of nLS-TPT and free TPT on body weight. A. Body weight monitoring results for mice associated with the efficacy experiments (Figure 4-3 and Figure 4-4). Group mean body

weights are shown, with SEM indicated for each. **A.** U-87MG model. **B.** GBM43 model. **C.** GBM6 model.

To compare myelosuppressive effects of free TPT and liposomal TPT, and to contrast TPT myelosuppressive effects against the most commonly used cytotoxic chemotherapeutic for treating GBM (temozolomide), athymic mice were either administered 10 mg/kg temozolomide (TMZ) for 5 consecutive days, or treated with TPT, using the same regimens as in the efficacy experiments (**Figures 4-3, 4-4**). Peripheral blood samples were collected weekly, and blood cell counts determined. For all time points tested, neither free TPT nor nLS-TPT treatment had a significant effect on hematocrit or hemoglobin levels (**Figure 4-9**), suggesting that nLS-TPT treatment is unlikely to cause anemia. In contrast, mice on TMZ experienced a near-significant decrease in hemoglobin levels (control vs. TMZ: $p = 0.08$). Platelet levels were unaffected by TPT or TMZ treatments (**Figure 4-10**). There was a significant decrease in neutrophil levels at the first time point following initiation of TMZ or TPT therapy (**Figure 4-11**, day 4: control vs. free TPT, $p = 0.01$; control vs. nLS-TPT, $p = 0.05$; control vs. TMZ, $p = 0.01$). Importantly, there was no significant difference in neutrophil levels between nLS-TPT and free TPT treated mice at any time point. Additionally, neutrophil levels recovered rapidly following completion of the treatment cycle, with baseline levels achieved within seven days following the last administration of TPT

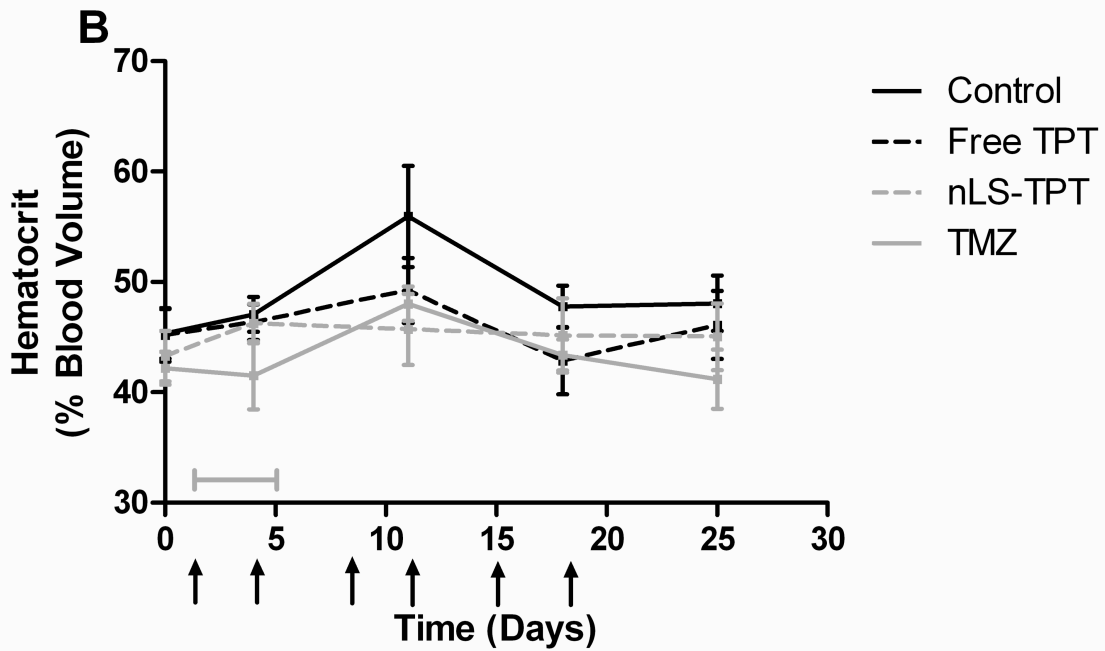
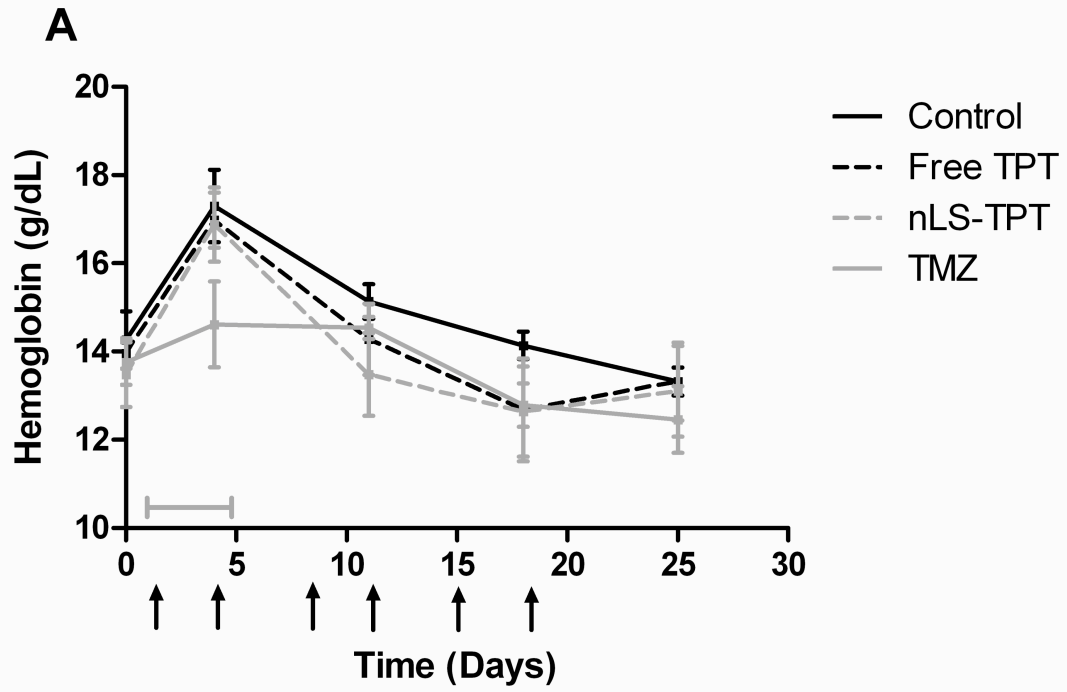


Figure 4-9 Effect of nLS-TPT treatment on hemoglobin and hemaocrit levels. Athymic mice were treated with 1 mg/kg doses (arrows) of either free TPT or nLS-TPT, following the same

schedule used in the efficacy experiments (biweekly dosing for three consecutive weeks). Mice in the temozolomide group (TMZ) were first administered 10 mg/kg TMZ daily for 5 consecutive days (gray bracket). Blood samples were collected weekly, and complete blood cell counts obtained. Group means are plotted (N = 5, all groups), with SEM indicated for each.

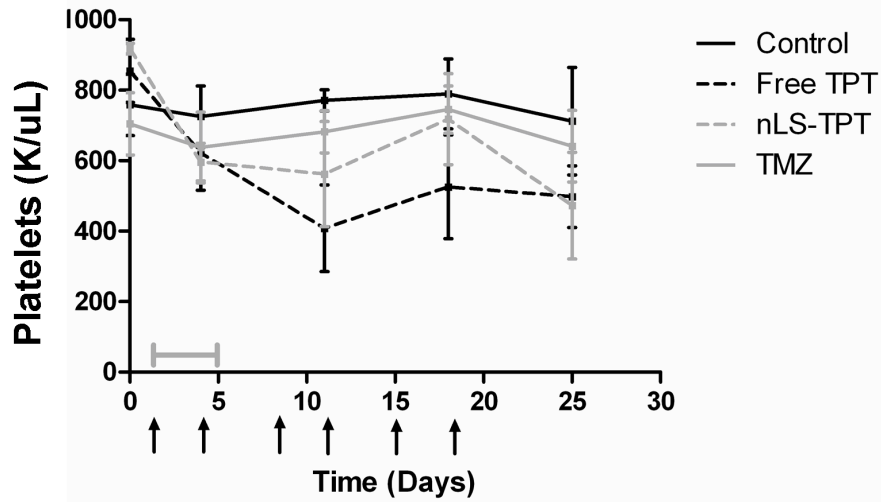


Figure 4-10 Effect of nLS-TPT treatment on platelet levels. Athymic mice were treated with 1 mg/kg doses of free TPT or nLS-TPT (arrows), following the same schedule used in the efficacy experiments (biweekly dosing for three consecutive weeks). Mice in the temozolomide group (TMZ) were first administered 10 mg/kg TMZ daily for 5 consecutive days (gray bracket), then followed until blood count results indicated a return to pre-treatment levels. Blood samples were collected weekly, and complete blood cell counts obtained for each sample. Group means are plotted (N = 5, all groups), with SEM indicated for each.

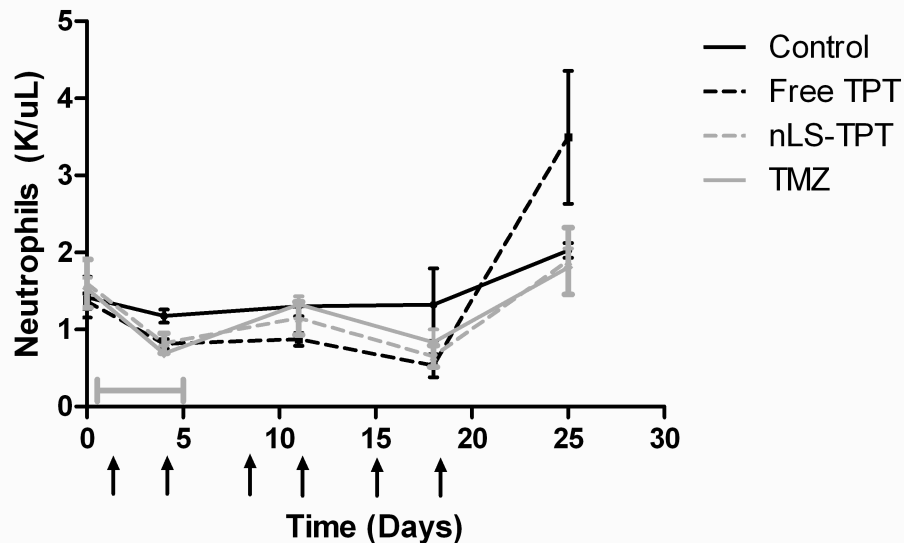


Figure 4-11 Neutrophil levels in mice treated with nLS-TPT. Athymic mice were treated with 1 mg/kg doses of either free TPT or nLS-TPT (arrows), following the same schedule used in the efficacy experiments (biweekly dosing for three consecutive weeks). Mice in the temozolomide group (TMZ) were administered 10 mg/kg TMZ daily for 5 consecutive days (Days 1-5, grey bracket), a regimen previously determined to be well-tolerated and demonstrating anti-tumor activity against most GBM intracranial xenografts. Blood samples were collected weekly, with complete blood cell counts obtained for each sample. Group means are plotted (N = 5, all groups), with SEMs indicated.

Following recovery of blood cell counts to pre-treatment levels for mice receiving TMZ, the same mice were administered nLS-TPT in order to investigate myelosuppressive effects of nLS-TPT when used as a salvage therapy for recurrent GBM. Results show that administration of nLS-TPT, following blood cell recovery from TMZ monotherapy, has lesser myelosuppressive effect than initial TMZ treatment (**Figure 4-12**).

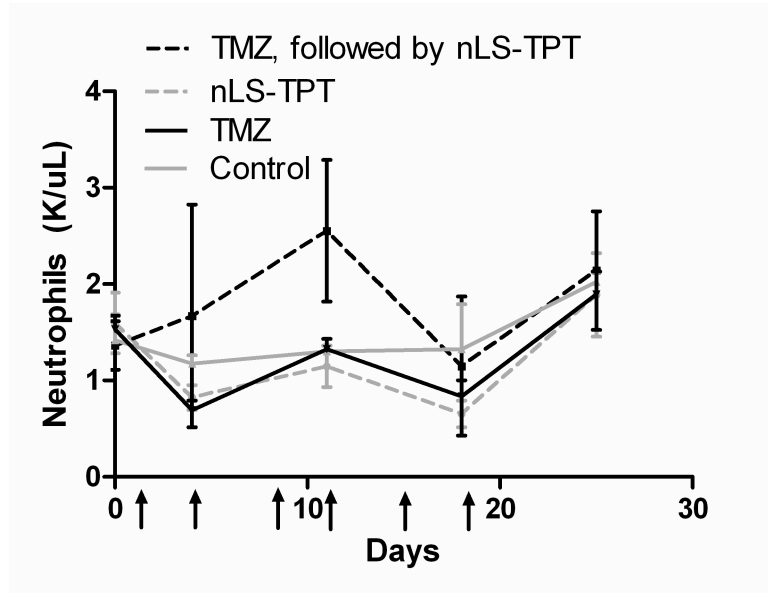


Figure 4-12 Neutrophil levels in mice treated nLS-TPT, with or without prior temozolomide treatment. Athymic mice were treated with 1 mg/kg doses of free TPT or nLS-TPT (arrows), following no treatment or treatment and recovery from 10 mg/kg TMZ for 5 days. Blood samples were collected weekly and complete blood cell counts obtained. Group means are plotted (N = 5, all groups), with SEMs indicated.

4.5 DISCUSSION

Although the use of camptothecins in treating primary brain tumors has been widely researched, these compounds have yet to see routine use in clinical practice, in large part due to their toxicity and related pharmacokinetic shortcomings[107, 123]. Liposomal encapsulation of chemotherapeutics has been shown to increase tumor drug exposure, as well as reduce systemic toxicity[124-127]. Due to the size of therapeutic liposomes, previous brain tumor studies have often focused on their direct, local delivery to tumors by CED[23, 24, 128, 129]. While nLS-TPT CED has shown efficacy in preclinical investigations employing rodent models of GBM[26], enthusiasm for use of this route of administration has been restrained due to the invasive nature of CED and the limited success of CED-associated clinical trials conducted to date[130].

In contrast to CED, intravenous delivery is less invasive and promotes a more uniform drug distribution throughout the brain, which is an important consideration given the invasive nature of GBM. Here, we have investigated intravenous administration of nanoliposomal topotecan for efficacy against three types of GBM xenografts, and report for the first time that liposomal encapsulation enhanced TPT concentration in the brain, resulting in increased anti-tumor activity. We have previously shown that empty liposomes do not have anti-tumor activity[82], indicating that it is the liposomal packaging of TPT, and not the liposomes themselves that is responsible for improved anti-tumor activity in relation to free TPT.

By intercalating into DNA, topotecan inhibits an essential process in proliferating cells, namely the role of topoisomerase I in DNA replication, ultimately resulting in DNA strand breaks that initiate programmed cell death. Indeed, the results of our TUNEL analysis

show increased DNA strand breaks in TPT treated tumors (**Figure 4-6**), and a corresponding increase in activated caspase-3 (**Figure 4-7**), a marker of programmed cell death. Importantly, DNA strand breaks as well as activated caspase-3 were significantly elevated by liposomal packaging of TPT. These results complement our previously published data indicating that TPT treatment depletes topoisomerase I in tumor cells[82], and, in combination, address mechanism and biologic consequence of TPT activity.

In contrast to targeted therapeutics, such as Tarceva, whose anti-tumor effect has been shown to be specific to a subclass of GBM[131], topotecan is expected to have a more generalized effect against GBM, due to the essential nature of topoisomerase I in tumor growth. In fact, an analysis of TCGA data for TOPI expression shows significantly elevated TOP1 mRNA levels irrespective of GBM subclassification (**Figure 4-13**). Results from our analysis of 3 distinct GBM cell sources (U87 MG and serially propagated subcutaneous xenografts GBM 6 and GBM 43) for topotecan treatment response (**Figures 4-3 and 4-4**), support the anti-tumor effect of this cytotoxic chemotherapeutic as being generalizable to most, if not all subtypes of GBM.

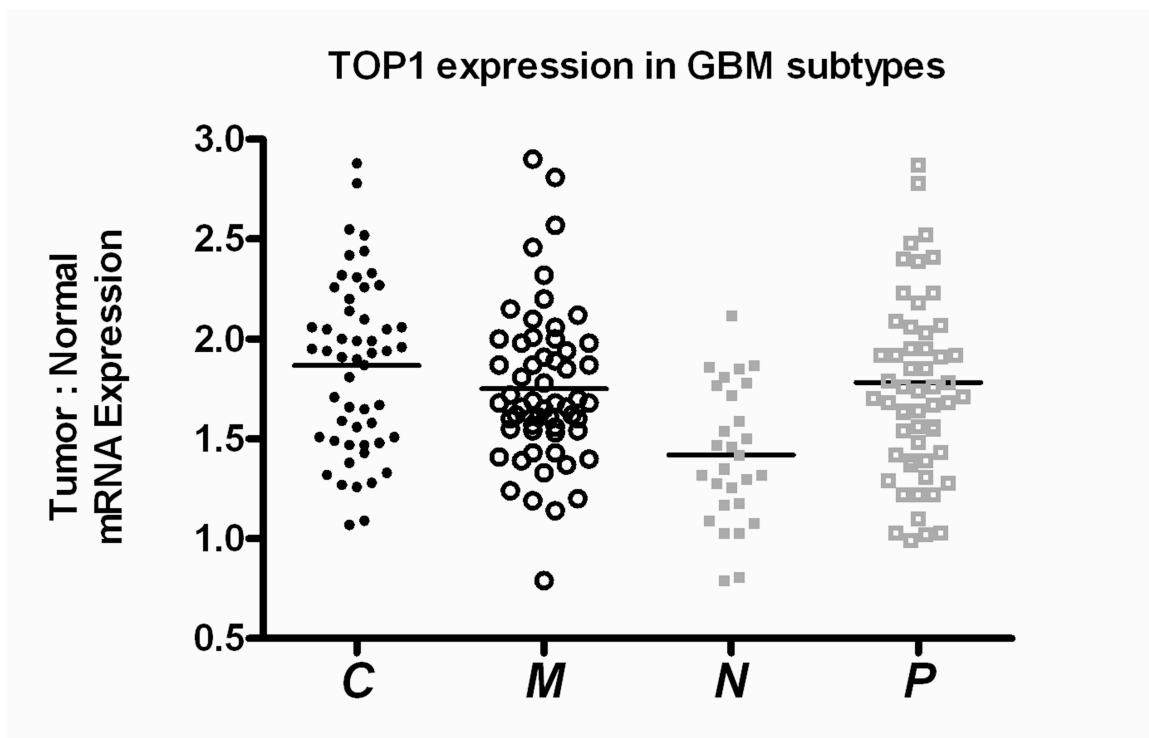


Figure 4-13 Distribution of topoisomerase I expression among GBM subtypes[121]. The expression of DNA topoisomerase I in tumor tissue, compared to normal brain tissue, is shown for 195 human glioblastoma samples subclassified by TCGA[121]. C – Classical, M – Mesenchymal, N – Neural, P – Proneural. All tumor subgroups express significantly more *TOP1* than normal brain.

The increased efficacy of nLS-TPT did not come at the expense of increased toxicity: there was not a significant difference in either mouse body weights or in neutrophil counts in mice treated with nLS-TPT versus free TPT (**Figures 4-11, 4-12**). Moreover, our analysis of blood cell counts in mice first treated with TMZ, followed by treatment with nLS-TPT, indicate that nLS-TPT has a favorable safety profile for use in treating recurrent GBM.

Previous studies have not shown a significant advantage to adding topotecan to radiation therapy[132, 133]. However, given the dramatic improvements in distribution and efficacy seen with nLS-TPT, further study into nLS-TPT combined with radiation seems warranted. In addition, it would be of interest to examine the efficacy of TPT when used in combination with inhibitors of proteins that prevent apoptosis, such as obatoclax mesylate

(GX15-070MS), a small molecule pan-Bcl-2 family inhibitor recently shown to be well-tolerated when administered with topotecan to cancer patients[134].

In total, our study results, as well as previous results from others, point to several promising possibilities for maximizing benefit from intravenous administration of nLS-TPT, and support additional investigation of this therapeutic agent and approach.

4.6 ACKNOWLEDGEMENTS

We thank the UCSF Brain Tumor Tissue Core and the UCSF Mouse Pathology Core for technical assistance.

CHAPTER 5: Convection-Enhanced Delivery of EGFR-targeted Topotecan Liposomes

The research in this section is the product of a collaboration with Dr. Charles O. Noble, formerly of Merrimack Pharmaceuticals.

5.1 ABSTRACT

Previously we have shown that direct administration of liposomal topotecan by convection-enhanced delivery (CED) is efficacious against rodent models of glioblastoma (GBM). To extend these results through tumor cell specific targeting of liposomal therapy, we have manufactured anti-EGFR immunoliposomes containing topotecan (EGFR-TPT-LS), and compared these for anti-tumor effect, and efficacy, in relation to non-targeted liposomal TPT (NT-TPT-LS). Flow cytometry and confocal microscopy were used to determine the level of binding and internalization of EGFR-TPT-LS in distinct cell lines that differed with respect to EGFR expression. High performance liquid chromatography (HPLC) and MTT assays were performed to determine the effect of increased internalization on drug content in tumor, as well as tumor cytotoxic response. Distribution of EGFR-TPT-LS *in vivo* was assessed by infusing fluorescently-labeled liposomes into intracranial xenograft tumor, followed by fluorescence microscopy of tumor tissue. Finally, efficacy was assessed in three different orthotopic models of GBM, including two cell sources that overexpress EGFR and one cell source that does not express detectable EGFR protein. *In vivo*, when delivered by CED, EGFR-TPT-LS demonstrates a similar distribution in intracranial xenograft tumor as NT-TPT-LS. In contrast, EGFR-TPT-LS was shown to specifically bind and internalize in EGFR overexpressing cells lines, resulting in a significantly improved cytotoxicity when

compared to non-targeted liposomal TPT NT-TPT-LS and free TPT. *In vivo*, when delivered by CED EGFR-TPT-LS are able to obtain a similar distribution in an intracranial xenografts tumor as NT-TPT-LS. Efficacy study results indicate that EGFR-TPT-LS confer a significant survival advantage to mice with intracranial tumors that overexpress EGFR, relative to NT-TPT-LS, while showing similar efficacy as NT-TPT-LS against tumors expressing low levels of EGFR. Our results suggest that CED of EGFR-targeted immunoliposomes is an attractive strategy for the treatment of gliomas that overexpress EGFR.

5.2 INTRODUCTION

The aggressive and infiltrative nature of glioblastoma (GBM) has long been accepted as a key factor in the poor prognosis for patients afflicted with this cancer. While the bulk of GBM can often be resected, malignant cells infiltrate at the tumor margin where they can multiply and re-establish the tumor. Current efforts for local treatment of these cells rely primarily on implantable drugs that diffuse away from the resection site[18]. However, drug diffusion only allows for minimal movement (1-2 mm) away from the implantation site, which does not lead to long-term tumor suppression or substantial increases in survival. Convection-enhanced delivery (CED) has offered promise in its ability to distribute therapeutics to greater distances than could be achieved from diffusion alone[79]. Previously, we have shown that combining CED with a long-lasting formulation of topotecan, liposomal topotecan (NT-TPT-LS), improves the efficacy of locally-administered topotecan and leads to long-term survival in a rodent model of GBM[26].

In seeking further improvement of these results, we have taken advantage of the high levels of EGFR amplification and overexpression in GBM[135]. EGFR-targeting has proven to be efficacious delivering therapeutics agents to solid tumors, when administered intravenously.[136-138] This has been explained, in part, by an increase in cellular internalization when using targeted liposomes against a cell source that expresses high levels of the target protein.[139, 140] Increased rates of internalization results in increased anti-tumor effect of therapy. In this report we address the advantages of combining local delivery via CED with cell-specific targeting of anti-EGFR immunoliposomal topotecan, as a technology amenable to the aggressive treatment of GBM that express high levels of EGFR.

5.3 METHODS

5.3.1 Materials

1,2-Distearoyl-*sn*-glycero-3-phosphocholine (DSPC), 1,2-distearoyl-*sn*-glycero-3-phosphoethanolamine (DSPE), 1,2-distearoyl-*sn*-glycero-3-phosphoethanolamine-*N*-[methoxy(polyethylene glycol)-2000] (PEG-DSPE), and 1,2-Distearoyl-*sn*-glycero-3-phosphoethanolamine-*N*-[maleimide(polyethylene glycol)2000] (Mal-PEG-DSPE) were purchased from Avanti Polar Lipids (Alabaster, AL), succinimidyl 4-*N*-maleimidomethyl]cyclohexane-1-carboxylate (SMCC) was obtained from Pierce, and Cholesterol (Chol) was obtained from Calbiochem (San Diego, CA). Sepharose CL-4B, Sephadex G-75, Sephadex G-25, and Ultrogel AcA 34 size exclusion resins and triethylamine (99.5%) were obtained from Sigma-Aldrich (St. Louis, MO). ADS-645WS was obtained from American Dye Source (Quebec, Canada). 1,1'-Dioctadecyl-3,3,3',3'-tetramethylindocarbocyanine perchlorate (1) (DiIC₁₈(3)), 3,3'-Dioctadecyloxacarbocyanine perchlorate (2) (DiOC₁₈(3)) were obtained from Invitrogen (Carlsbad, CA). Sucrose octasulfate (sodium salt) was purchased from Toronto Research Chemicals, Inc. (North York, ON, Canada). Topotecan was a kind gift from TLC (Taipei, Taiwan). All liposomes were kindly provided by Merrimack Pharmaceuticals (Cambridge, MA).

5.3.2 Cell culture

U87-EGFRvIII (U87 glioblastoma cells stably modified with lentivirus for high level EGFRvIII expression)[141] were provided by Russ Pieper (UCSF). LN229 and LN229-EGFR were provided by Theo Nicolaides (UCSF). J3T cells originated from M.E. Berens (Children's Hospital of Philadelphia). All other cell lines were obtained from the Brain

Tumor Research Center Tissue Bank at the University of California, San Francisco. All cells were maintained in either Eagle's Minimal Essential Medium (EMEM) or Dulbecco's Modified Eagle Medium (DMEM) supplemented with 10% fetal calf serum, 0.1 mg/ml streptomycin sulfate, and 100 U/ml penicillin G. All cells were maintained as monolayers at 37 °C in a humidified atmosphere consisting of 95% air and 5% CO₂.

5.3.3 C225 Fab' and p2/4 preparation

Throughout this chapter, EGFR-targeting was obtained using either the commercially available C225 (UCSF Pharmacy) or p2/4, a novel EGFR-targeting antibody kindly provided by Jim Marks (UCSF). C225 IgG₁ was treated with pepsin at 20:1 antibody to pepsin weight ratio in 0.1 M sodium acetate for 2 h at 37 °C, followed by dialysis against 5 mM MES, 135 mM NaCl (pH 6.0). The resulting (Fab')₂ was reduced with 17.5 mM mercaptoethylamine at 37 °C for 1 hour under argon followed by purification with a Sephadex G25 column eluted with 5 mM MOPS, 135 mM saline (pH 7.0). The degree of reduction was determined by gel electrophoresis and staining with coomassie brilliant blue. The C225-Fab' was stored at 4 °C under argon and used within 2 days of preparation.

Preparation of p2/4 scFv was initiated by dialysis against NaH₂PO₄ 0.1 M, EDTA 5 mM pH 6.0 (Ar purged) for 4 h, at 4 °C. To obtain monomer p2/4 scFv the dimer was reduced by addition of mercaptoethylamine hydrochloride 20 mM and pH of 6.0. Heat at 37 °C for 45 min and stop reduction by application to a sephadex G25 column and elute with 5 mM citrate, 100 mM NaCl, 1.0 mM EDTA, pH 6.0. The freshly reduced p2/4 scFv was conjugated to Mal-PEG-PE at a molar ratio of 1:5 by rocking for 2 h room temp then 24 h at 4 °C. Quenching of the unreacted maleimide groups was performed by addition of an equimolar portion of mercaptoethanol and after an initial gentle stirring, let sit at room

temperature for 5 min and then apply the solution to a sephacryl ACA 34 column and elute with 5 mM citrate, 1 mM EDTA, 100 mM NaCl pH 6.5, to remove the mercaptoethanol and the unconjugated scFv from the micellar p2/4 scFv-PEG-PE, which is stored at 4 °C until use.

5.3.4 *In vitro* binding/uptake of EGFR-LS

For studies involving the p2/4 targeting antibody, cells were plated at 3×10^5 cells/well 24 hours prior to treatment. The cells were then placed in fresh media containing either NT-LS or EGFR -LS at 0.49 mM phospholipid. For studies involving the C225 targeting antibody, cell lines were seeded in 12-well plates at a density of 1×10^5 cells/well 24 h prior to treatment. The cells were then exposed to NT-LS and EGFR-LS for 2 h at a concentration of 0.15 mM phospholipid.

After treatment, the cells were washed 3 times with PBS, detached and analyzed immediately by flow cytometry (Becton Dickonson FacsCalibur). The fluorescence of NT-LS and EGFR-LS were detected using the FL4 channel at an excitation of 635 nm and emission of 661/16 nm.

5.3.5 Tumor implantation

U87-EGFRvIII cells were harvested for intracranial injection by monolayer trypsinization followed by resuspension in DMEM at 1×10^8 cells/mL. For intracranial injection of GBM43 and GBM39, subcutaneous tumor was removed, minced with a scalpel, and subjected to three rounds of passage through a 40 μ m pore filter, with centrifugation after each round of filtering (increasing speed: 158g, 355g, 631g, 10 minutes each). After the final round of centrifugation, the cells were resuspended in 1mL of sterile DMEM media (without antibiotics), counted and diluted to 1×10^8 cells/mL for intracranial injection. All animal

experiments were conducted using protocols approved by the University of California, San Francisco, Institutional Animal Care and Use Committee. Briefly, four to six-week old female congenitally athymic nu/nu mice (Simonsen Labs: Gilroy, CA) were anesthetized by intraperitoneal injection of ketamine (100 mg/kg) and xylazine (10 mg/kg). A 1 cm sagittal incision was made along the scalp, and the skull suture lines exposed. A small hole was created by puncture with a 25g needle, at 2 mm to the right of the bregma and 0.5 mm anterior of the coronal suture. Using a sterile Hamilton syringe (Stoelting), 3×10^5 cells in 3 μ l were injected at a depth of 3 mm over a 60 second period. After injection, the syringe was held in place for 1 minute and then slowly removed. The skull was cleaned with 3% hydrogen peroxide and then sealed with bone wax. The scalp was closed using 7 mm surgical staples (Stoelting). Mice were monitored daily and euthanized when exhibiting significant neurological deficit or greater than 15% reduction from their initial body weight.

For studies performed in rats, cells were prepared as was done for the mouse studies, but the number injected was increased to 5×10^5 in 10 μ l. Injection co-ordinates were 0.5mm anterior and 3mm lateral from the bregma. The cells were injected in two 5 μ l portions, the first at a 4.5mm depth and the second at a 4mm depth. After surgery, the wound was sutured.

5.3.6 Convection-enhanced delivery

CED was performed using a cannula previously described.[77, 118] The cannula was placed through the existing burr hole at the same coordinates as the cell implantation. In mice, 10 μ l was infused using the following rates: 0.1 μ l/min (5 min), 0.2 μ l/min (5 min), 0.5 μ l/min (5 min), 0.8 μ l/min (7.5 min). In the rats, 20 μ l infusion volume was achieved with the following ascending rates: 0.2 μ l/min (15 min) + 0.5 μ l/min (10 min.) + 0.8 μ l/min (15

min). At the end of the infusion, the cannula was left in the infusion site for an additional minute and then slowly removed.

5.3.7 Effect of EGFR targeting on liposome distribution via CED

To determine effects of EGFR targeting on liposome distribution in brain tumors, fluorescently labeled anti-EGFR-ILs and NT-Ls were infused by CED into rats with U87-EGFRvIII tumors. The infusion was performed 10 days after tumor implantation. The animals were sacrificed immediately following infusion and tissue sections were analyzed for the distribution of each liposome. Images were obtained using an inverted microscope with epifluorescent capabilities and a FITC and TRITC filter combination. Images of cells with individual dyes were examined to confirm there was no interference. Intensity surface plots were obtained from the fluorescent images using ImageJ version 1.33u software.

5.3.8 *In Vitro* luciferase assay

Luciferase-modified U87-EGFRvIII cells were plated in a 96-well plate at a concentration of 5,000 cells per well. 24 hours later cells were treated for either 24 or 48 hours with 2.67×10^{-3} mg/mL NT-TPT-LS or EGFR (p2/4)-TPT-LS. After incubation, the cells were washed in pre-warmed PBS, and fresh media, without phenol red, was added to the cells. D-luciferin was added to each well at a final concentration of 0.6 mg/mL. After a 10 minute incubation cells were examined for luminescence using the IVIS Lumina System (Caliper Life Sciences, Alameda, CA, USA), as described in *Bioluminescence Imaging*.

5.3.9 *In vivo* binding/uptake of EGFR (C225)-LS

C225-ILs or NT-Ls were infused into rats 7 days after the implantation of U87 or U87-EGFRvIII tumors. Rhodamine 123 was co-infused with the liposomes as a surrogate marker to identify the portion of the tumor exposed to the CED infusion plume. The animals

were sacrificed 24 h after CED and the tumors were isolated from the healthy brain tissue. The tumor was minced and washed 3 times with PBS followed by disaggregation with trypsin/versine by gentle rocking at 37 °C for 20 min. The cell suspension was filtered and washed 2 times by centrifugation at 1000 RPM for 5 min followed by resuspension in PBS. The cells were fixed in 2% paraformaldehyde at room temperature for 15 min then washed once and placed in PBS for analysis by flow cytometry. Flow cytometry analysis was performed by gating on the cells exposed to rhodamine 123.

5.3.10 Bioluminescence imaging (BLI)

Mice were anesthetized by intraperitoneal injection of ketamine (100 mg/kg) and xylazine (10 mg/kg), and then injected intraperitoneally with 33.3 mg of D-luciferin (potassium salt, Gold Biotechnology, St. Louis, MO, USA) dissolved in sterile saline. Tumor bioluminescence was determined 10 minutes after luciferin injection, using the IVIS Lumina System (Caliper Life Sciences, Alameda, CA, USA) and LivingImage software, as the sum of photon counts/sec in regions of interest defined by a lower threshold value of 25% of peak pixel intensity. Imaging was performed biweekly beginning three days after tumor implantation until completion of study.

5.3.11 Western blots

Western blots of GBM12, GBM39, and GBM43 cell lysates were performed using standard methods[142]. For EGFR detection, membranes were incubated with 1:500 anti-EGFR (SC-03, Santa Cruz Biotechnology). For β -actin, membranes were incubated with 1:2000 anti- β -actin (AM4302, Ambion).

5.4 RESULTS

5.4.1 *In vitro* binding/internalization of EGFR-TPT-LS

To determine if EGFR-targeted liposomes demonstrate preferential binding/uptake to EGFR-overexpressing cells, we conducted flow cytometry experiments using two sets of paired cell lines: U87 and U87-EGFRvIII, as well as LN229 and LN229-EGFR (**Figure 5-1**). Both pairs consist of parental human GBM cell lines that were modified to constitutively express either EGFRvIII or wild type EGFR. In all cell lines tested, the amount of EGFR protein expressed by the cell correlated with an increase in EGFR (p2/4)-LS binding/uptake.

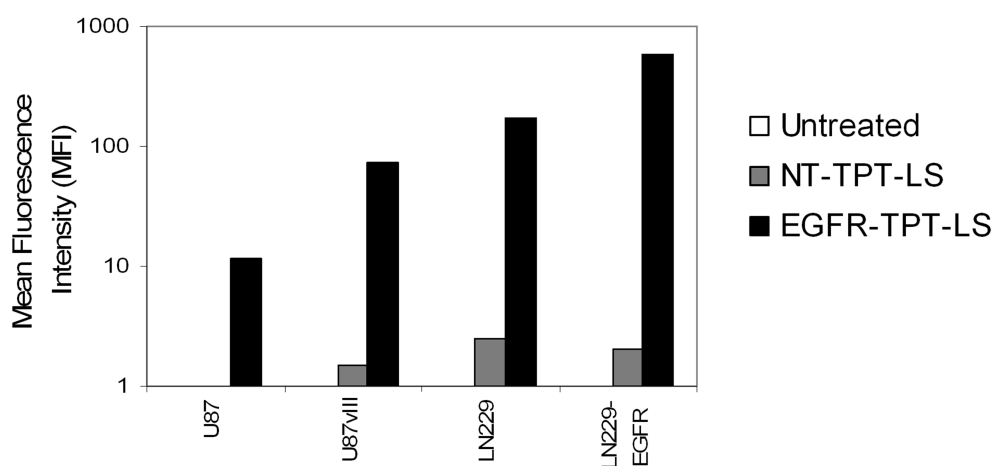


Figure 5-1 Binding/internalization studies of fluorescently labeled NT-TPT-LS and EGFR-TPT-LS. Binding/internalization studies were conducted using flow cytometry of cells exposed to either fluorescently labeled NT-TPT-LS or EGFR-TPT-LS. Graph of mean fluorescence intensity (MFI) from flow cytometry experiments using the indicated cell lines exposed to: no treatment (no fill), NT-TPT-LS (gray), or EGFR-TPT-LS (black).

The same analysis was also performed using the C225 anti-EGFR targeting antibody, on a panel of canine and human cell lines with varying levels of EGFR expression, with similar results obtained (**Figure 5-2**).

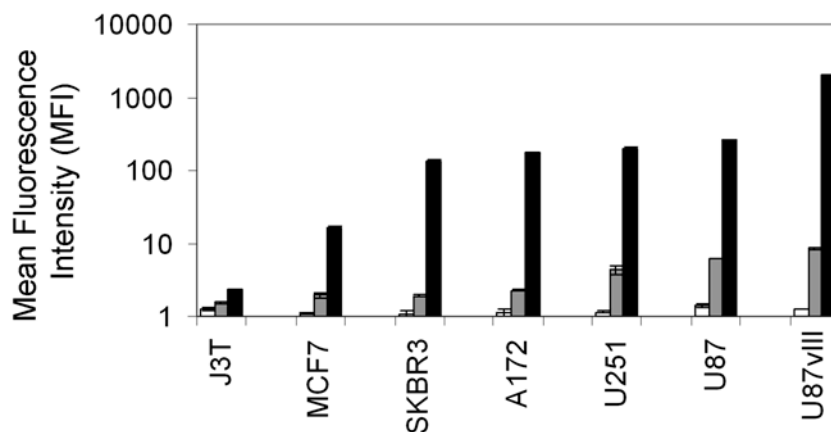


Figure 5-2 Binding/internalization studies of fluorescently labeled NT-TPT-LS and EGFR (C224)-TPT-LS Binding/internalization studies were conducted using flow cytometry of cells exposed to either fluorescently labeled NT-TPT-LS or EGFR (C225)-TPT-LS. Graph of mean fluorescence intensity (MFI) from flow cytometry experiments using the indicated cell lines exposed to: no treatment (no fill), NT-TPT-LS (gray), or EGFR-TPT-LS (black).

5.4.2 *In Vitro* drug uptake and cytotoxicity

Incubation of U87-EGFRvIII cells with various formulations of TPT showed highest intracellular drug concentrations from treatment with anti-EGFR(C225)-ILs-TPT (**Figure 5-3**). An 8 hour period of monitoring revealed intracellular maximums of 7.49×10^{-3} ng TPT/ 10^6 and 17.0×10^{-3} ng TPT/ 10^6 cells from incubations with free TPT and NT-Ls-TPT, respectively, whereas treatment with anti-EGFR(C225)-ILs-TPT resulted in 6.4 ng intracellular TPT/ 10^6 cells, which is a 376-fold greater uptake.

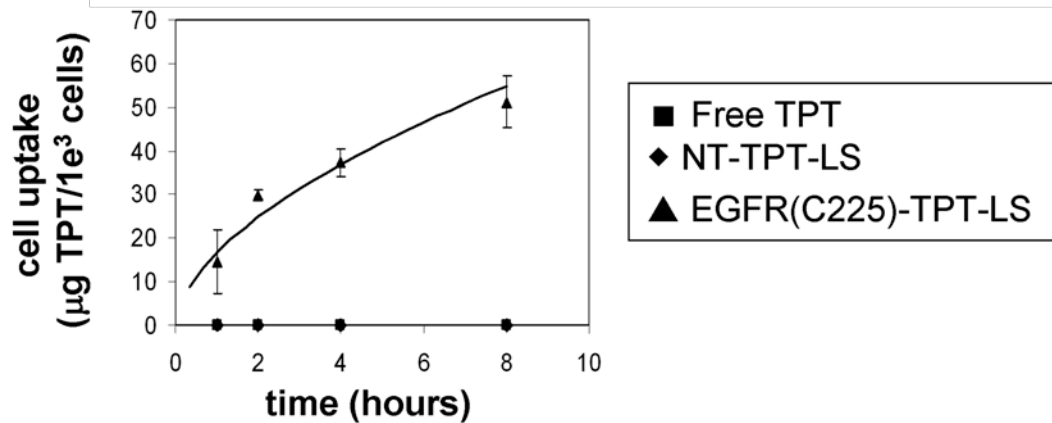


Figure 5-3 TPT uptake in cells that overexpress EGFR U87-EGFRvIII cells were treated for four hours with either NT-TPT-LS or EGFR-TPT-LS. Error bars represent standard error of the mean (SEM).

To determine if the increased binding/uptake of EGFR-TPT-LS in cells that express EGFR had a biologic consequence, we performed a luciferase assay using the U87-EGFRvIII cells (**Figure 5-4**). Luciferase-expressing U87-EGFRvIII cells were treated with either NT-TPT-LS or EGFR(p2/4)-TPT-LS for 4 hours, and cell viability was assayed by determining cell luminescence after luciferin addition. NT-TPT-LS are able to kill U87-EGFRvIII cells, as noted by the decrease in luminescence compared to untreated cells, however, there is significantly less cell viability in cells treated with EGFR(p2/4)-TPT-LS, relative to NT-TPT-LS treated cells.

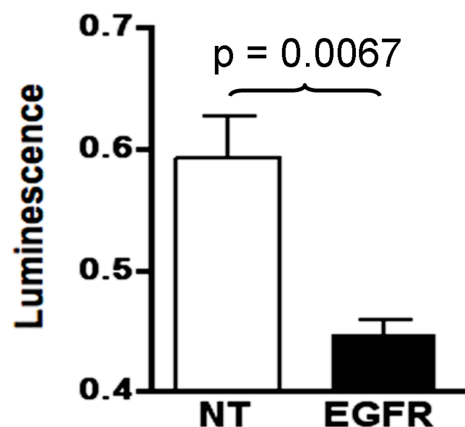


Figure 5-4 Luciferase assay of TPT-LS treated cells. U87-EGFRvIII cells were treated for four hours with either NT-TPT-LS or EGFR-TPT-LS. Error bars represent standard error of the mean (SEM).

5.4.3 Efficacy of systemic administration of EGFR-TPT-LS in EGFR-expressing xenografts

To determine if EGFR-TPT-LS could outperform NT-TPT-LS *in vivo*, we administered 1 mg/kg doses of either EGFR-TPT-LS or NT-TPT-LS intravenously to mice bearing orthotopic U87-EGFRvIII xenograft tumors. In this preliminary study, two doses were administered on days 8 and 13 post-tumor implantation. The bioluminescence scores from the tumors (**Figure 5-5**) indicated that both liposomal formulations were able to slow tumor growth, but that there was no benefit from EGFR-targeting. Given the small sample sizes of this experiment (n =3/group) survival analysis was not performed. We hypothesized that systemic administration of EGFR-targeted liposomes may adversely effect drug localization to orthotopic brain tumors, and thus conducted further studies using a local administration of EGFR-TPT-LS.

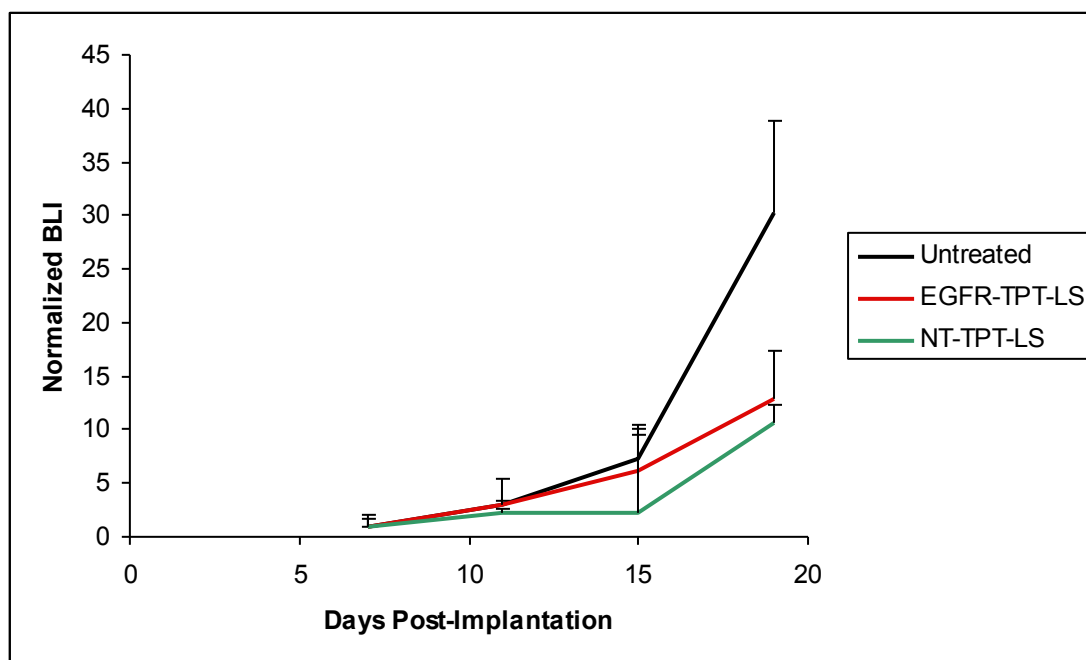


Figure 5-5 Systemic administration of EGFR-TPT-LS in mice bearing intracranial tumors that overexpress EGFRvIII. Mice (n =3/group) with U87-EGFRvIII tumors were administered 1 mg/kg doses of either NT-TPT-LS or EGFR-TPT-LS on days 8 and 13. Plot shows tumor growth, as determined by *in vivo* bioluminescence imaging.

5.4.4 Efficacy of local administration of EGFR-TPT-LS in EGFR-expressing xenografts

To determine if EGFR-TPT-LS could outperform NT-TPT-LS when delivered locally by CED, we administered a single dose (0.26 mg/kg) of either EGFR-TPT-LS or NT-TPT-LS to mice bearing intracranial U87-EGFRvIII xenografts. Using this administration, we saw no difference between EGFR-TPT-LS and NT-TPT-LS either in tumor growth delay or in overall survival (**Figure 5-6**). Given the aggressive nature of this tumor model (mouse survival mean: 15 days post tumor cell injection: see **Figure 5-6B**), we reasoned that multiple liposomal administrations may prove more efficacious, and distinguish survival benefit between non-targeted vs. EGFR-targeted liposomal preparations. To test this hypothesis, we repeated the study, adding a second administration of TPT. With the second treatment, we saw an increase in both tumor growth delay as well as in survival with the EGFR-TPT-LS compared to NT-TPT-LS (**Figure 5-7**). Consistent with our prior experiences[97], observed growth delay by bioluminescence imaging reliably indicates a significant increase in overall survival ($p = 0.004$). Histological examination revealed that all animal deaths were caused by tumor burden and there was no indication of drug toxicity observed in any animals.

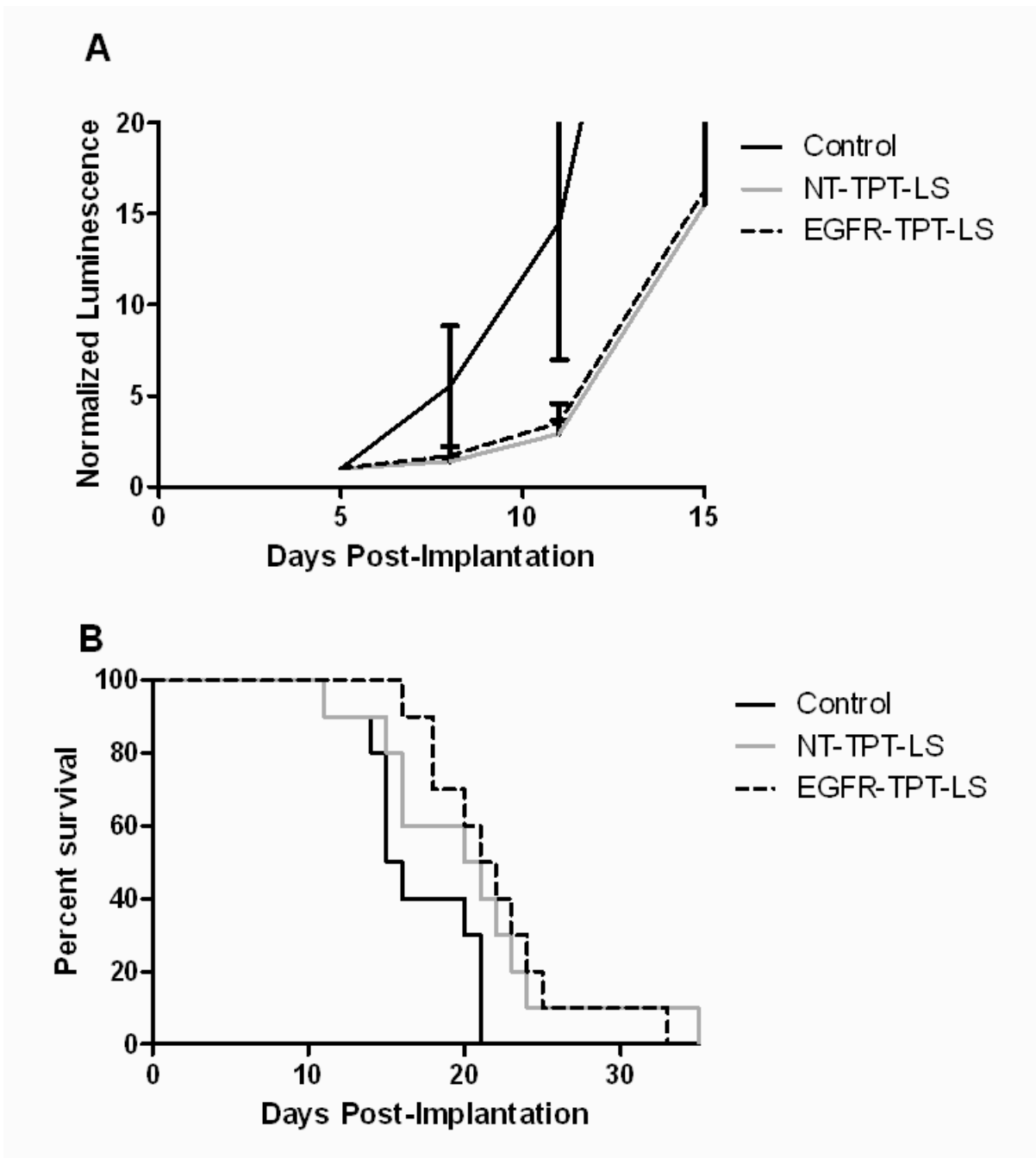


Figure 5-6 Effect of a single administration (0.26 mg/kg) of either EGFR-TPT-LS or NT-TPT-LS in mice bearing U87-EGFRvIII tumors. Mice (n =10/group) with intracranial tumors were treated once on Day 7 by CED with either NT-TPT-LS or EGFR-TPT-LS (0.26 mg/kg). **A.** Tumor growth, as determined by *in vivo* bioluminescence imaging. **B.** Corresponding Kaplan-Meier survival curve. There was no significant difference between EGFR (p2/4)-TPT-LS and NT-TPT-LS ($p = 0.74$).

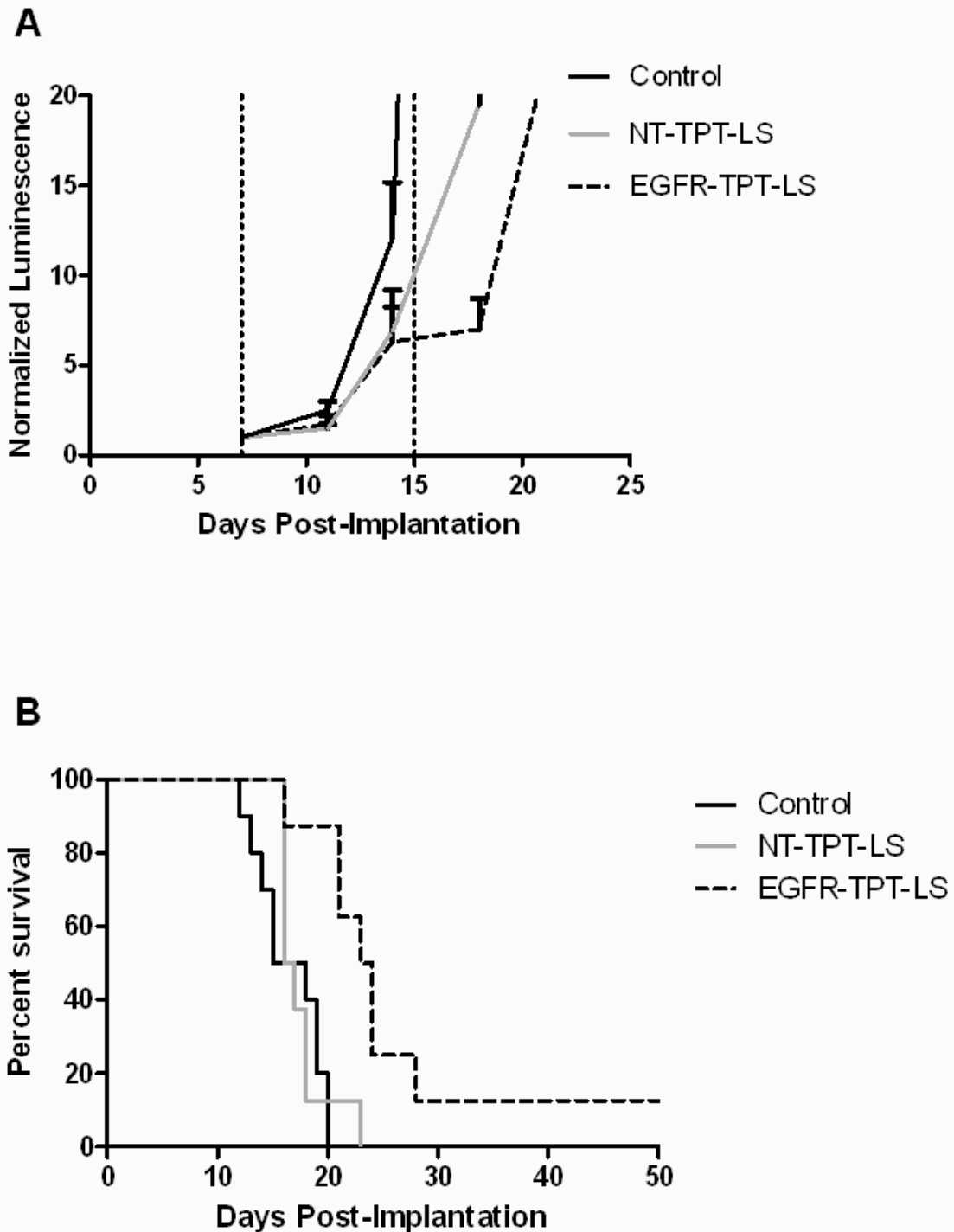


Figure 5-7 Effect of two administrations of EGFR-TPT-LS treatment on U87-EGFRvIII tumor growth and survival. Mice (10 per group) with intracranial U87-EGFRvIII tumors received two treatments of either NT-TPT-LS or EGFR-TPT-LS (0.26 mg/kg/dose) by CED. **A.** Tumor growth, as determined by *in vivo* bioluminescence imaging. Treatment times are indicated by vertical dashed lines. **B.** Corresponding Kaplan-Meier survival curve. EGFR (p2/4)-TPT-LS significantly extended survival compared to NT-TPT-LS ($p = 0.004$).

To determine whether the increased efficacy of EGFR-TPT-LS could be demonstrated using a distinct EGFR overexpressing xenograft, we repeated the efficacy study using GBM39, a subcutaneously-propagated GBM cell source that natively expresses high levels of EGFRvIII (**Figure 5-8**). This cell source grows more slowly than U87-EGFRvIII, and as a result we treated mice at day 21 post tumor cell implantation. As with the U87-EGFRvIII model, EGFR (p2/4)-TPT-LS treatment resulted in the most substantial tumor growth delay, and a significant survival advantage (NT-TPT-LS vs. EGFR-TPT-LS, $p = 0.02$).

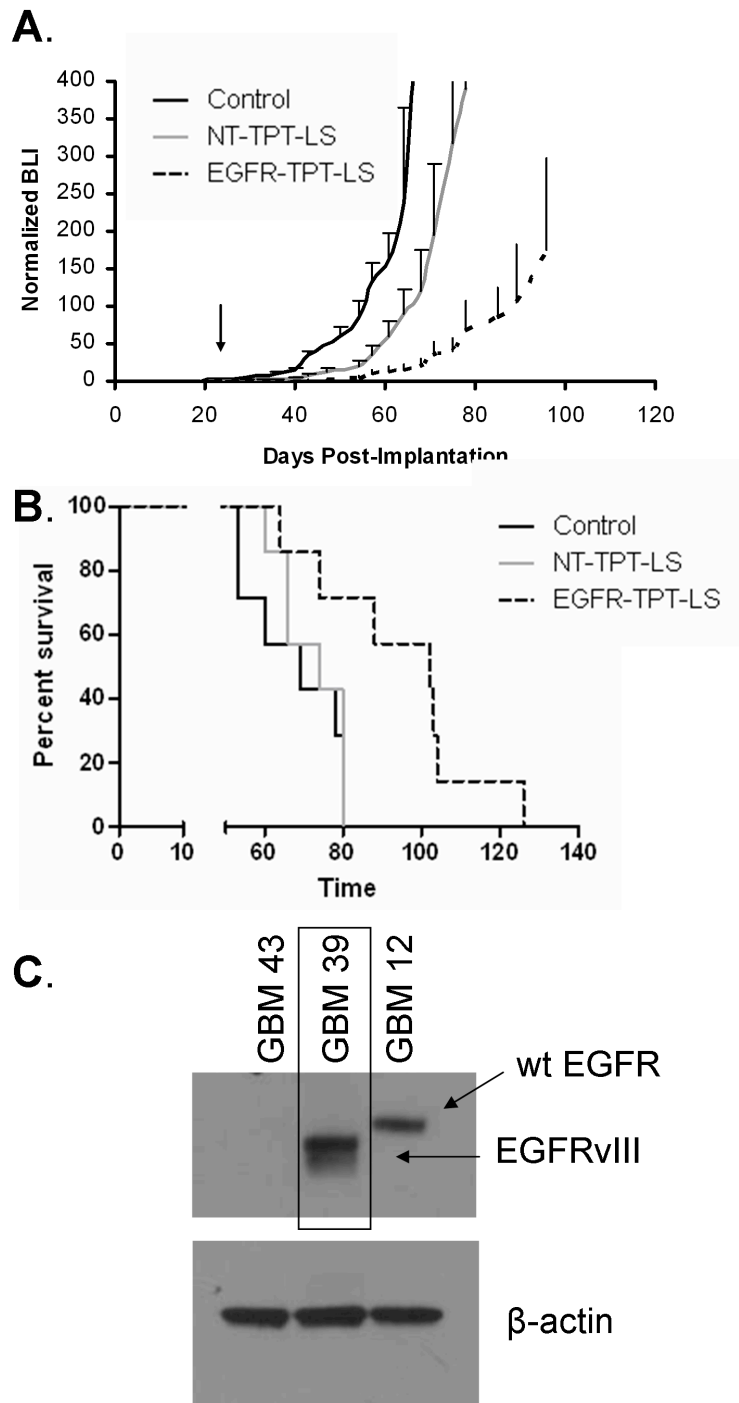


Figure 5-8 Effect of EGFR-TPT-LS treatment on intracranial xenografts established from a serially passed subcutaneous tumor with endogenous EGFRvIII amplification and overexpression. Mice ($n = 8$ per group) bearing intracranial GBM39 tumors were treated with a single dose of EGFR-TPT-LS (0.38 mg/kg) at Day 21 (arrow). **A.** Tumor growth was monitored by bioluminescence imaging. Error bars indicate SEM. **B.** Corresponding Kaplan-Meier survival curve.

EGFR (p2/4)-TPT-LS treatment extended survival significantly longer than NT-TPT-LS ($p = 0.02$).
C. Western blot showing EGFR expression levels in GBM39.

The importance of EGFR expression in tumor tissue, as a key determinant of enhanced efficacy due to EGFR liposomal targeting, can be seen in **Figure 5-9**. Using a cell source with low level EGFR expression, we see neither a delay in tumor growth, nor an increase in survival in mice bearing intracranial tumors treated with NT-TPT-LS vs. EGFR-TPT-LS.

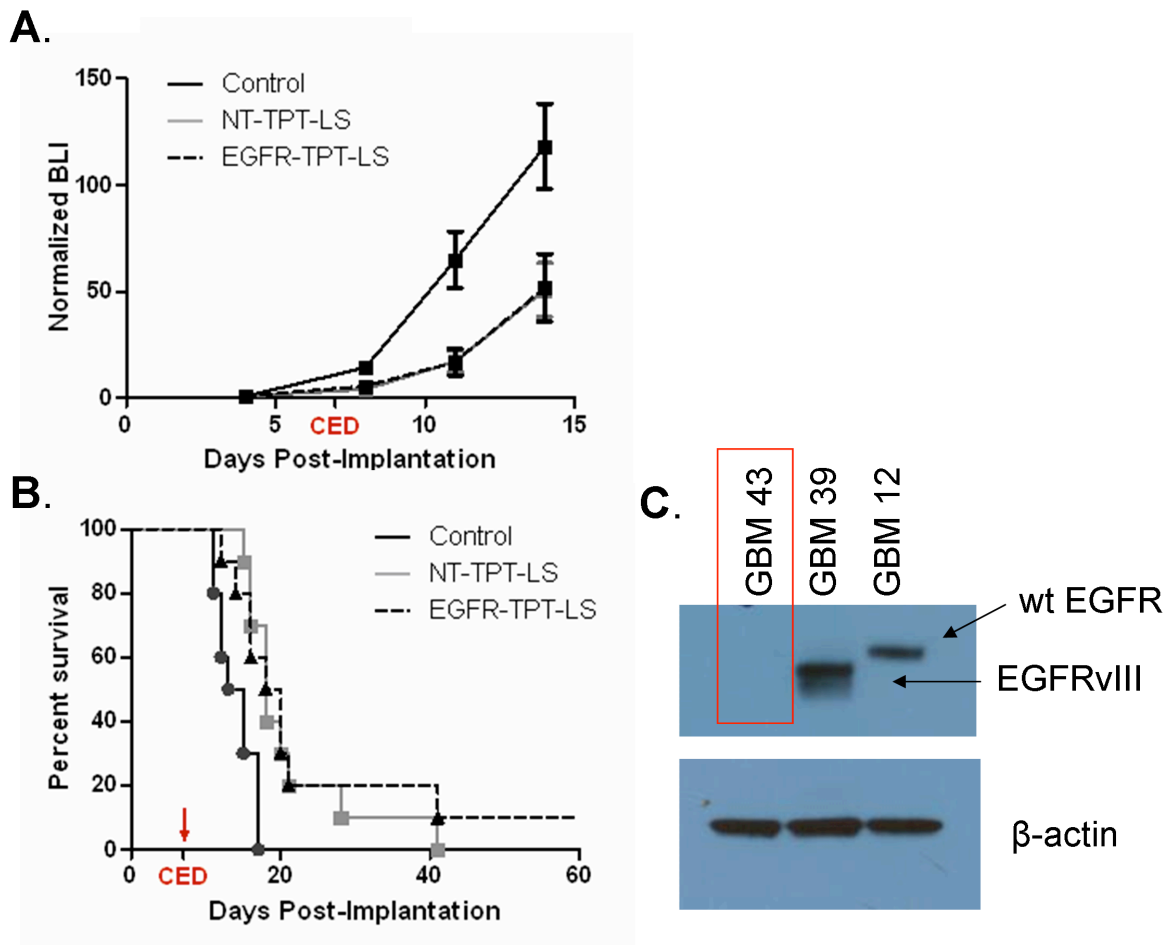


Figure 5-9 Effect of EGFR-TPT-LS on cell sources that lack EGFR. **A.** Mice bearing intracranial tumors established from cells obtained from subcutaneously-passaged GBM43 xenografts were treated with either NT-TPT-LS or EGFR (p2/4)-TPT-LS. Tumor growth was measured by bioluminescence imaging. Error bars indicate SEM. **B.** Corresponding Kaplan-Meier survival curve

for the mice in A. There was no significant difference between NT-TPT-LS and EGFR (p2/4)-TPT-LS treatment with regard to survival benefit ($p = 0.57$). C. Western blot showing the disparity in EGFR expression between GBM43 and GBM39 xenografts.

5.4.5 Effect of EGFR targeting on tumor distribution of immunoliposomes infused via CED

Infusion of fluorescently-labeled NT-LS and EGFR(C225)-LS by CED into U87-EGFRvIII tumors resulted in similar patterns of liposome distribution (**Figure 5-10**), although there is some indication of the EGFR(C225)-LS fluorescent signal being more concentrated in the center (near the infusion site) of the tumor, as indicated by surface plots of tumor fluorescence intensity (**Figures 5-10C, D**).

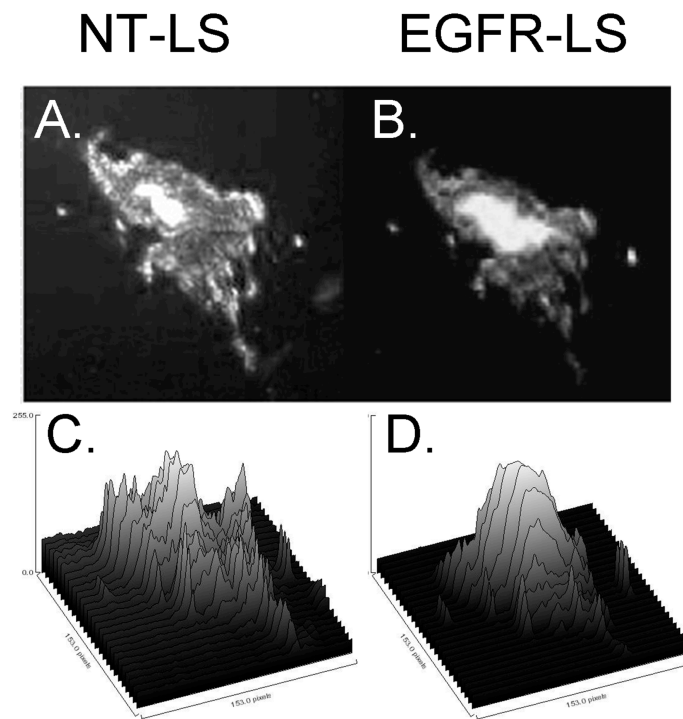


Figure 5-10 Distribution of NT-LS or EGFR (C225)-LS in U87-EGFRvIII tumors. Intracranial U87-EGFRvIII tumors were co-infused with a mixture fluorescently labeled NT-LS and EGFR(C225)-LS by CED with each liposome at a concentration 0.5 M phospholipid. **A and C.** Fluorescent image (top) and intensity surface plot (bottom) for NT-LS. **B and D.** Fluorescent image (top) and intensity surface plot (bottom) for anti-EGFR(C225)-LS.

5.5 DISCUSSION

The efficacy of immunoliposomes for treating various cancers has been shown by us[138, 139] and others[143, 144] in a variety of preclinical models. In the treatment of brain tumors, there has been increased focus on delivering agents directly to the tumor. CED, a surgical strategy proven effective in preclinical applications, is particularly suitable for delivering complex, nanoscale therapeutic constructs directly to the brain parenchyma. Such innovative approaches are important due to the limited improvements seen in the past decade for glioma chemotherapy. Our immunoliposome approach combined with CED introduces an opportunity for advancement in the field of glioma therapy. To our knowledge this is the first report describing delivery of receptor tyrosine kinase-targeted immunoliposomal anti-cancer drugs by CED.

Improved drug internalization is likely the primary basis for the enhanced efficacy seen with EGFR-TPT-LS. Additional benefit from EGFR-TPT-LS may also be found from a protection of the active form of TPT. The structure of TPT can exist in an active lactone or in inactive carboxylate form depending on solution pH[145]. Gradient loading into liposomes with a low interior pH has been shown to preserve topotecan and other camptothecin derivatives in the active lactone form[6, 113]; therefore, receptor mediated endocytosis of such particles via EGFR targeting may increase the intracellular concentration of active drug, further enhancing cytotoxicity.

The aggressive and refractory nature of GBM often necessitates the use of multiple therapies. While EGFR-TPT-LS has significant efficacy as a single agent, further improvement could be made through combination treatments. Radiation therapy, a mainstay of GBM treatment, has previously not shown any synergistic effects with topotecan treatment,

however, the improvement in topotecan retention previously shown with liposomal topotecan[26] may offer support for further study combining radiation with EGFR-TPT-LS.

The success of a CED administered therapeutic is heavily dependent on obtaining adequate drug distribution within the tumor, and avoiding drug leakage into areas of low pressure[19]. Future studies involving CED of EGFR-TPT-LS into larger animals or in clinical trials could include a co-infusion of gadolinium-filled liposomes, along with real-time MR imaging. This strategy has previously been shown to give reliable feedback regarding drug distribution[146], and should be considered an essential part of any future clinical trial involving EGFR-TPT-LS.

CED administration combined with immunoliposomal drug delivery is multi-component system offering several exciting avenues for discovery leading to improved treatment outcomes for GBM patients. The grave nature of GBM warrants the development of unconventional therapeutic approaches. Further study could lead to the establishment of immunoliposomal CED as a viable option in the treatment of glioblastoma.

CHAPTER 6: Conclusion

6.1 SUMMARY OF FINDINGS

The focus of my thesis research has been on drug delivery to brain tumors. While brain tumors have many unique biological features, compared to other cancers, perhaps their most important distinction lies in their location in one of the most sensitive and well protected regions of the body. Because of this, results from in vitro, as well as some in vivo investigations, especially those involving subcutaneous tumor growth and response to therapy, have to be interpreted with caution as concerns their potential applicability to treating brain tumor patients. We have many small molecule and biologic therapeutics that are able to disable and kill glioblastoma cells in a plate. The true challenge lies in replicating that success in a patient.

In Chapter 3, I explored the use of a protein therapeutic, cytosine deaminase, delivered locally to intracranial GBM xenografts by convection-enhanced delivery (CED). I found this therapeutic and route of administration to be successful in that sufficient activity was obtained to cause a response using an aggressive model of GBM. However, to achieve substantial survival effect it was necessary to treat animal subjects at an early timepoint after intracranial injection of tumor cells. Initiating treatment at a later timepoint resulted in only minor effect on survival, and suggests that therapeutic coverage of tumor, when administered by CED, is compromised when dealing with larger tumor volumes. Additionally, we found that the administered therapeutic protein, cytosine deaminase was cleared within 24 hours, which would necessitate multiple dosing, thereby complicating the translation of this therapy to the clinic.

Chapter 4 explores the use of a liposomal formulation of a small molecule chemotherapeutic, topotecan. Liposomal topotecan has previously been shown to be effective in the treatment of brain tumors when delivered directly to the tumor by CED[26], but has not advanced into the clinic, in part due to concerns about the invasive nature of CED. To investigate the potential of this therapeutic when used in association with an alternative route of administration, we treated mice with intracranial GBM xenografts intravenously and found, in several different xenograft models, that we were able to obtain improvements in length of tumor growth delay and corresponding extension of animal subject survival. Additionally, when we investigated systemic toxicity, we found that the liposomal topotecan caused neither greater weight loss, nor greater myelosuppression than equal doses of free topotecan. Given the improvements seen in efficacy, without accompanying increases in toxicity, I remain hopeful that the systemic delivery of liposomal drugs will see more frequent use in clinical neuro-oncology. Indeed, there is currently a Phase I trial at UCSF to address the safety of liposomal irinotecan, an analogue of topotecan: see below in section 6.2.2.

Chapter 5 addressed a potential improvement in liposome technology – the addition of targeting moieties to the liposome surface. Taking advantage of the high levels of EGFR expression and amplification in GBM, our collaborators produced EGFR antibody modified liposomes for CED efficacy study. *In vitro*, these liposomes were able to bind to and be internalized by EGFR-expressing cells at a much higher rate than non-targeted liposomes, and that translated to an improvement in drug uptake as well as cytotoxicity. *In vivo*, we found that these targeted liposomes were able to delay tumor growth and provide length of survival advantage.

6.2 FUTURE DIRECTIONS

6.2.1 Cytosine deaminase therapy

While the strategy of cytosine deaminase (CD) treatment we explored in Chapter 3 may never see the clinic, the concept of using CD to treat GBM is being actively pursued by many groups. A prominent example can be found in the work done by Tocagen, a biotechnology company. Scientists at Tocagen have created a replicating viral vector, containing a humanized CD protein, that when introduced to tumor by direct injection, should only infect replicating tumor cells, allowing for sustained production of CD. Preclinical studies in both xenograft and syngeneic models have shown this strategy, when combined with a slow-release formulation of 5-FU, to be efficacious in substantially extending survival and, in some cases, even curing animals of intracranial tumor. Given these findings, a multicenter Phase I/II trial is currently ongoing with sites at UCLA, UCSF, and the Cleveland Clinic. If Tocagen has succeeded in delivering CD in a specific and long-lasting way, this may prove to be a significant step forward in achieving improved treatment outcomes for GBM patients.

6.2.2 Ongoing clinical trials using liposomal drugs to treat GBM

Liposomal drugs are still a small subset of all cancer therapeutics, but they are beginning to get more attention, particularly in the treatment of GBM. Merrimack Pharmaceuticals developed a novel liposomal formulation of irinotecan, an analogue of topotecan, which has been shown to be efficacious in many preclinical models of solid tumors, and MM-398/PEP02 has progressed to Phase II trials for gastric and pancreatic cancers, and at UCSF this therapeutic is currently being used in a Phase I trial for treating

patients with recurrent glioblastoma. Positive results from the Phase I trial of MM-398 would likely increase interest in using other liposomal therapeutics to treat brain cancer, including liposomal topotecan.

6.2.3 Potential combination therapies with liposomal topotecan

Given the aggressive nature of GBM, it is unlikely that a single therapeutic will ever be sufficient to cause complete and sustained disease remission. While liposomal topotecan has proven efficacious in our hands, we may be able to further improve on these results through combination with synergistic agents. Radiation therapy is a mainstay of GBM treatment, and as such there have been many clinical trials investigating the effects of topotecan combined with radiation [133, 147]. The results from these trials have been disappointing, likely due to the poor pharmacokinetics as well as toxicity associated with free topotecan. Given the improvements in pharmacokinetics seen with the liposomal formulation of topotecan, without increased toxicity, there may be rationale to explore combining radiation with concurrent liposomal topotecan treatment. Indeed, in a preliminary experiment in mice bearing intracranial human GBM tumors (SF767), we found that combining whole brain radiotherapy (XRT) with liposomal topotecan inhibited tumor growth more than either treatment alone (**Figure 6-1**).

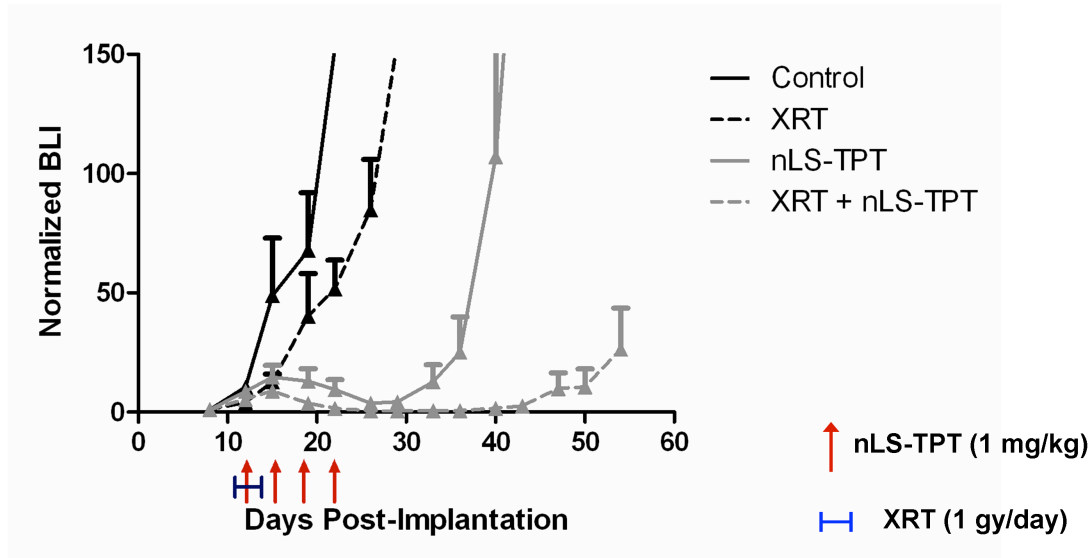


Figure 6-1 Combination of liposomal topotecan with whole brain radiotherapy in mice bearing SF767 intracranial tumors. Mice (n = 10/group) were injected with the glioblastoma cell line SF767 and treated as indicated: 1 Gy/day x 5 for XRT, beginning at day 10, and 4 intravascular administrations of liposomal topotecan, every third day, at 1 mg/kg per administration, beginning day 11 post tumor cell implantation. Tumor growth and response to therapy were assessed by bioluminescence imaging. XRT, nLS-TPT, and the combination regimen were well tolerated, with no treatment related pathology observed.

An additional approach of interest for combination therapies with liposomal topotecan would be to concurrently administer chemotherapy intended to promote the proapoptotic effect of TPT. For instance, specific inhibitors targeted to Bcl-2 family member proteins may be able to increase the cytotoxicity of topotecan as well as help prevent resistance. A Phase I trial recently performed in patients with recurrent small cell lung cancer combined free topotecan with obatoclax, a pan-Bcl-2 inhibitor[134] and found that this combination was sufficiently safe to warrant progression to larger studies. If this combination is found to be efficacious in other solid tumors, there may be rationale for combining obatoclax with liposomal topotecan in glioblastoma patients.

In summary, advances in drug delivery technology, combined with advances in our understanding of tumor biology are beginning to make progress in extending both the length

and importantly the quality of patients with glioblastoma. Collectively, the related research that has been conducted in recent years provides promise of a future in which CNS tumor patients will have multiple, efficacious treatment options for improved clinical management of their disease.

References

1. Reese TS, Karnovsky MJ, *Fine structural localization of a blood-brain barrier to exogenous peroxidase*. J Cell Biol, 1967. 34(1): p. 207-217.
2. Brightman MW, *Morphology of blood-brain interfaces*. Exp Eye Res, 1977. 25: p. 1-25.
3. Kroll RA, Neuwelt EA, *Outwitting the blood-brain barrier for therapeutic purpose: osmotic opening and other means*. Neurosurgery, 1998. 42(5): p. 1083-99.
4. Frank HJ, Jankovic-Vokes T, Pardridge WM, Morris WL, *Enhanced insulin binding to blood-brain barrier in vivo and to brain microvessels in vitro in newborn rabbits*. Diabetes, 1985. 34(8): p. 728-33.
5. Schinkel A, *P-Glycoprotein, a gatekeeper in the blood-brain barrier*. Adv Drug Deliv Rev, 1999. 36(2-3): p. 179-194.
6. Tamai I, Tsuji A, *Transporter-mediated permeation of drugs across the blood-brain barrier*. J Pharm Sci, 2000. 89(11): p. 1371-88.
7. Schlageter KE, Molnar P, Lapin GD, Groothuis DR, *Microvessel organization and structure in experimental brain tumors: microvessel populations with distinctive structural and functional properties*. Microvasc Res, 1999. 58(3): p. 312-28.
8. Port RE, Bernstein LJ, Barboriak DP, Xu L, Roberts TPL, van Brugen N, *Noncompartmental kinetic analysis of DCE-MRI data from malignant tumors: Application to glioblastoma treated with bevacizumab*. Magn Reson Med, 2010. 64(2): p. 408-417.
9. Yung WK, Prados MD, Yaya-Tur R, Rosenfeld SS, Brada M, Friedman HS, Albright R, Olson J, Chang SM, O'Neill AM, Friedman AH, Bruner J, Yue N, Dugan M, Zaknoen S, Levin VA, *Multicenter phase II trial of temozolomide in patients with anaplastic astrocytoma or anaplastic oligoastrocytoma at first relapse*. J Clin Oncol, 1999. 17(9): p. 2962-71.
10. Paz MF, Yaya-Tur R, Rojas-Marcos I, Reynes G, Pollan M, Aguirre-Cruz L, Garcia-Lopez JL, Piquer J, Safont MJ, Balana C, Sanchez-Cespedes M, Garcia-Villanueva M, Arribas L, Esteller M, *CpG island hypermethylation of the DNA repair enzyme methyltransferase predicts response to temozolomide in primary gliomas*. Clin Cancer Res, 2004. 10(15): p. 4933-8.
11. Hegi ME, Diserens AC, Gorlia T, Hamou MF, de Tribolet N, Weller M, Kros JM, Hainfellner JA, Mason W, Mariani L, Bromberg JEC, Hau P, Mirimanoff RO,

- Cairncross JG, Janzer RC, Stupp R, *MGMT gene silencing and benefit from temozolomide in glioblastoma*. *N Engl J Med*, 2005. 352(10): p. 997-1003.
12. Hansen RJ, Nagasubramanian R, Delaney SM, Samson LD, Dolan ME, *Role of O6-methylguanine-DNA methyltransferase in protecting from alkylating agent-induced toxicity and mutations in mice*. *Carcinogenesis*, 2007. 28(5): p. 1111-6.
 13. Stupp R, Hegi ME, Gilbert MR, Chakravarti A, *Chemoradiotherapy in Malignant Glioma: Standard of Care and Future Directions*. *J Clin Oncol*, 2007. 25(26): p. 4127-4136.
 14. Friedman HS, Prados MD, Wen PY, Mikkelsen T, Schiff D, Abrey LE, Yung WKA, Paleologos N, Nicholas MK, Jensen R, Vredenburgh J, Huang J, Zheng M, Cloughesy T, *Bevacizumab alone and in combination with irinotecan in recurrent glioblastoma*. *J Clin Oncol*, 2009. 27(28): p. 4733-40.
 15. Desjardins A, Reardon DA, Herndon JE, Marcello J, Quinn JA, Rich JN, Sathornsumetee S, Guyuyangan S, Sampson J, Bailey L, Bigner DD, Friedman AH, Friedman HS, Vredenburgh JJ, *Bevacizumab plus irinotecan in recurrent WHO grade 3 malignant gliomas*. *Clin Cancer Res*, 2008. 14(21): p. 7068-73.
 16. Chamberlain MC, *Emerging clinical principles on the use of bevacizumab for the treatment of malignant gliomas*. *Cancer*, 2010. 116(17): p. 3988-99.
 17. Buonerba C, Di Lorenzo G, Marinelli A, Federico P, Palmieri G, Imbimbo M, Conti P, Peluso G, De Placido S, Sampson JH, *A comprehensive outlook on intracerebral therapy of malignant gliomas*. *Crit Rev Oncol Hematol*, 2010. In Press.
 18. Westphal M, Hilt DC, Bortey E, Delavault P, Olivares R, Warnke PC, Whittle IR, Jaaskelainen J, Ram Z, *A phase 3 trial of local chemotherapy with biodegradable carmustine (BCNU) wafers (Gliadel wafers) in patients with primary malignant glioma*. *Neuro Oncol*, 2003. 5(2): p. 78-88.
 19. Varenika V, Dickinson P, Bringas J, LeCouteur R, Higgins R, Park J, Fiandaca M, Berger M, Sampson J, Bankiewicz K, *Detection of infusate leakage in the brain using real-time imaging of convection-enhanced delivery*. *J Neurosurg*, 2008. 109(5): p. 874-80.
 20. Sampson JH, Raghavan R, Brady ML, Provenzale JM, Herndon JE, Croteau D, Friedman AH, Reardon DA, Coleman RE, Wong T, Bigner DD, Pastan I, Rodriguez-Ponce MI, Tanner P, Puri R, Pedain C, *Clinical utility of a patient-specific algorithm for simulating intracerebral drug infusions*. *Neuro Oncol*, 2007. 9(3): p. 343-53.
 21. Ding D, Kanaly CW, Bigner DD, Cummings TJ, Herndon JE, Pastan I, Raghavan R, Sampson JH, *Convection-enhanced delivery of free gadolinium with the recombinant immunotoxin MRI-1*. *J Neuro-Oncol*, 2010. 98(1): p. 1-7.
 22. Weaver M, Laske DW, *Transferrin receptor ligand-targeted toxin conjugate (Tf-CRM107) for therapy of malignant gliomas*. *J Neuro-Oncol*, 2003. 65(1): p. 3-13.
 23. Noble CO, Krauze MT, Drummond DC, Yamashita Y, Saito R, Berger MS, Kirpotin DB, Bankiewicz KS, Park JW, *Novel nanoliposomal CPT-11 infused by convection-enhanced delivery in intracranial tumors: pharmacology and efficacy*. *Cancer Res*, 2006. 66(5): p. 2801-2806.
 24. Dickinson PJ, LeCouteur RA, Higgins RJ, Bringas JR, Roberts B, Larson RF, Yamashita Y, Krauze M, Noble CO, Drummond D, Kirpotin DB, Park JW,

- Berger MS, Bankiewicz KS, *Canine model of convection-enhanced delivery of liposomes containing CPT-11 monitored with real-time magnetic resonance imaging: laboratory investigation*. J Neurosurg, 2008. 108(5): p. 989-998.
25. Dickinson PJ, LeCouteur RA, Higgins RJ, Bringas JR, Larson RF, Yamashita Y, Krauze M, Forsayeth J, Noble CO, Drummond D, Kirpotin DB, Park JW, Berger MS, Bankiewicz KS, *Canine spontaneous glioma: a translational model system for convection-enhanced delivery*. Neuro Oncol, 2010. 12(9): p. 928-40.
 26. Saito R, Krauze MT, Noble CO, Drummond DC, Kirpotin DB, Berger MS, Park JW, Bankiewicz KS, *Convection-enhanced delivery of Ls-TPT enables an effective continuous, low dose chemotherapy against malignant glioma xenograft model*. Neuro Oncol, 2006. 8(3): p. 205-214.
 27. Gupta B, Levchenko TS, Torchilin VP, *TAT peptide-modified liposomes provide enhanced gene delivery to intracranial human brain tumor xenografts in nude mice*. Oncol Res, 2007. 16(8): p. 351-9.
 28. Vyas TK, Shahiwala A, Marathe S, Misra A, *Intranasal drug delivery for brain targeting*. Current drug delivery, 2005. 2(2): p. 165-75.
 29. Muhs A, Hickman DT, Pihlgren M, Chuard N, Giriens V, Meerschman C, van der Auwera I, van Leuven F, Sugawara M, Weingertner MC, Bechinger B, Greferath R, Kolonko N, Nagel-Steger L, Riesner D, O'Brady R, Pfeifer A, Nicolau C, *Liposomal vaccines with conformation-specific amyloid peptide antigens define immune response and efficacy in APP transgenic mice*. Proc. Natl. Acad. Sci. USA, 2007. 104(23): p. 9810-5.
 30. Kao HD, Traboulsi A, Itoh S, Dittert L, Hussain A, *Enhancement of the systemic and CNS specific delivery of L-dopa by the nasal administration of its water soluble prodrugs*. Pharm Res, 2000. 17(8): p. 978-84.
 31. Hanson LR, Frey WH, *Intranasal delivery bypasses the blood-brain barrier to target therapeutic agents to the central nervous system and treat neurodegenerative disease*. BMC Neurosci, 2008. 9(Suppl 3): p. 55.
 32. Wang F, Jiang X, Lu W, *Profiles of methotrexate in blood and CSF following intranasal and intravenous administration to rats*. International Journal of Pharmaceutics, 2003. 263(1-2): p. 1-7.
 33. Wang D, Gao Y, Yun L, *Study on brain targeting of raltitrexed following intranasal administration in rats*. Cancer Chemother Pharmacol, 2006. 57(1): p. 97-104.
 34. Shingaki T, Hidalgo IJ, Furubayashi T, Katsumi H, Sakane T, Yamamoto A, Yamashita S, *The transnasal delivery of 5-fluorouracil to the rat brain is enhanced by acetazolamide (the inhibitor of the secretion of cerebrospinal fluid)*. International Journal of Pharmaceutics, 2009. 377(1-2): p. 85-91.
 35. Hashizume R, Ozawa T, Gryaznov SM, Bollen AW, Lamborn KR, Frey WH, Deen DF, *New therapeutic approach for brain tumors: Intranasal delivery of telomerase inhibitor GRN163*. Neuro Oncol, 2008. 10(2): p. 112-120.
 36. Hohl RJ, Lewis K, *Differential effects of monoterpenes and lovastatin on RAS processing*. J Biol Chem, 1995. 270(29): p. 17508-12.
 37. Dafonseca C, Masini M, Futuro D, Caetano R, Rochagattass C, Quiricosantos T, *Anaplastic oligodendroglioma responding favorably to intranasal delivery of*

- perillyl alcohol: a case report and literature review. Surgical Neurology*, 2006. 66(6): p. 611-615.
38. Stayrook KR, McKinzie JH, Barbhuiya LH, Crowell PL, *Effects of the antitumor agent perillyl alcohol on H-Ras vs. K-Ras farnesylation and signal transduction in pancreatic cells. Anticancer Res*, 1998. 18(2A): p. 823-8.
 39. Gimenez F, Krauze MT, Valles F, Hadaczek P, Bringas J, Sharma N, Forsayeth J, Bankiewicz KS, *Image-guided convection-enhanced delivery of GDNF protein into monkey putamen. Neuroimage*, 2011. 54(Suppl 1): p. S189-95.
 40. Pollack IF, Hurtt M, Pang D, Albright AL, *Dissemination of low grade intracranial astrocytomas in children. Cancer*, 1994. 73(11): p. 2869-78.
 41. D'Haene N, Coen N, Neugroschl C, Baleriaux D, Salmon I, *Leptomeningeal dissemination of low-grade intramedullary gliomas: about one case and review. Clin Neurol Neurosurg*, 2009. 111(4): p. 390-4.
 42. Groothuis DR, Benalcazar H, Allen CV, Wise RM, Dills C, Dobrescu C, Rothholtz V, Levy RM, *Comparison of cytosine arabinoside delivery to rat brain by intravenous, intrathecal, intraventricular and intraparenchymal routes of administration. Brain Research*, 2000. 856(1-2): p. 281-90.
 43. Rubertone JA, Woo DV, Emrich JG, Brady LW, *Brain uptake of thallium-201 from the cerebrospinal fluid compartment. J Nucl Med*, 1993. 34(1): p. 99-103.
 44. Clayton J, Vloeberghs M, Jaspan T, Walker D, MacArthur D, Grundy R, *Intrathecal chemotherapy delivered by a lumbar-thecal catheter in metastatic medulloblastoma: a case illustration. Acta Neurochir (Wien)*, 2008. 150(7): p. 709-12.
 45. Edwards MS, Levin VA, Seager ML, Wilson CB, *Intrathecal chemotherapy for leptomeningeal dissemination of medulloblastoma. Childs Brain*, 1981. 8(6): p. 444-51.
 46. Fulton DS, Levin VA, Gutin PH, Edwards MS, Seager ML, Stewart J, Wilson CB, *Intrathecal cytosine arabinoside for the treatment of meningeal metastases from malignant brain tumors and systemic tumors. Cancer Chemother Pharmacol*, 1982. 8(3): p. 285-91.
 47. Uemura S, Matsukado Y, Fujioka S, Kuratsu J, Sonoda H, Yano T, Ohtsuka T, Yoshioka S, *Treatment of meningeal carcinomatosis--neocarzinostatin perfusion therapy in the CSF pathway. Gan To Kagaku Ryoho*, 1985. 12(9): p. 1794-800.
 48. Levin VA, Chamberlain M, Silver P, Rodriguez L, Prados M, *Phase I/II study of intraventricular and intrathecal ACNU for leptomeningeal neoplasia. Cancer Chemother Pharmacol*, 1989. 23(5): p. 301-7.
 49. Conroy S, Garnett M, Vloeberghs M, Grundy R, Craven I, Walker D, *Medulloblastoma in childhood: revisiting intrathecal therapy in infants and children. Cancer Chemother Pharmacol*, 2010. 65(6): p. 1173-89.
 50. Witham TF, Fukui MB, Meltzer CC, Burns R, Kondziolka D, Bozik ME, *Survival of patients with high grade glioma treated with intrathecal thiotriethylenephosphoramidate for ependymal or leptomeningeal gliomatosis. Cancer*, 1999. 86(7): p. 1347-53.
 51. Groves MD, Glantz MJ, Chamberlain MC, Baumgartner KE, Conrad CA, Hsu S, Wefel JS, Gilbert MR, Ictech S, Hunter KU, Forman AD, Puduvalli VK, Colman H, Hess KR, Yung WKA, *A multicenter phase II trial of intrathecal*

- topotecan in patients with meningeal malignancies. Neuro Oncol, 2008. 10(2): p. 208-215.*
52. Yoshimura J, Nishiyama K, Mori H, Takahashi H, Fujii Y, *Intrathecal chemotherapy for refractory disseminated medulloblastoma. Childs Nerv Syst, 2008. 24(5): p. 581-5.*
 53. Blaney SM, Balis FM, Berg S, Arndt CAS, Heideman R, Geyer JR, Packer R, Adamson PC, Jaeckle K, Klenke R, Aikin A, Murphy R, McCully C, Poplack DG *Intrathecal mafosfamide: a preclinical pharmacology and phase I trial. J Clin Oncol, 2005. 23(7): p. 1555-63.*
 54. Slavc I, Schuller E, Falger J, Gunes M, Pillwein K, Czech T, Dietrich W, Rossler K, Dieckmann K, Prayer D, Hainfellner J, *Feasibility of long-term intraventricular therapy with mafosfamide (n = 26) and etoposide (n = 11): experience in 26 children with disseminated malignant brain tumors. J Neuro-Oncol, 2003. 64(3): p. 239-47.*
 55. Passarin MG, Moretto G, Musso AM, Ottaviani S, Masotto B, Ghimenton C, Iuzzolino P, Buffone E, Ruda R, Soffietti R, Vattemi E, Pedersini R, *Intrathecal liposomal cytarabine in combination with temozolomide in low-grade oligoastrocytoma with leptomeningeal dissemination. J Neuro-Oncol, 2010. 97(3): p. 439-44.*
 56. Bourdon MA, Wikstrand CJ, Furthmayr H, Matthews TJ, Bigner DD, *Human glioma-mesenchymal extracellular matrix antigen defined by monoclonal antibody. Cancer Res, 1983. 43(6): p. 2796-805.*
 57. Brown MT, Coleman RE, Friedman AH, Friedman HS, McLendon RE, Reiman R, Felsberg GJ, Tien RD, Bigner SH, Zalutsky MR, Zhao XG, Wikstrand CJ, Pegram CN, Herndon JE, Vick NA, Paleologos N, Fredericks RK, Schold SC, Bigner DD, *Intrathecal 131I-labeled antitenascin monoclonal antibody 81C6 treatment of patients with leptomeningeal neoplasms or primary brain tumor resection cavities with subarachnoid communication: phase I trial results. Clin Cancer Res, 1996. 2(6): p. 963-72.*
 58. Merrill MK, Bernhardt G, Sampson JH, Wikstrand CJ, Bigner DD, Gromeier M, *Poliovirus receptor CD155-targeted oncolysis of glioma. Neuro Oncol, 2004. 6(3): p. 208-17.*
 59. Ochiai H, Campbell SA, Archer GE, Chewning TA, Dragunsky E, Ivanov A, Gromeier M, Sampson JH, *Targeted therapy for glioblastoma meningitis with intrathecal delivery of an oncolytic recombinant poliovirus. Clin Cancer Res, 2006. 12(4): p. 1349-54.*
 60. Aboody KS, Brown A, Rainov NG, Bower KA, Liu S, Yang W, Small JE, Herrlinger U, Ourednik V, Black PM, Breakefield XO, Snyder EY, *Neural stem cells display extensive tropism for pathology in adult brain: evidence from intracranial gliomas. Proc. Natl. Acad. Sci. USA, 2000. 97(23): p. 12846-51.*
 61. Shimato S, Natsume A, Takeuchi H, Wakabayashi T, Fujii M, Ito M, Ito S, Park IH, Bang JH, Kim SU, Yoshida J, *Human neural stem cells target and deliver therapeutic gene to experimental leptomeningeal medulloblastoma. Gene Ther, 2007. 14(15): p. 1132-42.*

62. Gu C, Li S, Tokuyama T, Yokota N, Namba H, *Therapeutic effect of genetically engineered mesenchymal stem cells in rat experimental leptomeningeal glioma model*. *Cancer Lett*, 2010. 291(2): p. 256-62.
63. Rapoport SI, Robinson PJ, *Tight-junctional modification as the basis of osmotic opening of the blood-brain barrier*. *Ann N Y Acad Sci*, 1986. 481(250-67).
64. Nakano S, Matsukado K, Black KL, *Increased brain tumor microvessel permeability after intracarotid bradykinin infusion is mediated by nitric oxide*. *Cancer Res*, 1996. 56(17): p. 4027-31.
65. Neuwelt EA, Frenkel EP, Rapoport S, Barnett P, *Effect of osmotic blood-brain barrier disruption on methotrexate pharmacokinetics in the dog*. *Neurosurgery*, 1980. 7(1): p. 36-43.
66. Boockvar JA, Tsiouris AJ, Hofstetter CP, Kovanlikaya I, Fralin S, Kesavabhotla K, Seedial SM, Pannullo SC, Schwartz TH, Stieg P, Zimmermann RD, Knopman J, Scheff RJ, Christos P, Vallabhajosula S, Riina HA, *Safety and maximum tolerated dose of superselective intraarterial cerebral infusion of bevacizumab after osmotic blood-brain barrier disruption for recurrent malignant glioma. Clinical article*. *J Neurosurg*, 2011. 114(3): p. 624-32.
67. Nilaver G, Muldoon LL, Kroll RA, Pagel MA, Breakefield XO, Davidson BL, Neuwelt EA, *Delivery of herpesvirus and adenovirus to nude rat intracerebral tumors after osmotic blood-brain barrier disruption*. *Proc. Natl. Acad. Sci. USA*, 1995. 92(21): p. 9829-33.
68. Doran SE, Ren XD, Betz AL, Pagel MA, Neuwelt EA, Roessler BJ, Davidson BL, *Gene expression from recombinant viral vectors in the central nervous system after blood-brain barrier disruption*. *Neurosurgery*, 1995. 36(5): p. 965-70.
69. Blasberg RG, Kobayashi T, Horowitz M, Rice JM, Groothuis D, Molnar P, Fenstermacher JD, *Regional blood-to-tissue transport in ethylnitrosourea-induced brain tumors*. *Ann Neurol*, 1983. 14(2): p. 202-215.
70. Zunkeler B, Carson RE, Olson J, Blasberg RC, DeVroom H, Lutz RJ, Saris SC, Wright DC, Kammerer W, Patronas NJ, Dedrick RL, Herscovitch P, Oldfield EH, *Quantification and pharmacokinetics of blood-brain barrier disruption in humans*. *J Neurosurg*, 1996. 85(6): p. 1056-65.
71. Black KL, King WA, Ikezaki K, *Selective opening of the blood-tumour barrier by intracarotid infusion of leukotriene C4*. *Acta Neurochir Suppl (Wien)*, 1990. 51: p. 140-1.
72. Matsukado K, Inamura T, Nakano S, Fukui M, Bartus RT, Black KL, *Enhanced tumor uptake of carboplatin and survival in glioma-bearing rats by intracarotid infusion of bradykinin analog, RMP-7*. *Neurosurgery*, 1996. 39(1): p. 125-33.
73. Friden PM, Olson TS, Obar R, Walus LR, Putney SD, *Characterization, receptor mapping and blood-brain barrier transcytosis of antibodies to the human transferrin receptor*. *J Pharmacol Exp Ther*, 1996. 278(3): p. 1491-8.
74. Huwyler J, Wu D, Pardridge WM, *Brain drug delivery of small molecules using immunoliposomes*. *Proc. Natl. Acad. Sci. USA*, 1996. 93(24): p. 14164-9.
75. Zhang Y, Zhang YF, Bryant J, Charles A, Boado RJ, Pardridge WM, *Intravenous RNA interference gene therapy targeting the human epidermal growth factor receptor prolongs survival in intracranial brain cancer*. *Clin Cancer Res*, 2004. 10(11): p. 3667-77.

76. Carcaboso AM, Elmeliogy MA, Shen J, Juel SJ, Zhang ZM, Calabrese C, Tracey L, Waters CM, Stewart CF, *Tyrosine kinase inhibitor gefitinib enhances topotecan penetration of gliomas*. *Cancer Res*, 2010. 70(11): p. 4499-508.
77. Krauze MT, Saito R, Noble C, Tamas M, Bringas J, Park JW, Berger MS, Bankiewicz K, *Reflux-free cannula for convection-enhanced high-speed delivery of therapeutic agents*. *J Neurosurg*, 2005. 103: p. 923-929.
78. Jain RK, *Delivery of novel therapeutic agents in tumors: physiological barriers and strategie*. *J Natl Cancer Inst*, 1989. 81(8): p. 570-6.
79. Bobo RH, Laske DW, Akbasak A, Morrison PF, Dedrick RL, Oldfield EH, *Convection-enhanced delivery of macromolecules in the brain*. *Proc. Natl. Acad. Sci.*, 1994. 91: p. 2076-2080.
80. Gill SS, Patel NK, Hotton GR, O'Sullivan K, McCarter R, Bunnage M, Brooks DJ, Svendsen CN, Heywood P, *Direct brain infusion of glial cell line-derived neurotrophic factor in Parkinson disease*. *Nat Med*, 2003. 9(5): p. 589-85.
81. Szerlip NJ, Walbridge S, Yang L, Morrison PF, Degen JW, Jarrell ST, Kouri J, Kerr PB, Kotin R, Oldfield EH, Lonser RR, *Real-time imaging of convection-enhanced delivery of viruses and virus-sized particles*. *J Neurosurg*, 2007. 107(3): p. 560-567.
82. Yamashita Y, Krauze MT, Kawaguchi T, Noble CO, Drummond DC, Park JW, Bankiewicz KS, *Convection-enhanced delivery of a topoisomerase I inhibitor (nanoliposomal topotecan) and a topoisomerase II inhibitor (pegylated liposomal doxorubicin) in intracranial brain tumor xenografts*. *Neuro Oncol*, 2007. 9(1): p. 20-28.
83. MacKay JA, Deen DF, Szoka FC, *Distribution in brain of liposomes after convection enhanced delivery; modulation by particle charge, particle diameter, and presence of steric coating*. *Brain Research*, 2005. 1035: p. 139-153.
84. Dickinson PJ LeCouteur RA, Higgins RJ, Bringas JR, Roberts B, Larson RF, Yamashita Y, Krauze M, Noble CO, Drummond D, Kirpotin DB, Park JW, Berger MS, Bankiewicz KS, *Canine model of convection-enhanced delivery of liposomes containing CPT-11 monitored with real-time magnetic resonance imaging: laboratory investigation*. *J Neurosurg*, 2008. 108(5): p. 989-998.
85. Krauze MT Vandenberg SR, Yamashita Y, Saito R, Forsayeth J, Noble C, Park JW, Bankiewicz K, *Safety of real-time convection-enhanced delivery of liposomes to primate brain: a long-term retrospective*. *Exp Neurol*, 2008. 210(2): p. 638-844.
86. Degen JW Walbridge S, Vortmeyer AO, Oldfield EH, Lonser RR, *Safety and efficacy of convection-enhanced delivery of gemcitabine or carboplatin in a malignant glioma model in rats*. *J Neurosurg*, 2003. 99(5): p. 893-898.
87. Saito R, Bringas JR, Panner A, Tamas M, Pieper RO, Berger MS, Bankiewicz KS, *Convection-enhanced delivery of tumor necrosis factor-related apoptosis-inducing ligand with system administration of temozolomide prolongs survival in an intracranial glioblastoma xenograft model*. *Cancer Res*, 2004. 64(19): p. 6858-6862.
88. Murad GJ, Walbridge S, Morrison PF, Garmestani K, Degen JW, Brechbiel MW, Oldfield EH, Lonser RR, *Real-time, image-guided, convection-enhanced delivery of interleukin 13 bound to pseudomonas exotoxin*. *Clin Cancer Res*, 2006. 12(10): p. 3145-3151.

89. Yamashita Y Krauze MT, Kawaguchi T, Noble CO, Drummond DC, Park JW, Bankiewicz KS, *Convection-enhanced delivery of a topoisomerase I inhibitor (nanoliposomal topotecan) and a topoisomerase II inhibitor (pegylated liposomal doxorubicin) in intracranial brain tumor xenografts.* Neuro Oncol, 2007. 9(1): p. 20-28.
90. Saito R Bringas JR, Panner A, Tamas M, Pieper RO, Berger MS, Bankiewicz KS, *Convection-enhanced delivery of tumor necrosis factor-related apoptosis-inducing ligand with system administration of temozolomide prolongs survival in an intracranial glioblastoma xenograft model.* Cancer Res, 2004. 64(19): p. 6858-6862.
91. Murad GJ Walbridge S, Morrison PF, Garmestani K, Degen JW, Brechbiel MW, Oldfield EH, Lonser RR, *Real-time, image-guided, convection-enhanced delivery of interleukin 13 bound to pseudomonas exotoxin.* Clin Cancer Res, 2006. 12(10): p. 3145-3151.
92. Miller CR, Williams CR, Buchsbaum DJ, Gillespie GY, *Intratumoral 5-Fluorouracil Produced by Cytosine Deaminase/5-Fluorocytosine Gene Therapy Is Effective for Experimental Human Glioblastomas.* Cancer Research, 2002. 62: p. 773-780.
93. Nishiyama T, Kawamura Y, Kawamoto K, Matsumura H, Yamamoto N, Ito T, Ohyama A, Katsuragi T, Sakai T, *Antineoplastic effects in rats of 5-fluorocytosine in combination with cytosine deaminase capsules.* Cancer Res, 1985. 45(4): p. 1753-61.
94. Greco O, Dachs GU, *Gene directed enzyme/prodrug therapy of cancer: historical appraisal and future perspectives.* J Cell Physiol, 2001. 187(1): p. 22-36.
95. Senter PD, Su PC, Katsuragi T, Sakai T, Cosand WL, Hellstrom I, Hellstrom KE, *Generation of 5-fluorouracil from 5-fluorocytosine by monoclonal antibody-cytosine deaminase conjugates.* Bioconj Chem, 1991. 2(6): p. 447-51.
96. Korkegian A, Black ME, Baker D, Stoddard BL, *Computational thermostabilization of an enzyme.* Science. 308(5723): p. 857-60.
97. Dinca EB, Sarkaria JN, Schroeder MA, Carlson BL, Voicu R, Gupta N, Berger MS, James CD, *Bioluminescence monitoring of intracranial glioblastoma xenograft: response to primary and salvage temozolomide therapy.* J Neurosurg, 2007. 108(3): p. 610-616.
98. Krauze MT Saito R, Noble C, Bringas J, Forsayeth J, McKnight TR, Park JW, Berger MS, Bankiewicz K, *Effects of the perivascular space on convection-enhanced delivery of liposomes in primate putamen.* Exp Neurol, 2005. 196(1): p. 104-111.
99. Fuchita M, Ardiani A, Zhao L, Serve K, Stoddard BL, Black ME, *Bacterial cytosine deaminase mutants created by molecular engineering show improved 5-fluorocytosine-mediated cell killing in vitro and in vivo.* Cancer Res, 2009. 69(11): p. 4791-9.
100. Bookman MA, Malmstrom H, Bolis G et al., *Topotecan for the treatment of advanced epithelial ovarian cancer: an open-label phase II study in patients treated after prior chemotherapy that contained cisplatin or carboplatin and paclitaxel.* J Clin Oncol, 1998. 16: p. 3345-3352.

101. Depierre A, von Pawel J, Hans K, et al, *Evaluation of topotecan (Hycamtin) in relapsed small cell lung cancer (SCLC). A multicentre phase II study.* . Lung Cancer, 1997. 18(suppl 1): p. 35.
102. ten Bokkel Huinink W, Gore M, Carmichael J, Gordon A, Malfetano J, Hudson I, Broom C, Scarabelli C, Davidson N, Spanczynski M, Bolis G, Malmstrom H, Coleman R, Fields SC, Heron JF, *Topotecan versus paclitaxel for the treatment of recurrent epithelial ovarian cancer.* J Clin Oncol, 1997. 15: p. 2183-2193.
103. ten Bokkel Huinink W, Lane SR, Ross GA, and the International Topotecan Study Group, *Long-term survival in a phase III, randomised study of topotecan versus paclitaxel in advanced epithelial ovarian carcinoma.* Ann Oncol, 2004. 15: p. 100-103.
104. Ciusani E, Croci D, Gelati M, Calatozzolo C, Sciacca F, Fumagalli L, Balzarotti M, Fariselli L, Boidardi A, Salmaggi A, *In vitro effects of topotecan and ionizing radiation on TRAIL/Apo2L-mediated apoptosis in malignant glioma.* J Neuro-Oncol, 2005. 71: p. 19-25.
105. Rapisarda A, Zalek J, Hollingshead M, Braunschweig T, Uranchimeg B, Bonomi CA, Borgel SD, Carter JP, Hewitt SM, Shoemaker RH, Melillo G, *Schedule-dependent inhibition of hypoxia-inducible factor-1alpha protein accumulation, angiogenesis, and tumor growth by topotecan in U251-HRE glioblastoma xenografts.* Cancer Res, 2004. 64: p. 6845-6848.
106. Baker SD, Heideman RL, Crom WR et al, *Cerebrospinal fluid pharmacokinetics and penetration of continuous infusion topotecan in children with central nervous system tumors.* Cancer Chemother Pharmacol, 1996. 37: p. 195-202.
107. Macdonald D, Cairncross G, Stewart D, Forsyth P, Sawka C, Wainman N, Eisenhauer E, *Phase II study of topotecan in patients with recurrent malignant glioma.* National Clinical Institute of Canada Clinical Trials Group. Ann Oncol, 1996. 7(2): p. 205-7.
108. Friedman HS, Kerby T, Fields S, Zilisch JE, Graden D, McLendon RE, Houghton PJ, Arbuck S, Cokgor I, Friedman AH, *Topotecan treatment of adults with primary malignant glioma.* The Brain Tumor Center at Duke. Cancer, 1999. 85(5): p. 1160-5.
109. Blaney SM, Phillips PC, Packer RJ, Heideman RL, Berg SL, Adamson PC, Allen JC, Sallan SE, Jakacki RI, Lange BJ, Reaman GH, Horowitz ME, Poplack DG, Balis FM, *Phase II evaluation of topotecan for pediatric central nervous system tumors.* Cancer, 1996. 78(3): p. 527-31.
110. Mi Z, Malak H, Burke TG, *Reduced albumin binding promotes the stability and activity of topotecan in human blood.* Biochemistry, 1995. 34(42): p. 13722-8.
111. Tardi P, Choice E, Masin D, Redelmeier T, Bally M, Madden TD, *Liposomal encapsulation of topotecan enhances anticancer efficacy in murine and human xenograft models.* Clin Cancer Res, 2001. 60: p. 3389-3393.
112. Drummond DC, Noble CO, Guo Z, Hayes ME, Connolly-Ingram C, Gabriel BS, Hann B, Liu B, Park JW, Hong K, *Development of a highly stable and targetable nanoliposomal formulation of topotecan.* Journal of Controlled Release, 2010. 141(1): p. 13-21.
113. Burke TG, Gao X, *Stabilization of topotecan in low pH liposomes composed of distearoylphosphatidylcholine.* J Pharm Sci, 1994. 83: p. 967-969.

114. Tardi P, Choice E, Masin D, Redelmeier T, Bally M, Madden TD, *Liposomal encapsulation of topotecan enhances anticancer efficacy in murine and human xenograft models*. Clin Cancer Res, 2000. 60: p. 3389-3393.
115. Bartlett GR, *Phosphorus assay in column chromatography*. J Biol Chem, 1959. 234(3): p. 466-468.
116. Roland M, Tozer T, *Clinical Pharmacokinetics: Concepts and Applications*. Third ed. 1995: Lippincott Williams & Wilkins.
117. *UCSF Animal Care & Use Program - Standard Procedures & Guidelines*. [cited 2011 June 9]; Available from: <http://www.iacuc.ucsf.edu/Policies/awStandardProcedures.asp>.
118. Serwer L, Hashizume R, Ozawa T, James CD, *Systemic and local drug delivery for treating diseases of the central nervous system in rodent models*. J Vis Exp, 2010. 42.
119. Sarkaria JN, Yang L, Grogan PT, Kitange GJ, Carlson BL, Schroeder MA, Galanis E, Giannini C, Wu W, Dinca EB, James CD, *Identification of Molecular Characteristics Correlated with Glioblastoma Sensitivity to EGFR Kinase Inhibition Through Use of an Intracranial Xenograft Test Panel*. Mol Cancer Ther, 2007. 6: p. 1167-74.
120. Giannini C, Sarkaria JN, Saito A, Uhm JH, Galanis E, Carlson BL, Schroeder MA, James CD, *Patient tumor EGFR and PDGFRA gene amplifications retained in an invasive intracranial xenograft model of glioblastoma multiforme*. Neuro Oncol, 2005. 7(2): p. 164-176.
121. Verhaak RG, Hoadley KA, Purdom E, Wang V, Qi Y, Wilkerson MD, Miller CR, Ding L, Golub T, Mesirov JP, Alexe G, Lawrence M, O'Kelly M, Tamayo P, Weir BA, Bagriel S, Winckler W, Gupta S, Jakkula L, Feiler HS, Hodgson JG, James CD, Sarkaria JN, Brennan C, Kahn A, Spellman PT, Wilson RK, Speed TP, Gray JW, Meyerson M, Getz G, Perou CM, Hayes DN. Cancer Genome Atlas Research Network, *Intergrated genomic analysis identifies clinically relevant subtypes of glioblastoma characterized by abnormalities in PDGFRA, IDH1, EGFR, and NF1*. Cancer Cell, 2010. 17(1): p. 98-110.
122. Michaud K, Solomon DA, Oermann E, Kim JS, Zhong WZ, Prados MD, Ozawa T, James CD, Waldman T, *Pharmacologic inhibition of cyclin-dependent kinases 4 and 6 arrests the growth of glioblastoma multiforme intracranial xenografts*. Cancer Res, 2010. 70(8): p. 3228-3238.
123. Quinn JA, Jiang SX, Reardon DA, Desjardins A, Vredenburgh JJ, Friedman AH, Sampson JH, McLendon RE, Herndon JE, Friedman HS, *Phase II trial of temozolomide (TMZ) plus irinotecan (CPT-11) in adults with newly diagnosed glioblastoma multiforme before radiotherapy*. J Neuro-Oncol, 2009. 95(3): p. 393-400.
124. Drummond DC, Noble CO, Guo Z, Hong K, Park JW, Kirpotin DB, *Development of a Highly Active Nanoliposomal Irinotecan Using a Novel Intraliposomal Stabilization Strategy*. Cancer Res, 2006. 66: p. 3271-7.
125. Allen TM, Cullis PR, *Drug delivery systems: Entering the mainstream*. Science, 2004. 303: p. 1818-1822.

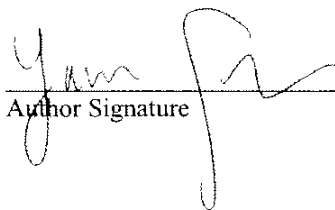
126. Drummond DC, Meyer O, Hong KL, Kirpotin DB, Papahadjopoulos D, *Optimizing liposomes for delivery of chemotherapeutic agents to solid tumors*. Pharmacological Reviews, 1999. 51: p. 691-743.
127. Drummond DC, Noble CO, Hayes ME, Park JW, Kirpotin DB, *Pharmacokinetics and in vivo drug release rates in liposomal nanocarrier development*. J Pharm Sci, 2008. 97(11): p. 4696-4740.
128. Saito R, Bringas JR, McKnight TR, Wendland MF, Mamot C, Drummond DC, Kirpotin DB, Park JW, Berger MS, Bankiewicz KS, *Distribution of liposomes into brain and rat brain tumor models by convection-enhanced delivery monitored with magnetic resonance imaging*. Cancer Res, 2004. 64: p. 2572-2579.
129. Mamot C, Nguyen JB, Pourdehnad M, Hadaczek P, Saito R, Bringas JR, Drummond DC, Hong KL, Kirpotin DB, McKnight T, Berger MS, Park JW, Bankiewicz KS, *Extensive distribution of liposomes in rodent brains and brain tumors following convection-enhanced delivery*. J Neuro-Oncol, 2004. 68: p. 1-9.
130. Sampson JH, Akabani G, Archer GE, Berger MS, Coleman RE, Friedman AH, Friedman HS, Greer K, Herndon JE, Kunwar S, McLendon RE, Paolino A, Petry NA, Provenzale JM, Reardon DA, Wong TZ, Zalutsky MR, Pastan I, Bigner DD, *Intracerebral infusion of an EGFR-targeted toxin in recurrent malignant brain tumors*. Neuro Oncol, 2008. 10(3): p. 320-329.
131. Mellinghoff IK, Wang MY, Vivanco I, Haas-Kogan DA, Zhu S, Dia EQ, Lu KV, Yoshimoto K, Huang JH, Chute DJ, Riggs BL, Horvath S, Liau LM, Cavenee WK, Rao PN, Beroukhi R, Peck TC, Lee JC, Sellers WR, Stokoe D, Prados M, Cloughesy TF, Sawyers CL, Mischel PS, *Molecular determinants of the response of glioblastomas to EGFR kinase inhibitors*. N Engl J Med, 2005. 353: p. 2012-24.
132. Neuhaus T, Ko Y, Muller RP, Grabenbauer GG, Hedde JP, Schueller H, Kocher M, Stier S, Fietkau R, *A phase III trial of topotecan and whole brain radiation therapy for patients with CNS-metastases due to lung cancer*. Br J Cancer, 2009. 100(2): p. 291-297.
133. Fisher B, Won M, Macdonald D, Johnson DW, Roa W, *Phase II study of topotecan plus cranial radiation for glioblastoma multiforme: results of Radiation Therapy Oncology Group 9513*. Int J Radiat Oncol Biol Phys, 2002. 53(4): p. 980-986.
134. Paik PK, Rudin CM, Brown A, Rizvi NA, Takebe N, Travis W, James L, Ginsberg MS, Juergens R, Markus S, Tyson L, Subzwari S, Kris MG, Krug LM, *A phase I study of obatoclox mesylate, a Bcl-2 antagonist, plus topotecan in solid tumor malignancies*. Cancer Chemother Pharmacol, 2010. 66: p. 1079-1085.
135. Ekstrand AJ, James CD, Cavenee WK, Seliger B, Pettersson RF, Collins VP, *Genes for epidermal growth factor receptor, transforming growth factor alpha, and epidermal growth factor and their expression in human gliomas in vivo*. Cancer Res, 1991. 51: p. 2164-72.
136. Sapra P, Allen TM, *Internalizing antibodies are necessary for improved therapeutic efficacy of antibody-targeted liposomal drugs*. Cancer Res, 2002. 62(24): p. 7190-4.
137. Noble CO, Kirpotin DB, Hayes ME, Mamot C, Hong K, Park JW, Benz CC, Marks JD, Drummond DC, *Development of ligand-targeted liposomes for cancer therapy*. Expert Opin Ther Targets, 2004. 8(4): p. 335-53.

138. Park JW, Hong K, Carter P, Asgari H, Guo LY, Keller GA, Wirth C, Shalaby R, Kotts C, Wood WI, *Development of anti-p185HER2 immunoliposomes for cancer therapy*. Proc. Natl. Acad. Sci. USA, 1995. 92(5): p. 1327-31.
139. Kirpotin D, Park JW, Hong K, Zalipsky S, Li WL, Carter P, Benz CC, Papahadjopoulos D, *Sterically stabilized anti-HER2 immunoliposomes: design and targeting to human breast cancer cells in vitro*. Biochemistry, 1997. 36(1): p. 66-75.
140. Park JW, Hong K, Kirpotin DB, Colbern G, Shalaby R, Baselga J, Shao Y, Nielsen UB, Marks JD, Moore D, Papahadjopoulos D, Benz CC *Anti-HER2 immunoliposomes: enhanced efficacy attributable to targeted delivery*. Clin Cancer Res, 2002. 8(4): p. 1172-81.
141. Sonoda Y, Ozawa T, Hirose Y, et al., *Formation of intracranial tumors by genetically modified human astrocytes defines four pathways critical in the development of human anaplastic astrocytoma*. Cancer Res, 2001. 61(13): p. 4956-4960.
142. Lowe C, *Western Blotting - A Beginner's Guide*, Current Protocols.
143. Sapa P, Allen TM, *Improved outcome when B-cell lymphoma is treated with combinations of immunoliposomal anticancer drugs targeted to both the CD19 and CD20 epitopes*. Clin Cancer Res, 2004. 10(14): p. 4893.
144. Ahmad I, Longenecker M, Samuel J, Allen TM, *Antibody-targeted delivery of doxorubicin entrapped in sterically stabilized liposomes can eradicate lung cancer in mice*. Cancer Res, 1993. 53(7): p. 1484-1488.
145. Garcia-Carbonero R, Supko JG, *Current perspectives on the clinical experience, pharmacology, and continued development of the camptothecins*. Clin Cancer Res, 2002. 8(3): p. 641-661.
146. Krauze MT, Vandenberg SR, Yamashita Y, Saito R, Forsayeth J, Noble C, Park JW, Bankiewicz K, *Safety of real-time convection-enhanced delivery of liposomes to primate brain: a long-term retrospective*. Exp Neurol, 2008. 210(2): p. 638-844.
147. Bernier-Chastagner V, Grill J, Doz F, Bracard S, Gentet JC, Marie-Cardine A, Luporsi E, Margueritte G, Lejars O, Laithier V, Mechinaud F, Millot F, Kalifa C, Castagner P, *Topotecan as a radiosensitizer in the treatment of children with malignant diffuse brainstem gliomas: results of a French Society of Paediatric Oncology Phase II Study*. Cancer, 2005. 104(12): p. 2792-7.

Publishing Agreement

It is the policy of the University to encourage the distribution of all theses, dissertations, and manuscripts. Copies of all UCSF theses, dissertations, and manuscripts will be routed to the library via the Graduate Division. The library will make all theses, dissertations, and manuscripts accessible to the public and will preserve these to the best of their abilities, in perpetuity.

I hereby grant permission to the Graduate Division of the University of California, San Francisco to release copies of my thesis, dissertation, or manuscript to the Campus Library to provide access and preservation, in whole or in part, in perpetuity.



Author Signature

9/19/11

Date